LÉKAŘ A TECHNIKA • CLINICIAN AND TECHNOLOGY

ČÍSLO 2 • ČERVEN 2012 • ROČNÍK 42

LÉKAŘ A TECHNIKA

Vydává *Česká lékařská společnost J. E. Purkyně*, Sokolská 31, 120 26 Praha 2 a *Fakulta biomedicínského inženýrství Českého vysokého učení technického v Praze,* nám. Sítná 3105, 272 01 Kladno.

Vedoucí redaktor *doc. Ing. Karel Roubík, Ph.D.*
Výkonný redaktor *MUDr. Ing. David Macků*
Odpovědná redaktorka *Ing. Ida Skopalová*
Předplatné *Soňa Stehlíková, DiS.*

Vychází 4krát ročně.
Po dobu řešení projektu **„Prohloubení odborné spolupráce a propojení ústavů lékařské biofyziky na lékařských fakultách v ČR“**, kód CZ.1.07/2.4.00/17.0058 bude časopis vydáván zdarma.

Registrační značka MK ČR E 5085.

Rukopisy zasílejte na adresu: *ČVUT FBMI, Redakce, nám. Sítná 3105, 272 01 Kladno*, *e-mail: redakce@fbmi.cvut.cz.*
Rukopis byl dán do výroby v červnu 2012.

ISSN 0301-5491

EDITORIAL

Biomedical engineering and medical informatics represent challenging and rapidly growing areas. Applications of advanced electronics and information technology in these areas are of paramount importance. Building on the success of the four previous YBERC conferences, the aim of the fifth YBERC conference is to continue in bringing together especially young scientists, researchers and practitioners from different disciplines, namely from mathematics, computer science, bioinformatics, biomedical engineering, medicine, biology, and different fields of life sciences, so that they can present and discuss their research results in biomedical engineering and medical informatics. We hope that YBERC will serve as a platform for fruitful discussions between all attendees, where participants can exchange their recent results, identify future directions and challenges, and initiate possible collaborative research. The importance of computer-aided diagnosis and therapy continues to draw attention worldwide and has laid the foundations for modern medicine with excellent potential for promising applications in a variety of fields, such as, telemedicine, Web-based healthcare, analysis of genetic information and personalized medicine.

The articles can be found in the proceedings. The papers show how broad the spectrum of topics in applications of information technology and electronics to biomedical engineering and medical informatics is.

The editors would like to thank all the participants for their high quality contributions and all pC members and reviewers for their efficient and excellent work.

June 2012
Lenka Lhotská
Jan Havlík

CONTENT

THE FIFTH BIOMEDICAL ENGINEERING CONFERENCE OF YOUNG BIOMEDICAL ENGINEERS AND RESEARCHERS

YBERC 2012

Prague, Czech Republic • July 11–13, 2012

CONFERENCE ORGANIZERS

Czech Technical University in Prague	Faculty of Electrical Engineering Faculty of Biomedical Engineering
VŠB - Technical University of Ostrava	Faculty of Electrical Engineering and Computer Science Department of Measurement and Control
Technical University of Kosice	Faculty of Mechanical Engineering Department of Biomedical Engineering, Automation and Measurement
elfa, s. r. o.	

EDITORS

doc. Ing. Lenka Lhotská, CSc.	FEL ČVUT v Praze
Ing. Jan Havlík, Ph.D.	FEL ČVUT v Praze

PROGRAM COMMITTEE

Chairperson

doc. Ing. Lenka Lhotská, CSc.	FEL ČVUT v Praze

Members

Ing. Michal Augustynek	FEI VŠB-TU Ostrava
Ing. Elena Cocherová, PhD.	FEI STU Bratislava
Ing. Martin Černý, Ph.D.	FEI VŠB-TU Ostrava
Ing. Jan Havlík, Ph.D.	FEL ČVUT v Praze
Ing. Zdeněk Horčík	FEL ČVUT v Praze
doc. Ing. Jiří Hozman, Ph.D.	FBMI ČVUT v Praze
Ing. Radovan Hudák, Ph.D.	FME TUK Košice
Ing. Václav Chudáček, Ph.D.	FEL ČVUT v Praze
Ing. Václav Křemen, Ph.D.	FEL ČVUT v Praze
Ing. Martin Macaš	FEL ČVUT v Praze
Ing. Marek Penhaker, Ph.D.	FEI VŠB-TU Ostrava
Ing. Jozef Púčik, PhD.	FEI STU Bratislava
doc. Ing. Karel Roubík, Ph.D.	FBMI ČVUT v Praze
prof. Ing. Pavel Sovka, CSc.	FEL ČVUT v Praze

CONFERENCE YBERC 2012

NONINVASIVE SYSTEM FOR LOCALIZATION OF SMALL REPOLARIZATION CHANGES IN THE HEART

Olena Punshchykova[1,3], Peter Kneppo[1] and Milan Tyšler[1,2]

[1]Faculty of Biomedical Engineering, Czech Technical University in Prague, Kladno, Czech Republic

[2]Institute of Measurement Science, Slovak Academy of Science, Bratislava, Slovakia

[3]Intercollegiate Faculty of Medical Engineering, National Technical University of Ukraine "Kyiv Polytechnic Institute", Kyiv, Ukraine

Abstract

Novel noninvasive method for localization of areas of myocardium with changed repolarization that can lead to life threatening cardiac arrhythmias is presented. Method is based on multichannel ECG measurement, body surface potential mapping and solving the inverse problem of electrocardiology to find one or two dipoles representing the pathological sources in the heart. Body surface potential mapping system ProCardio-8 using up to 144 active electrodes was used for multichannel ECG measurement. For the inverse calculations, inhomogeneous model of the shape of thorax with lungs and ventricles including cavities was used. Ability of the system to identify selected cardiac pathologies is demonstrated on cases with one or two ischemic foci. In this paper, analysis of existing system and algorithms for cardiac pathology localization is given in detail. Further software development will include ventricular premature beat foci localization.

Keywords

multichannel ECG recording, body surface potentials, inverse problem of electrocardiography, repolarization changes, arrhythmia

Introduction

According to the European Heart Rhythm Association White Book 2011, in 2009 the proportion of deaths resulting from cardiovascular diseases was 50% in the Czech Republic and 65% in Ukraine [1]. Therefore it is vital to decrease these numbers using new diagnostic and treatment methods.

Necessary precondition for the use of advanced diagnostic methods enabling precise cardiac pathology localization in various cardiovascular diseases is availability of quality high resolution measurement of electrocardiograms.

Diagnostic information contained in body surface potential maps and acquired from multichannel ECG signals is much more detailed than that obtained from standard 12-lead ECG or Frank VCG lead system.

For high quality measurement of required ECG signals special multichannel electrocardiographic system ProCardio-8 was developed [2].

Material and Methods

Body surface potential mapping (BSPM) is a technologically advanced method that helps in detailed diagnostics of various cardiovascular diseases. Using BSPM for localization of areas with changed repolarization can significantly improve the understanding of electrophysiological processes in the heart in different clinical cases. The procedure is noninvasive and non-fluoroscopic and can provide highly useful diagnostic information without substantially loading the patient. In addition, its safety, possibility of repeated examinations and their automation gives BSPM more important advantages in comparison to other diagnostic procedures.

BSPM is based on multichannel measurement of body surface cardiac potentials using special multichannel electrocardiograph. Detailed registration of the surface cardiac potentials requires high number of sensing electrodes accurately placed on the thorax.

BSPM is one of the several cardiac mapping methods. "Cardiac mapping" is a wide term which also

covers endocardial and epicardial mapping. Endocardial mapping is performed with catheters, which are inserted into heart cavities and navigated using fluoroscopy. Inserted catheters sequentially record endocardial electrograms and enable to identify temporal and spatial distributions of electrical potentials generated by the myocardium during normal and abnormal rhythms.

In contrast to the above mentioned two methods of cardiac mapping, noninvasive assessment of the electrical state of the heart by solution of the inverse problem of electrocardiography requires high quality surface ECG measurement with correct and precise electrode positioning and an appropriate model of the patient torso volume conductor. This model can be either some simplified approximation of a real torso, or can be precisely derived from CT or MRI scans of the patient torso what considerably increases accuracy of the method. The variety of cardiovascular pathologies that can be identified using such noninvasive inverse procedure includes ischemia, WPW, ventricular ectopy and other arrhythmias [4].

Multichannel ECG mapping system ProCardio-8

In order to record and analyse high quality multichannel ECG recordings, a special system ProCardio-8 was designed. This device consists of a set of active electrodes (up to 144), a data acquisition system and a hosting personal computer. Rechargeable Li-ion battery power supply with advanced power management is used for achieving excellent recordings quality and possibility of its using for one working day without replacement or recharging.

The data acquisition system is placed in a patient terminal box and connected via USB cable to the host personal computer. Its small geometric dimensions (14 × 19 × 20 cm) minimize capacitive coupling with external environment. The data acquisition system is modular and built from up to 9 measuring boards that are plugged into a motherboard. The system can be configured to record ECG signals simultaneously from 64 to 144 electrodes. Each measuring board records 16 ECG signals. One of the boards is configured as the reference board and is used for recording of 3 signals from the limb electrodes R, L and F. The mean value from the limb electrodes - the potential of the Wilson's central terminal (WCT) that is commonly used as the reference for all unipolar leads - is generated in a resistor network as the 4th signal from the board. Resting 12 channels on the board can be used for signals from additional chest electrodes.

The reference board also contains additional circuitry for the common mode sense electrode (CMS) and the driven right leg (DRL) electrode that provides active grounding of the patient and reduces the common mode voltage. DRL circuit also limits the current through the patient body to 50 μA. For patient protection in case of possible electrical defects, additional protection circuit is used that generates a power-down signal in case when the current through the patient body remains close to 50 μA. In such a case the microcontroller disables the power supply of the measuring boards.

To get optimal signal quality, all recorded signals are originally measured relatively to the properly placed CMS electrode. Potentials of unipolar electrocardiographic leads are then computed in the PC by subtracting the WCT potential from the electrode signals, while bipolar leads are computed as difference signals between corresponding electrodes. Each measuring channel is low-noise (< 0.75 μV_{RMS}) and equipped with a DC-coupled instrumentation amplifier (Analog Devices AD 627) with fixed gain of 40 and a 22-bit Σ-δ A/D converter (Analog Devices AD 7716). Sampling frequency can be selected between 125 and 2000 Hz and provides corresponding effective dynamic resolution between 19 and 16 bits.

The data acquisition system is controlled by a 16-bit CISC Fujitsu microcontroller placed on the motherboard. It scans the data sampled from analogue channels and sends it to the connected host PC. To minimize the capacitive coupling between the USB port of the host PC and the patient terminal, a fibre optic USB extension cable is used.

Disposable Ag-AgCl electrodes with active adapters are used for ECG signals sensing. Each electrode is made in SMD technology and has a thermally compensated amplifier (Analog Devices OP 193). Therefore each electrode has high input and very low output impedance, what effectively reduces disturbing signals, guarantees low noise induced in electrode cables and enables high quality ECG measurement. Disposable electrodes usage eliminates risk of patient infections as well.

The host personal computer of the ProCardio-8 system runs Microsoft Windows® based measuring and data analysis application software containing five basic modules:

1. Configuration of the data acquisition system,
2. Testing of electrode contacts and signal calibration,
3. Measurement of ECG signals,
4. Off-line ECG signal processing,
5. Computation and analysis of body surface potential maps.

The first three user-friendly programmed modules enable to set all necessary parameters of the system, to test electrode-skin connections and optimize signal processing depending on ECG amplitudes, read the ECG data stream into the host PC, monitor recorded ECG signals on the screen and store recorded measurements. Measured and processed data are stored as GDF files (general data format for biosignals) in selected directory. The fourth module performs off-line ECG signal filtering and baseline correction, enables to select desired time instants in the ECG records and finally the fifth module computes, displays and analyses body surface potential maps, integral maps and desired difference or departure integral maps.

Creating, debugging and consecutive testing of any real-time measuring software is a very difficult and time consuming process, especially in so sensitive field as medical sciences. The classical approach is to develop an application source code in C++ language what certainly takes a large amount of programmer's time and labour. To simplify and accelerate this process, we decided to use the MATLAB environment and its supporting background also for measurement control and communication with the external hardware. This concept offers the opportunity to utilize all digital signal processing and analysis functions included in the MATLAB for processing of the data stream during the data acquisition and subsequent off-line processing and analysis of measured ECG signals [3].

Cardiac pathology localization method

The location of some cardiac pathology can be found noninvasively by solving the inverse problem of electrocardiology. In our study, possibility to locate one or two ischemic areas with changed repolarization was analysed.

The noninvasive inverse method was based on a dipole model of the cardiac electric generator representing small pathological lesions and realistic model of the geometry and electrical properties of an inhomogeneous human torso [5], [6].

The method evaluates differences between surface potentials recorded in the same patient under conditions without manifestation of ischemia and during ischemia developed during a stress test or by progress of the disease.

Differences within the depolarization - repolarization period can be topologically represented as one difference integral map (DIM) showing the surface distribution of differences between integrals of ECG potentials over the QRST interval recorded in corresponding surface points. Assuming a multiple dipole generator and piecewise homogeneous torso as the volume conductor, boundary element method can be applied for computation of body surface potentials yielding a linear matrix equation.

Computation of the DIM by subtracting the normal integral map from the integral map with manifested ischemia is then equivalent to the computation of an integral map for a difference multiple dipole generator Δs representing only the pathological changes:

$$\Delta p = A.s_i - A.s_n = A.(s_i - s_n) = A.\Delta s \,, \quad (1)$$

where Δp is the vector of computed values in the DIM, A is the transfer matrix representing the torso volume conductor, s_i and s_n are dipolar sources in the normal and ischemic myocardium and Δs represents dipolar generators in ischemic lesions; physically s represents time integrals of dipole moments of current dipoles.

In the inverse solution, a single dipole or a pair of dipoles was searched as the equivalent generator (EG) representing the small lesions. The inverse solution was based on singular value decomposition of a submatrix of the transfer matrix A. The submatrix was composed of columns of the matrix A corresponding to every possible position of an EG located in the predefined points evenly distributed within the modelled ventricular myocardium (N possible dipoles, or $N.(N-1)/2$ possible dipole pairs).

As the transfer submatrix for each dipole or pair of dipoles is strongly over-determined, unique solution in the sense of the minimum least-squares criterion can be always obtained. The best representative dipole or pair of dipoles with minimal rms difference (DIF) between the measured DIM and the map generated by the inversely estimated equivalent generator was then considered to represent the analysed cardiac pathology.

However, especially for dipole pairs, this criterion usually had no sharp minimum and several dipole pairs gave results with DIF varying very slightly from the minimum. Therefore also results with DIF within 1% difference from the best solution were analysed. To identify the cases, where the inversely computed dipoles really represented 2 lesions, two clusters of dipoles were created from the obtained dipole pairs by applying the modified K-means iterative algorithm for K=2, based on Euclidean distance between the dipoles. Dipole positions of the dipole pair with smallest DIF value were used as the initial positions of the cluster centres. Dipoles from another dipole pairs were then assigned to the cluster with the nearest cluster centre.

Because dipoles from one pair should represent different ischemic lesions, they should belong to different clusters. If both dipoles were assigned to the same cluster, the pair was excluded from the evaluation. At the end of each iteration, new cluster centres were recalculated from assigned dipoles and next iteration was started. If no more changes occurred during the iteration, the algorithm finished dividing dipoles into 2 clusters. The final gravity centre of each cluster was considered as the centre of an identified lesion and the mean dipole moment computed from all dipoles in one cluster was assigned to that lesion. At the end of the iteration process, the DIM was claimed to represent two distinct lesions only if all pairs of the inverse dipoles have their dipoles located in different clusters and the distance between the clusters was big enough.

Patient analysis

To locate the heart repolarization changes, body surface potentials from multiple chest leads were measured using the ProCardio-8 in a group of patients (8 men and 3 women, age 45-69) after myocardial infarction and surface QRST integral maps were computed. In order to calculate equivalent current dipoles representing the regions with changed repolarization, inhomogeneous torso model with lungs and both, realistic and analytical heart model were used. Integral maps before and during the exercise test at load of 75W were computed for each patient and the corresponding EG was considered as the representation of possible local repolarization changes induced due to the stress test and was compared with perfusion images obtained by single photon emission computer tomoghraphy (SPECT). Analysis of the results showed that in 80% of cases the EG representing the QRST DIMs was located in areas identified also by the SPECT, so the method could be a useful tool for localization of ischemic heart lesions [5].

Moreover, information on individual torso structure from MRI, CT or ultrasound systems could significantly increase the quality and accuracy of this advanced inverse diagnostic method for identification of local repolarization changes [6].

Ventricular arrhythmias belong to the main causes of mortality in the western society. Ablation of the ectopic centre, which causes ventricular cardiac rhythm pathology, can significantly improve the stability of the heart function and decrease the number of life threatening arrhythmias. O. Dössel's group [7] has used anatomical data of the patient and a model based on the cellular automaton principle to demonstrate possibility of ectopic focus localization. Their method showed reliable localization of premature ventricular beat foci with reconstruction error less than 6.1 mm. Therefore we are going to supplement the ProCardio-8 software with new algorithms which will enable to detect ventricular ectopic centres using the Tikhonov regularization method [8].

Conclusion

Analysis of the normal electrophysiology of the heart, cardiac arrhythmia mechanisms origin and ECG genesis specifics showed that using body surface potentials together with patient torso model (using cardiac CT or MRI scans) is possible instrument for cardiac arrhythmia substrate localization. Physical and mathematical aspects of the inverse solution using simplified dipole-based model of cardiac pathologies were experimentally verified and ProCardio-8 mapping system, for computation and evaluation of body surface potential maps was developed. Efficiency of the solution of the inverse problem of electrocardiography and its possibility to locate cardiac pathologies was demonstrated on localization of one or two simultaneous ischemic lesions with changed repolarization properties.

Further software development will include ventricular premature beat foci localization. Application of this method for arrhythmia diagnostics can expand understanding of electrophysiological processes in the heart in different clinical cases.

Acknowledgement

This work has been supported by the research grants No. NT/11532-5 from the Ministry of Health of the Czech Republic IGA, No. SGS11/143/OHK5/2T/17 from Czech Technical University in Prague SGS, No. 2/0210/10 from the VEGA Grant Agency and No. APVV-0513-10 from the Slovak Research and Development Agency.

References

[1] Vardas, P., Auricchio, A., Merino, J.L. *The EHRA White Book 2011. The Current Status of Cardiac Electrophysiology in ESC Member Countries*. p. 498, www.escardio.org/EHRA.

[2] Karas, S., Hebláková, E., Rosík, V., Tyšler, M. *Multichannel high-resolution electrocardiograph developed in Matlab*. Technical Computing Prague. 16th Annual Conference Proceedings, Praha, Czech Republik, 2008, p. 55.

[3] Tyšler, M., Rosík, V., Kneppo, P. *Multichannel ECG measurement for noninvasive identification of heart regions with changed repolarization.* XVIII IMEKO World Congress. Metrology for a Sustainable Development, Rio de Janeiro, Brasil, 2006.

[4] Rosík, V., Karas, S., Hebláková, E., Tyšler, M., Filipová, S. *Portable device for high resolution ECG mapping*. Measurement science review, 2007, vol. 7, no. 6, p. 57-61.

[5] Tyšler, M., Svehlikova, J., Rosík, V., Karas, S., Hebláková, E., Kneppo, P., Muzik, J., Kania, M., Zaczek R., Kobylecka, M. *Model-based method and instrumentation for noninvasive identification of local ischemic lesions in the heart*. World Congress on Medical Physics and Biomedical Engineering. IFMBE Proceedings, Munich, Germany, 2009, p.1403-1406.

[6] Svehlikova, J., Lenkova, J., Turzova, M., Tysler, M., Kania, M., Maniewski R. *Influence of individual torso geometry on inverse solution to 2 dipoles*. J Electrocardiol, 2012, vol. 45, no. 1, p. 7-12.

[7] Farina, D., Dössel, O. *Non-invasive model-based localization of ventricular ectopic centers from multichannel ECG.* International Journal of Applied Electromagnetics and Mechanics, 2009, vol. 30, no. 3-4, p. 289-297.

[8] Denisov, A. M., Zakharov, E. V., Kalinin, A. V., Kalinin, V. V. *Numerical solution of the inverse electrocardiography problem with the use of the Tikhonov regularization method.* Moscow University Computational Mathematics and Cybernetics, 2008, vol. 32, no. 2, p. 61-68.

Olena Punshchykova, Mgr.
Department of Biomedical Technology
Faculty of Biomedical Engineering
Czech Technical University in Prague
nám. Sítná 3105, CZ-272 01 Kladno

E-mail: olena.punshchykova@fbmi.cvut.cz
Phone: +420 777 093 734

INDUCTION SENSORS FOR MEASUREMENT OF VIBRATION PARAMETERS OF ULTRASONIC SURGICAL WAVEGUIDES

D. Stepanenko[1], V. Minchenya[1], A. Avtushko[1], K. Bogdanchuk[1], E. Dlusskaya[1], I. Yanovich[1], T. Stepanenko[2]

[1]Belarussian national technical university, Minsk, Republic of Belarus

[2]Research institute of automation means, Minsk, Republic of Belarus

Summary
The article describes design, fabrication technology and results of experimental studies of induction sensors for measurement of vibration parameters of ultrasonic surgical waveguides. The developed sensors are based on effect of inverse magnetostriction and have simple and miniature design. They have improved locality of measurements and this provides possibility to study distribution of vibration parameters along the length of the waveguide. The described sensors can be used during design and testing of ultrasonic waveguides for minimally-invasive surgery and as feedback sensors in ultrasonic surgical devices.

Keywords
ultrasonic waveguide, induction sensor, inverse magnetostriction

Introduction

Measurement of parameters of ultrasonic vibrations, particularly, amplitude of mechanical stresses, is actual practical problem, because ultrasound is widely used in engineering and medicine. At present there is a number of non-contact sensors for measurement of vibration parameters of ultrasonic waveguides including fibre-optic sensors, laser Doppler vibrometers (LDVs), inductive and induction sensors. Direct measurement of amplitude of ultrasonic vibrations can be implemented by means of microscope and this method is used for calibration of the above mentioned sensors. The main drawbacks of fibre-optic sensors and LDVs are their high cost, complexity of design and signal processing. The most easily implemented sensors are inductive and induction ones. For example, the authors previously described design of induction sensor for measurement of vibration amplitude of ultrasonic surgical waveguides and application of this sensor for control of amplitude-frequency response functions of such waveguides [1]. As a special case of induction sensors one can consider sensors based on effect of inverse magnetostriction. This effect, also known as Villari effect, consists in alteration of magnetization of ferromagnetic materials under the action of mechanical stresses. Application of time-varying stresses to the material will create alternating magnetic field, which can be detected by means of induction coil. This method of detection of ultrasonic stresses was for the first time described by Langenecker [2]. Effect of inverse magnetostriction is widely used in non-destructive evaluation and for study of magnetic properties of materials. For example, Hatafuku describes application of inverse magnetostriction induced by ultrasonic stresses for determination of effective magnetic field in ferromagnetic bars [3]. The main drawback of measurement of parameters of ultrasonic vibrations by means of induction sensors on the basis of effect of inverse magnetostriction is non-locality of measurement. This non-locality is manifested in the fact that electromotive force (EMF) induced by alternating magnetic field in long helical induction coil is determined by mechanical stresses acting in all cross-sections of the waveguide encircled by loops of the coil. This makes impossible determination of stresses in specific cross-section. This article considers design, manufacturing technology and results of experimental studies of sensors of ultrasonic stresses based on effect of inverse magnetostriction with improved locality of measurements as well as possibility of application of these sensors for control of vibration parameters of ultrasonic surgical waveguides.

Design and fabrication methods of the sensors

Locality of measurements using induction sensors on the basis of effect of inverse magnetostriction can be improved by means of application of flat (spiral) induction coils. This idea was used for development and fabrication of three types of induction sensors with flat coils. In two of these sensors coil was fabricated by means of single-layer spiral winding of insulated wire conductor, and in the third sensor it was produced using electrochemical etching of thin-film conductive material (foil). Photographs of appearance of the developed sensors are presented in the Fig. 1.

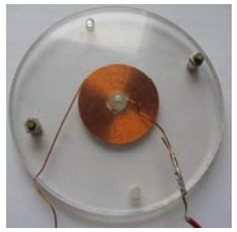
a)


b)


c)

Fig. 1: Photographs of the sensors

Sensor of the first type was fabricated using copper wire with diameter 0.7 mm coated with insulating lacquer. Wire was wound on non-ferromagnetic core in the form of short-length polystyrene tube. For ensuring single-layer packaging of wire winding of coil was implemented between two plates made of organic glass. Fixed clearance with value equal to diameter of wire was set between the plates. Core was inserted with small interference into the openings made in the centres of the plates. Length of core was chosen to be slightly smaller than sum of thicknesses of the plates and clearance between them. Clearance was set by inserting single turn of wire between the plates with their subsequent fixation by means of screw passing through the opening of core, washer and nut. Central turn of wire was fed from the sensor body through axial slot made in opening of one of the plates and radial cut in the washer. After winding of the necessary number of coil turns fixation screw was removed from the opening of core, and plates were kept in compressed state by means of screws inserted in openings circumferentially arranged at the outer edges of the plates. Utilization of plates made of transparent material enabled visual inspection of winding, particularly, presence of close packaging of coil turns.

In the sensor of the second design coil was wound using copper wire with diameter 0.06 mm. This enabled miniaturization of sensor (dimension with electronic components is Ø40 mm × 3 mm). Special feature of the sensor consists in the presence of built-in signal amplifier with low supply power. Power supply of amplifier is implemented using auxiliary coil, which transforms alternating magnetic field arising during vibration of the waveguide into supply voltage. In other words, power supply of amplifier is implemented using principle of magnetostrictive harvesting of vibration energy [4].

Sensor of the third type was fabricated using foil-coated cloth laminate with thin-film copper coating. Foil was mechanically polished, after that it was coated with mask protecting conductive tracks of coil from etching. In this work we generated mask using simplified technology applied by radioamateurs for production of homemade circuit boards and based on application of laser printer. First of all mirror image of mask was created. This task was implemented using AutoCad software and specially developed macro in VBA programming language for drawing of spirals. Image of mask was transferred onto paper carrier (tracing paper) using laser printer. After that toner powder was transferred from paper carrier onto copper coating of cloth laminate substrate using heating element with temperature about 180° C. Under uniform pressure and heating toner powder strongly adheres to the copper coating, and tracing paper can be removed by means of water. Drawback of the method consists in spreading of toner powder as a consequence of melting, resulting in spreading and non-uniform width of tracks of the mask. Under excessive pressure and heating spreading can result in formation of bridges between adjacent tracks of the mask. After etching these bridges give origin to cross-track short-circuiting. For avoidance of this problem one needs to remove bridges by means of needle or other sharp tool. Etching of copper was implemented using water solution of chloride of trivalent iron ($FeCl_3$). Duration of etching was about 2.5 hours, however, it can be substantially reduced by heating solution up to 50° C. It should be noted that large duration of etching is not a critical factor from the view of productivity since it is possible to use batch processing enabling simultaneous fabrication of large quantity of sensors. Under insufficiently strong adherence of toner powder to the substrate small underetching of tracks was observed, appearing as matt areas of the surface in the Fig. 1c. After etching toner powder was washed away from the substrate using acetone, drilling of central opening and soldering of signal wires were carried out. For protection of harmful external physical and chemical conditions tracks of the sensor can be coated with layer of insulating lacquer. In industrial conditions fabrication of foil sensors can be implemented using foil-coated polyimide films used in production of flexible circuit boards and having thickness down to 45 µm. Small thickness of the films provides potential possibility for creation of compact multilayer sensors, for example consisting of one or several layers of signal-detecting coils and one or several layers of energy-harvesting coils. Such sensors will preserve locality of measurements and posses enhanced sensitivity and efficiency of energy harvesting. Fabrication of coils can be implemented by means of photolithography, laser ablation or Focused Ion Beam (FIB) milling as well as by means of electrochemical etching with application of mask produced by direct printing on the substrate [5]. Above-listed methods provide possibility of fabrication of coils with precise dimensions and very small features (small pitch of conductive tracks).

Study of operational characteristics of the sensors

Experimental studies of the developed sensors were implemented on wire ultrasonic waveguides and bars made of austenitic steel 316L. EMF induced in the sensor coil can be determined from Faraday law:

$$E = \frac{d\Phi}{dt} = 2\pi f \Phi_0 \cos(2\pi f t), \qquad (1)$$

where $\Phi(t)$ is time-varying magnetic flux traversing coil; Φ_0 is amplitude of magnetic flux; f is vibration frequency.

It is supposed that magnetic flux varies in harmonic law:

$$\Phi(t) = \Phi_0 \sin(2\pi f t). \qquad (2)$$

As it follows from Eq. (1), amplitude of EMF is proportional to vibration frequency. For high vibration frequencies (20-30 kHz) this provides possibility to detect signal with sufficiently large amplitude even for very small variations of magnetization.

Testing of linearity of the developed sensors was implemented by measuring amplitude of stresses in longitudinally vibrating rigid bar with diameter 4 mm. Signal observed in all sections of the waveguide had harmonic form and this proves linearity of the sensors. Distribution of stress amplitude along the length of the waveguide is in agreement with theoretically predicted sinusoidal distribution (Fig. 2). Maximum amplitude of the signal is observed in nodal points of vibratory displacements corresponding to antinodes of mechanical stresses.

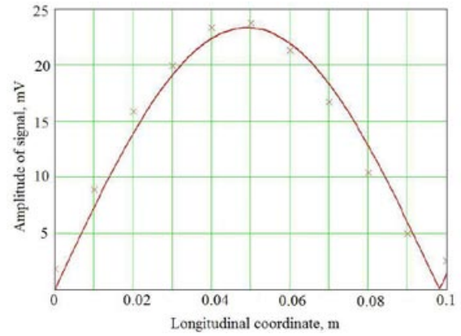

Fig. 2: Distribution of signal amplitude along the waveguide

In the case of flexible waveguides with diameter of input section 2 mm waveguide will also perform flexural vibrations besides longitudinal ones. As a result of nonlinear mechanical interaction of these two vibration modes output signal of the sensors will become non-harmonic. Spectral analysis of the signal can provide information on amplitudes of longitudinal and flexural components of vibration. Spectral analysis can be implemented by means of oscillograph with functions of mathematical processing of signals. Mathematical processing can be also performed using standard mathematical software, for example, MathCad. In this work we used photographic registration of the signal with subsequent software processing of image in MathCad. Image was saved in BMP format after that we extracted green channel of the image and represented intensities of its pixels in the form of matrix (selection of color channel is related to the green color of cathode-ray-tube phosphor in oscillograph). Extraction of signal curve from the background of image was implemented using threshold segmentation [6]. Example of the image with superimposed segmented curve is presented in the Fig. 3.

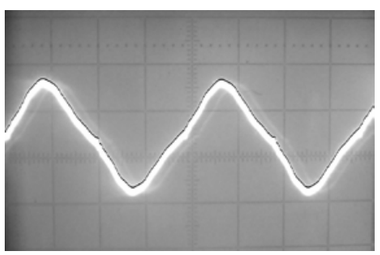

Fig. 3: Image of the signal with segmented signal curve

Spectral analysis of the given signal showed prevalence of fundamental and third harmonics. Fundamental harmonic presumably corresponds to longitudinal component of vibration, and third harmonic – to flexural component.

Longitudinal and flexural components can be separated by means of bias magnetization and this will be objective of the future studies. In the presence of uniform bias magnetic field (for example, created by Helmholtz coils) sensor will detect only component of stresses related to longitudinal deformation, and in the presence of asymmetric bias field created by permanent magnets it will detect only stress component related to transverse (flexural) deformation [7]. In the presence of asymmetric bias field induction detection of flexural deformation becomes possible even for non-ferromagnetic materials with high electric conductance, for example, aluminum [8]. Such possibility is based on reversed Lorentz-force mechanism used in electromagnetic acoustic transducers (EMATs): movement of conductive material in magnetic field under the action of external force results in generation of eddy current inducing EMF in detection coil.

In the future it is also planned to calibrate developed sensors. Calibration can be implemented using direct measurement of amplitude of vibratory displacements by means of microscope with account for theoretical relations between vibratory displacements and stresses. It is also possible to measure amplitude of stresses by means of tensoresistive transducers [9].

Another interesting problem is experimental modal analysis of waveguides. Such analysis demonstrated in other works on induction sensors [10] will be especially useful for explanation of nonlinear mechanical interactions between longitudinal and flexural vibrations.

The developed sensors can be used for study of vibratory processes in ultrasonic surgical waveguides during their development and testing and as feedback sensors in ultrasonic surgical devices with adaptive keeping of resonance.

Conclusions

In conclusion, we developed three types of inductive sensors for measurement of mechanical stresses in ultrasonic surgical waveguides and technology of fabrication of these sensors. The developed sensors have good linearity, improved locality of measurement, simple and compact design. They can be applied in research laboratories during design and testing of ultrasonic waveguides for minimally-invasive surgery as well as in surgical ultrasonic devices as feedback sensors. We also described future directions in experimental studies and practical applications of the developed sensors.

Acknowledgements

The authors would like to acknowledge Roustam Asimov and specialists of Sensotronica Co. Ltd., Resident of the High Technologies Park for assistance in development of the sensor with built-in amplifier.

References

[1] Stepanenko, D. et al. *Computer modelling and experimental studies of wire ultrasonic waveguides for minimally-invasive surgery*. Lékař a Technika, 2010, vol. 40, No. 2, p. 1-5.
[2] Langenecker, B. *Inverse magnetostrictive effect of ultrasonic stress waves in steel.* Journal of Acoustical Society of America, 1965, vol. 38, p. 234-238.
[3] Hatafuku, H. *Estimation of effective magnetic field in a nickel rod by the magnetoacoustic effect*. Journal of Magnetism and Magnetic Materials, 2002, vol. 239, p. 94-96.
[4] Wang, L., Yuan, F.G. *Vibration energy harvesting by magnetostrictive material*. Smart Materials and Structures, 2008, vol. 17, article 045009.
[5] Rapid Microsystem Prototyping – Stanford NEMS. http://nems.stanford.edu/mediawiki/index.php/Rapid_Microsystem_Prototyping
[6] Handbook of medical imaging processing and analysis. Editor-in-chief I.N. Bankman. – San Diego, San Francisco, New York, Boston, London, Sydney, Tokyo: Academic Press, 2000. – 893 p.
[7] Lee, H., Kim, Y.Y. *Wave selection using a magnetomechanical sensor in a solid cylinder*. Journal of Acoustical Society of America, 2002, vol. 112, p. 953-960.
[8] Kim, Y.Y., Han, S.W. *Magnetic sensor for noncontact modal testing of a nonferromagnetic cylinder*. Modal Analysis Conference 2007 (IMAC-XXV): A Conference and Exposition on Structural Dynamics, Orlando, USA, February 19-22, 2007.
[9] Lamport, H., Zinsser, H.H. *Strain gauge measurement of output of magnetostrictive ultrasonic transducer – pitfalls of optical measurement*. Journal of Acoustical Society of America, 1950, vol. 31, p. 435-438.
[10] Han, S.W., Kim, Y.Y. *Magnetostrictive sensor applications for the modal testing of insulated pipe*. The 32nd International Congress and Exposition on Noise Control Engineering, Seogwipo, Korea, August 25-28, 2003, p. 397-403.

Dmitry Stepanenko, Ph.D.
Department of construction
and production of instruments
Instrument-making faculty
Belarussian national technical university
65 Nezavisimosty Ave.,
220027 Minsk, Republic of Belarus

E-mail: stepd@tut.by
Phone: +375 17 2939101

Linear Modelling of Cardiovascular Parameter Dynamics during Stress-Test in Horses

Terézia Hodásová[1,2], Jiří Holčík[1,3]

[1] Institute of Biostatistics and Analyses, Masaryk University, Brno, Czech Republic
[2] Department of Mathematics and Statistics of the Faculty of Science, Masaryk University, Brno, Czech Republic
[3] Institute of Measurement Science, Slovak Academy of Sciences, Bratislava, Slovakia

Abstract
This paper deals with a processing of ECG signal parameters and modelling the parameter dynamics during the stress-test in horses. The standard Box-Jenkins methodology was applied for the linear model design. The order of the AR model (equal to 6) was estimated according to properties of autocorrelation and partial autocorrelation functions of the ECG parameter time series. Further, frequency responses of the model systems as well as distribution of their poles and zeros were determined for different stages of the stress test examination. The preliminary examination of the computed data and their dynamics indicates that they can carry useful information for evaluation the health and fitness conditions of the examined horses. All the computational procedures were implemented in MATLAB®.

Keywords
Stress-test examination in horses, ECG signal parameters, stationary process, transfer function, AR model

Introduction

The aim of the work was to find proper mathematical model of ECG parameter dynamics during the stress-test in horses. The stress-test examination consists of several stages. It starts with walk, lope and then gallop stages follow. The gallop stages ordinarily take 1 or 2 minutes starting with speed of 7m/s. After that the treadmill speed increases by 1 m/s usually up to 10 or 11 m/s.

The parameters of ECG signal change depending on the stress-test load. So the question is: is there any functional dependency based on the ECG signal parameters, which could describe the dynamics of the ECG parameters and which could characterise either the fitness level of the horse or state of its health?

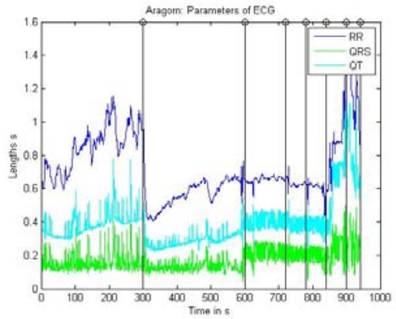

Fig. 1 : Parameters of ECG signal recorded during the stress-test in horses separated by steps.

Cardiovascular system condition can be characterised by several ECG parameters as the lengths of RR and/or QT intervals or duration of QRS complexes. In spite of the fact that all of these parameters were available, in this paper the lengths of RR intervals were considered only. It is because this parameter provides vets with a very fundamental information on the heart rate, its variability and ways of cardiovascular control.

The problematic of modelling dynamic ECG parameters is neglected part, therefore there were not known related works.

Signal processing

Data descriptions

The parameters were calculated from ECG signal recorded throughout stress-test [1]. The determined irregularly sampled parameter time series were then resampled by frequency of 10 Hz for next processing (Fig.1). The origin samples were linear interpolated to obtain the continuous signal and this signal was in next

step sampled by frequency of 10 Hz to obtain equidistant time series.

Stationarity and frequency spectrum

The basic well known approach for a description of a time series dynamics is based on the Box-Jenkins methodology. However, the approach prefers if the data represent stationary processes. That is why it was necessary to test how severe the non-stationarity of stress test process is.

There are several types of tests for stationarity. Testing stationarity in the mean proved to be sufficient for our purpose because of data character. Stationarity in the mean means that the value of the data mean does not depend on time. Therefore the analysed time series were divided to four intervals of the same lengths. Values of the mean were calculated for each interval and compared. Then the ANOVA test was used and the hypotheses that the values are equal, was rejected with p-value p=0 on significance level 0.05. The fact signified non-stationarity of the process and that is why the data had to be preprocessed to eliminate a data drift component.

To model the drift the frequency approach was used based on knowledge of time series frequency spectrum (Fig. 2).

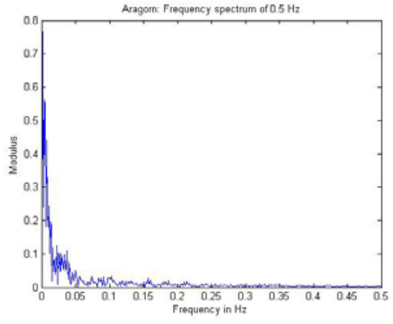

Fig. 2: Frequency spectrum of data.

There are some significant frequency clusters in the depicted spectrum. Each of them describes specific process as breathing during the stress-test or noise generated by some technical artificial sources (electrode contact artefacts, movement of ECG leads, etc).

From the Fig. 2 it is obvious that the most significant cluster is that at very low frequencies, typical for the slow drift in the data. Shape of the frequency spectrum can be also used for specification of the cut-off frequency of a low-pass filter that can be applied to remove the drift. It was determined as a frequency, the absolute value of which had the biggest difference from the previous sample. Further, order of the moving average filter (that was planned to use for removing of the data drift) had to be chosen. Provided filter with Hamming window [5] and sampling frequency of 10 Hz the degree of 700 samples proved to be of the best performance based on the trial and error method. If the degree was lower, the higher frequencies were much more attenuated. The trend obtained by filtering signal using the low-pass filter with Hamming window is shown in Fig. 3.

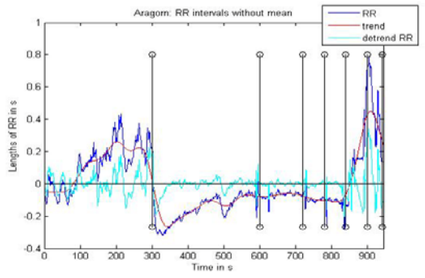

Fig. 3: Signal with and without the trend.

It is possible to see corresponding changes in the frequency spectrum in the Fig. 4. It is obvious from the figure, that the higher frequencies were really not inconveniently influenced.

The stationary signal after drift elimination (by subtracting estimated drift from the original RR interval time series) is shown in the Fig. 3, too.

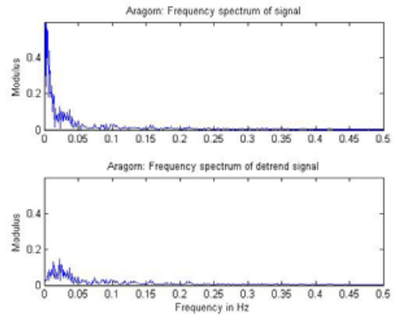

Fig. 4: Frequency spectrum of signal with and without the drift.

The test of stationarity in mean for the signal without drift does not rejected the null hypothesis, the p-value was p=0.1928 on significance level 0.05. That meant, that the signal without drift could be supposed to represent a stationary process.

Time series model

The proper linear model describing the RR interval data was looked for generally in the ARMA system family.

As it was mentioned before, the dynamics of parameters is connected to changes of the treadmill speed. Therefore the signal was divided into parts belonging to each step of the stress-test before next processing. These parts are obvious in the Fig. 3.

Each data interval was modelled individually, but the structure of the model was the same for all the cases. To determine such a structure it was necessary to decide which type of the model is the most applicable for the processed experimental data, then the order of model had to be set.

Both the tasks were solved by means of properties of an autocorrelation (ACF) and partial autocorrelation (PACF) function (see Fig. 5), [3].

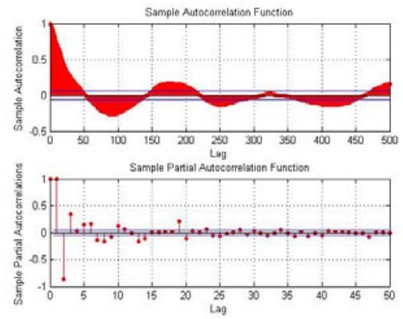

Fig. 5: ACF and PACF for step of gallop with speed 7 m/s.

For every stress-test step the estimated ACF was quickly decreasing curve shaped as attenuated sinusoid. Such a type of ACF function is typical for an autoregressive process, so the AR structure of the model proved to be the best choice. The degree of 6 of the AR model was estimated using the graph of PACF made for each part. It is not so clear from the Fig. 5. PACFs for all the stress-test steps were considered and rather simpler model than that with more complicated structure (higher order) was finally chosen.

On both of these graphs the 95% confidence intervals (blue lines) are shown. This interval is useful especially for estimation the degree of model. The values of lag numbers represent the model coefficients. If their values are outside of the confidence interval, then they are statistically significant and therefore they had to be included into the model.

Characteristics of AR(6)

The AR model of the order of 6 is defined by the difference equation according to eq. (1), [2].

$$Y_t = -\alpha_1 Y_{t-1} - \alpha_2 Y_{t-2} - \alpha_3 Y_{t-3} - \alpha_4 Y_{t-4} - \\ -\alpha_5 Y_{t-5} - \alpha_6 Y_{t-6} + \varepsilon_t \qquad (1)$$

and its transfer function is

$$H(z) = \frac{z^6}{z^6+\alpha_1 z^5+\alpha_2 z^4+\alpha_3 z^3+\alpha_4 z^2+\alpha_5 z+\alpha_6} \qquad (2)$$

Character of the transfer function can be also described by a map of its zeros and poles (see Figs. 6, 7, 8). In Fig. 6 there are obvious some clusters of poles that belong to transfer functions for different stress-test stages. These groups describe the movement of one pole (sometimes the real pole splits into two complex conjugate poles and vice versa). So the clusters can be used to describe the trajectory of pole dynamics.

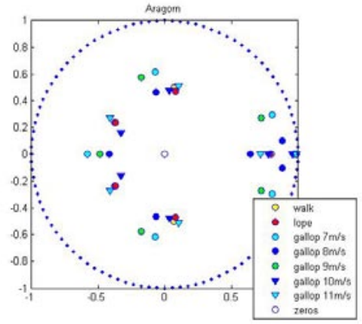

Fig. 6: Map of zeros and poles of the transfer function for horse Aragorn.

The question is, if this map can be useful for obtain the fitness level in horses. Let us examine the maps for two other horses, (Fig. 7 and 8). The pole map structure is different in both the figures. The most concentrated poles in one place are in Fig.7 (Line Honey, well trained athlete with the best fitness level). That demonstrates the low dynamics of heart rate (RR intervals) in successive steps of the stress-test.

In the Fig. 8 (Jarys, horse with the worst level of fitness in the group of examined horses) the concentration of poles is rather poor, the poles are distributed within the whole unit circle. That describes high level dynamics of the parameter.

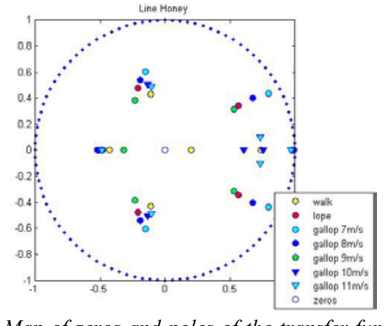

Fig. 7: Map of zeros and poles of the transfer function for horse Line Honey.

The concentration of poles for horse named Aragorn (Fig.6) is somewhere in a middle. Aragorn runs the races of the 3rd category. The previously mentioned examples demonstrate that the movement of poles of

the model describing time series of RR intervals could provide us with useful information for assessing the fitness level in horses.

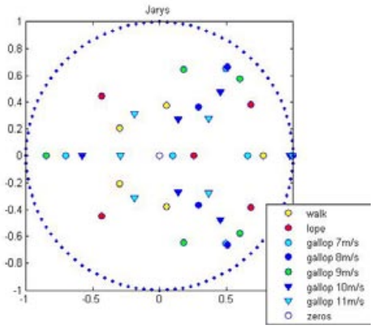

Fig. 8: Map of zeros and poles of the transfer function for horse Jarys.

Position of pole clusters in the complex Z plane (for example defined by an angle between real axis and the line connecting origin of the coordinates and centre of the pole cluster) characterizes also frequencies of processes that influence the heart rate. As it can be seen in all the mentioned figures the examined horses could be also assessed by means of such a parameter.

Conclusion

Experiments and calculations done with the experimental data up to now demonstrate that AR models and their characteristics could be considered as a useful tool for assessing especially fitness level in horses.

To verify such an idea it will be necessary to verify the hypothesis with larger set of experimental signals. Then the algorithms for machine classification of fitness level in horses will be developed.

Acknowledgement

The research was partly granted by the project of the Czech Science Foundation No.102/09/H083: „Information Technology in Biomedical Engineering“ and by the VEGA project No. 2/0210/10 “Methods and Systems for Multichannel Measurement and Evaluation of Bioelectric Signals of Heart and Brain”.

References

[1] Svačinová,J.: *Evaluation of Stress Test ECG Signal Parameters in Horses*. [Diploma Thesis], Brno, Masaryk University, 2011. (in Czech)

[2] Box, G. E., Jenkins, G. M., Reinsel, G. C. : *Time Series Analysis Forecasting and Control*. 4th. ed., Hoboken, New Jersey: John Wiley & Sons, Inc. 2008. ISBN 978-0-470-27284-8.

[3] Forbelská, M.: *Stochastic modelling of one-dimensional time series*. 1st ed., Brno: Masaryk University, 2009. (in Czech) ISBN 978-80-210-4812-6.

[4] Bitschnau, C. et al.: *Performance parameters and post excersice heart rate recovery in Warmblood sports horses of different performance level*. Equine veterinary journal 42, 2010. 17-22

[5] Harris, F. J.: *On the use of windows for harmonic analysis with the discrete Fourier transform*. IEEE vol. 66, 1978. 51- 83

Terézia Hodásová
Institute of Biostatistics and Analyses
Masaryk University
Kamenice 3, 62500 Brno

E-mail: 211192@mail.muni.cz
Tel. +420 775 119 908

MONITORING OF BREATHING BY BIOACOUSTIC METHOD

Jiri Kroutil, Alexandr Laposa, Miroslav Husak
Department of Microelectronics, Faculty of Electrical Engineering,
Czech Technical University in Prague, Prague, Czech Republic

Abstract
This paper describes a method of the breathing detection based on the sensing of acoustic signals in trachea. Parameters of the breathing, detection inspiration and expiration and apnoea pause are possible to determine from these signals. This method is simple and easy to use, portable and provides an accurate measurement and seems to be well suited for use as a modern breathing monitor. Monitoring of Respiration is important for monitoring respiration towards observation quality sleeping or The Sudden Infant Death Syndrome (SIDS).

Keywords
Breathing, biomedical sensors, biological signals

Introduction

Organism needs the energy for an arrangement of the all vital function. Energy is released by the oxidation of the energy matter (saccharides, lipids and proteins). Water and carbon dioxide are evolved too. Continuous supply of the oxygen and removing carbon dioxide are necessary by the oxidative processes. Therefore, the respiration falls into basic vital functions. In medicine this function is needed to sense and to detect its parameters. This article describes a solution of respiration diagnostics. Concretely it is thought the external respiration (pulmonary).

The organism is possible to imagine as the biological system generating biological signals that transfer information of the biological system. These signals are nearly always continuous. Bio signals are possible to divide according to origin into electrical, magnetic, acoustic, chemical, mechanical, optical, impedance, thermal, radiological and ultrasonic [5, 6].

The respiration can be detected in various ways. One of methods is the detection of the gas flow (Fleish pneumotachometer). Further, the respiration is possible to detect from the EEG signal. The method based on the imaging of the acoustic signals appears as very attractive.

Typical lung volumes and mechanism of the respiration are measured by the functional examine of lungs. One of the ways of study regulation respiration cycle is monitoring of breathing paradigm – depending among basic quantities of ventilation: respiration frequency, minute ventilation, inspiration and expiration time, apnoea pause, the respiration volume. Further parameters are: pressures and flow rates of respiration gases, lung plasticity, depending between the flow and the volume, resistance of airways [1, 2].

Characterization of Breathing

The breathing cycle is divided into four different successive phases: inspiratory phase, inspiratory pause, expiratory phase and expiratory pause. The breathing cycle is defined here as starting with the onset of inspiration at the moment when the air inflow starts. When the airflow stops, the inspiratory phase ends and the inspiratory pause begins and lasts until the air begins to flow out from the lungs and the expiratory phase starts. The expiratory phase is followed by the expiratory pause, which lasts until the end of the breathing cycle [3].

Method of Monitoring

Bioacoustic method is based on measuring acoustic signals originating in the trachea (Fig. 1). The microphone is used to measure these acoustic signals. The acquired signal of the microphone m(t) is consisted of different sources. Additional signals are added to the desired signal a(t). The equation (1) describes the relationship between the signal m(t) and the signal components. Constituent components are divided in four categories originating from: a) the airflow in the trachea, b) disturbances at the interface between the microphone and skin, c) internal components from the body without relation to the airflow and d) external components generated by the

events in the environment where the measurements are made [3].

$$m(t) = a(t) + y(t) + i_1(t) + \\ + i_2(t) + e_1(t) + e_2(t) \quad (1)$$

where
$m(t)$ ... signal observed by the microphone
$a(t)$ ... vibration airflow in the trachea
$y(t)$ ... disturbances from the interface between the microphone and skin
$i_1(t)$ ... internal disturbances from the blood flow
$i_2(t)$ ... other internal disturbances, e.g. from vessel movements
$e_1(t)$ ... external continuous disturbances
$e_2(t)$ ... external transient disturbances

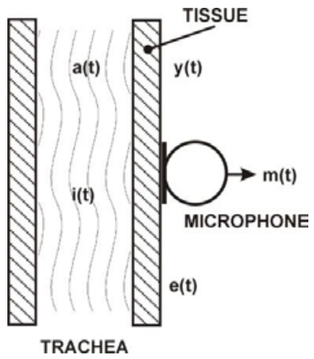

Fig. 1: The microphone applied over the trachea

The measure system in Fig. 2 was used for finding the information about the measured acoustic signal. Measure system is composed of four parts: microphone part, signal preprocessing, interface and PC.

The microphone part converts acoustic signal into electrical signal. Microphone 1 senses breathing signal originated in trachea – signal a(t). This microphone also senses additional signals added to the desired signal a(t) – external signals. The microphone 2 is used only for sensing external signals. Signals from both microphones are subtracted to cancellation of external signals. These signals from microphones are amplified by signal preprocessing block and converted to digital form by interface. Processing of signals is provided in PC by software LabView. Fig. 3 shows microphone part with MEMS microphone and its electrical scheme.

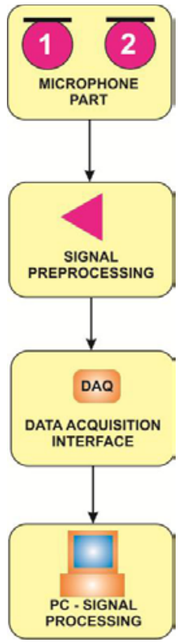

Fig. 2: Block diagram of the measure system

Fig. 3: Microphone part (10x8 mm)

In Fig. 4 is illustrated algorithm for processing signals of microphones. Signals from both microphones are converted to digital form by DAQ device. These signals are subtracted to cancellation of external signals. Level adjustment block serve for equalization of both signal level from microphones. Afterwards it follows filtration of signal in band 200Hz – 800Hz. This eliminates the remaining spurious signals. FFT block pursues conversion signal from time domain to frequency domain (spectrum). Finally, signal in time domain and its spectrum are displayed. RMS block calculates RMS value of signal. The RMS signal is compared with level of service set for detection of apnea.

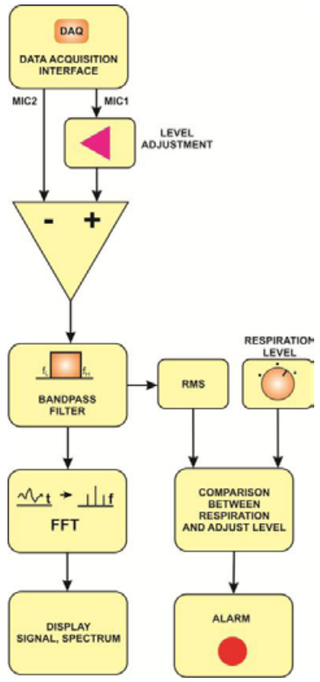

Fig. 4: Algorithm for processing signals of microphones

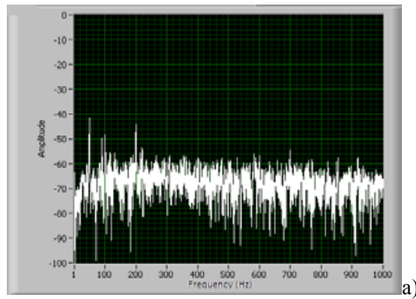

a)

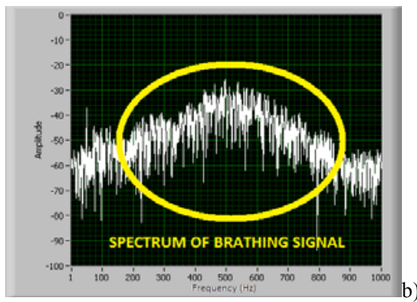

b)

Fig. 5: Spectrum of the acoustic signal: a) phase of the air flow – breathing, b) the air does not flow

The acoustic signal of the breathing occurs in frequency band from 200Hz to 800Hz, see Fig. 5. Therefore, the sampling frequency must be greater than 1600 Hz. The repeated breathing pattern and differences between inspiration and expiration are possible to read in the time behavior of the signal. The smooth beginning and the abrupt ending are often obvious during the inspiration. On the other hand, the behavior of the expiration shows the abrupt beginning and the smooth ending. Both phases are separated with the inspiratory and expiratory pauses. Fig. 6 illustrates breathing pattern – inspiration and expiration.

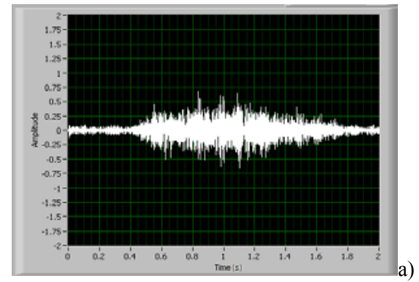

a)

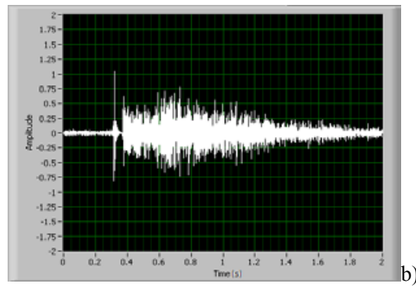

b)

Fig. 6: Breathing pattern: a)inspiration and b)expiration

Recent advances in Micro-Electro–Mechanical System (MEMS) technology enable complex miniaturized systems for biomedical applications – e.g. the integration of the Surface Acoustic Wave (SAW) sensors with a MEMS microphone [4]. The small size and wireless operation shows wide range of its potential patient monitoring applications including monitoring breathing sounds in apnea patients, monitoring chest sounds after cardiac surgery and also monitoring chest sounds of the newborns by causing minimal discomfort. Fig. 7 represents the concept of the SAW based wireless acoustic sensor. Acoustic signal from trachea are detected by microphone cause the change of the impedance of the sensor (microphone) connected across the output Interdigital Transducer (IDT) and the amplitude and phase of the reflected signal is as well as change and this is transmitted by the antenna.

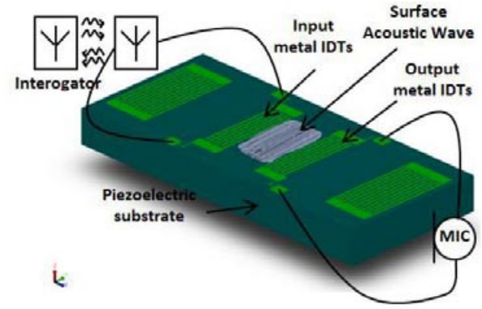

Fig. 7: Sketch of the SAW based wireless passive acoustic sensor

Another concept is depicted in Fig. 8. Sensory system contains cheap commercially available MEMS microphones. The detection of the breathing is based on the pick-up of the acoustic signal by the sensor and subsequent processing in PC. The communication between sensor and PC is wireless. The input part comprises the microphone which converts the acoustic signal to the electric signal. After this signal is amplified and digitalized. Subsequently, the signal is coded and sent by the transmitter. The receiver gives the information to PC where the breathing is analyzed. Two microphones are used in this system. The microphone 1 is used for sensing of the breathing – signal a(t). This microphone also senses additional signals added to the desired signal a(t) – external signals. The microphone 2 is used only for sensing external signals. Signals from both microphones are added to cancellation of external signals. The power part is used for the feeding sensor (battery, thermo or vibration principle).

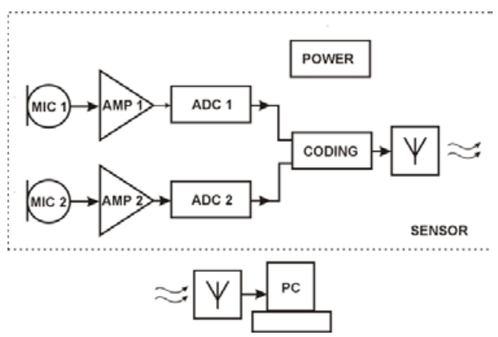

Fig. 8: Block diagram of sensory system

Conclusion

Methods, based on the monitoring of the chest motion, do not inconvenience patient with sensors placed on the body. On the other hand, it is necessary that the patient is at rest on bed. Acoustic method is very interesting for the non-invasive measurement of the breathing and for the possibility of CMOS MEMS integration. Further, this method is simple and easy to use, portable and provides an accurate measurement and seems to be well suited for the use as a modern breathing monitor. Parameters of the breathing, the detection of inspiration and expiration and the apnoea pause are possible to determine from the time behavior.

Acknowledgement

This research has been supported by the Czech Science Foundation project No. 102/09/1601 "Intelligent Micro and Nano Structures for Microsensor Realized Using Nanotechnologies" and partially by The Ministry of Interior of the Czech Republic research program No. VG20102015015.

References

[1] Rozman J a kol. *Elektronické přístroje v lékařství.* Nakladatelství Academia, Praha 2006, ISBN 80-200-1308-3.

[2] Bronzino J. D. *The Biomedical Engineering HandBook.* Second Edition, CRC Press LLC, ISBN 0-8493-0461-X.

[3] Hult P., Wranne B, Ask P. *A bioacoustic method for timing of the different phases of the breathing cycle and monitoring of breathing frequency.* Medical Engineering & Physics 22, 2000, p. 425–433.

[4] Sezen A. S., Sivaramakrishnan S., Hur S., Rajamani R., Robbins W., Nelson B.J. *Passive Wireless MEMS Microphones for Biomedical Applications*, Journal of Biomechanical Engineering, Vol.127, Iss.6, p.1030, 2005, ISSN 01480731.

[5] Webser J. G. *Measurement, Instrumentation, and Sensors HandBook*, CRC Press LLC, ISBN 0-8493-2145-X.

[6] Kroutil J., Husak M., Laposa A. Monitorování dýchání, Slaboproudý obzor, 2010, vol. 67, no. 1, p. 19–25., ISSN 0037-668X.

Jiri Kroutil,M.Sc.
Department of Microlectronics
Faculty of Electrical Engineering
Czech Technical University in Prague
Technicka 2, CZ-166 27Prague

E-mail:kroutj1@fel.cvut.cz
Phone: +420 224 352 356

APPLICATION OF TIME DOMAIN REFLECTOMETRY FOR CHARACTERIZATION OF HUMAN SKIN

Ľubomír Sládek[1], Alexander Šatka[1]

[1]Slovak University of Technology, Faculty of Electrical Engineering and Information, Institute of Electronics and Photonics, Ilkovičova 3, 812 19, Bratislava, Slovak Republic

Abstract
In this paper, we report on time domain reflectometry (TDR) and transmission (TDT) measurement and characterization of skin using biosignal electrodes, normally used for monitoring of EMG biosignals. Basic principles of TDR and TDT methods are presented for various skin equivalent circuit configurations. Using the methods, the reflected and transmitted waves were measured at three different parts of the human body skin. The measured differences reveal differences in transient phenomena related to charging-discharging cells in a skin and underneath layers.

Keywords
Time domain reflectometry, reflection, transmission, biosignal electrodes, transmission line

Introduction

Many electric measurement methods can be used for the in vivo examination of the skin properties. These methods of human skin measurement allow the tracking of various skin affection or of the effect of therapy or cosmetic methods. Also tracking changes of these properties in time is very valuable.

Using electrical measurement methods, desired skin properties can be evaluated in frequency or time domain. Both are equally useful in electronic characterization, but the measurement in time domain gives direct information about signal propagation through its electrical path. In our work, transient analysis of biosignal electrode used for evaluation of skin properties and EMG monitoring was our main point of interest. This characterization is required due to optimal design of analog matching network of electronic EMG monitoring system and evaluation of skin properties using TDR.

Time Domain Reflectometry

TDR is measuring method which evaluates the step response of electronic devices or circuits to the voltage step in time domain. In comparison to other measurement techniques, time domain reflectometry provides direct view at the device under test (DUT) characteristics. Equipment (Fig. 1) used for this type of measurement consists of a step generator, an oscilloscope and transmission line ended by measured device. Using ultrafast step generator, fast leading or trailing edge is launched into the transmission line (TL) under investigation. As the incident wave (E_i) propagate trough the TL, reflected wave (E_r) is generated by a load at the end of the line (Fig. 1a) [1].

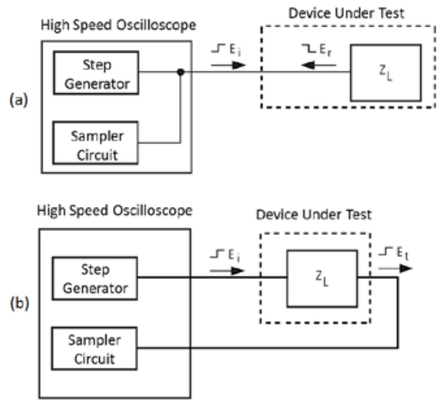

Fig. 1 Function block diagram of a time domain reflectometry system (a) and a time domain transmission system (b)

Character of the reflected wave, sampled by the sampling circuit of a high speed oscilloscope

unambiguously reveals character of the load (series or shunt, resistive, capacitive, or inductive). Similarly, part of the incident wave transmits through the measured object. Evaluating transmitted wave (E_t) gives additional information about transmission properties of the load (Fig. 1b).

Analyzing Reflections

Schematic of the TL with characteristic impedance Z_0 ended by load impedance Z_L and the basic relationship between E_r and E_i is shown in Figure 2. In this Figure, there is an impedance discontinuity at the distance x at the TL. At this discontinuity, part of the incident wave is reflected, which can be quantitatively characterized by reflection coefficient ρ:

$$\rho = \frac{E_r}{E_i} = \frac{Z_L - Z_0}{Z_L + Z_0} . \qquad (1)$$

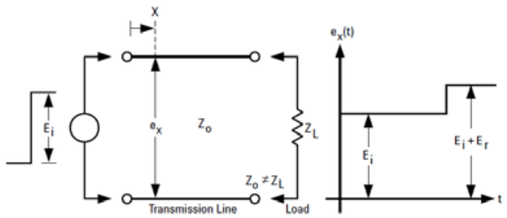

Fig. 2 Voltage vs. time at a particular point on a mismatched transmission line driven with a step of height E_i [2]

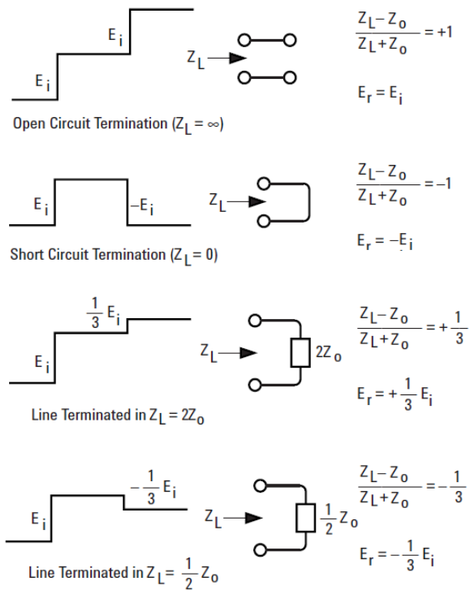

Fig. 3 TDR traces for typical loads[3]

Shape of the reflections reveals nature and also magnitude of the mismatch. Figure 3 shows four typical reflected waves and the load impedance responsible for each. Assuming Z_0 is real it is seen that resistive mismatches reflect a voltage of the same shape as the driving voltage, with the magnitude and polarity of E_r determined by the relative values of Z_0 and R_L. These reflections are of interest for evaluation of load connection to the TL, e.g. electrical length of the connection to the tested device or impedance mismatch at the connectors etc.

In our case, main focus of our interests is the reflections produced by complex load impedances of biosignal electrodes. Examples of these reflections for four basic loads are depicted in Figure 4. In case of inductive load, impedance of inductor is high at the beginning, so part of incident wave is reflected back to input of TL, but as the impedance decreases, the inductor acts like short circuit on TL. In case of capacitive load, capacitor represents a short circuit on TL in first moment and as the capacitor charges, its impedance is rising and the rest of energy of incident pulse is reflected back to input of TL. The most interesting case which corresponds to our skin measurements is depicted in Figure 4b and lately explained in part with results.

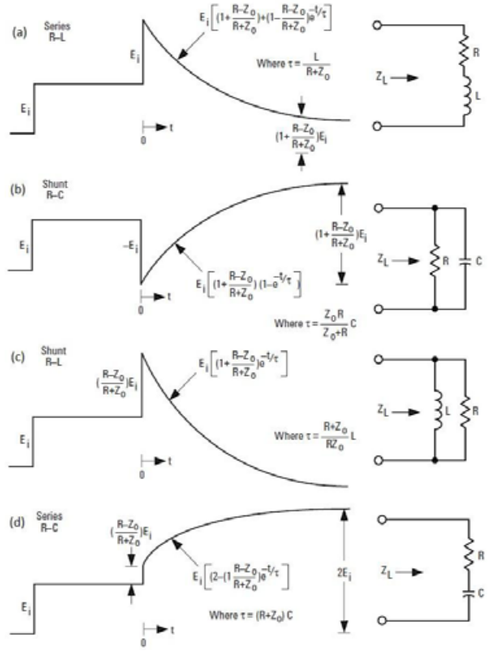

Fig. 4 TDR Oscilloscope displays for complex Z_L [4]

Experimental setup

The setup for TDR measurement features a digital serial analyzer DSA-8200 and TDR sampling modules 80E02 manufactured by Tektronics. In this configuration, TDR measurement system allows true-differential TDR measurements up to 30 GHz bandwidth with 12 ps incident rise time and 15 ps sampling time of reflected waves.

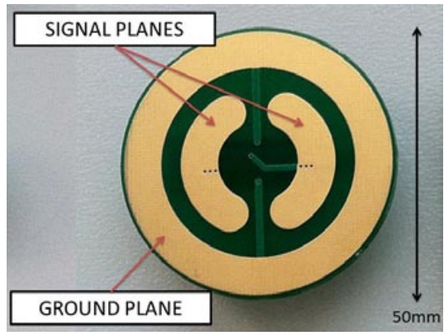

Fig. 5 Biosignal electrode

Biosignal electrodes are fabricated using printed circuit board (PCB) technology [5]. Their structure consists of FR-4 core material, conductive copper layer coated with gold, preventing electrode surface degradation due to the aggressive sweat. Topology and geometry of the electrodes is depicted in Fig. 5 [6], [7].

Connection of the electrodes to the measurement system is realized by BNC connectors and coaxial cables with characteristic impedance of 50Ω.

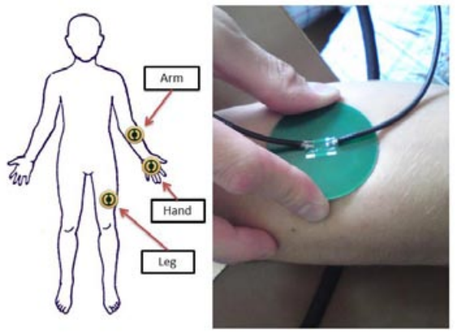

Fig. 6 Placement of electrodes on human body

Results

Example of measured reflected and transmitted waves at three different places of human body (see Fig.6) are shown in Figure 7 and Figure 8. In all three traces, the reflected wave comprised of fast negative transient (see Figure 7a) corresponding to a capacitive short and a negligible low serial resistance, followed by a nearly exponential increase of the signal above the incident value. This corresponds to the situation depicted in Fig. 4b, where resistive component represents conductivity of the skin and capacitance component represent charging of the electrolyte at the cells.

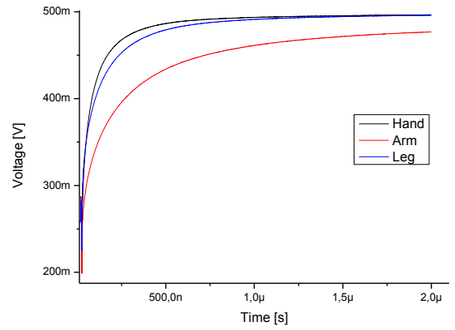

a)

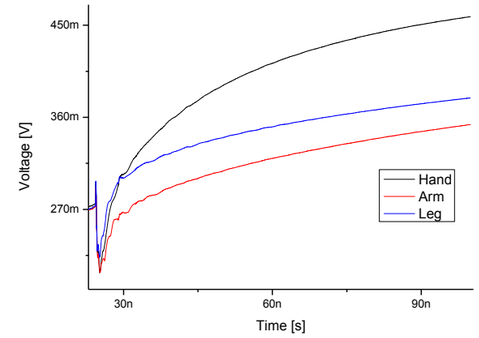

b)

Fig. 7 Reflected waves measured by biosignal electrode at three different positions (a) and detail (b)

Similarly, transmitted wave (Fig. 8) comprised of a fast, very short peak, corresponding to a serial capacitive short and a negligible low serial resistance between electrodes, followed by charging of the electrolyte at the cells and a slow relaxation to a steady state, where skin serial resistance dominates.

Using this information, the equivalent electrical circuit of skin measurements using TDR and TDT methods can be created, as depicted in Figure 9. Parameters of R_1, C_1 and R_3, C_3 can be quantified separately from TDR measurements, whereas R_2, C_2 from TDT measurements.

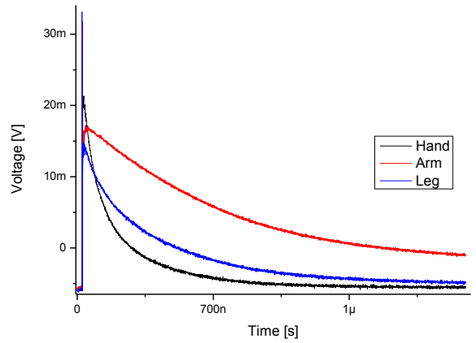

a)

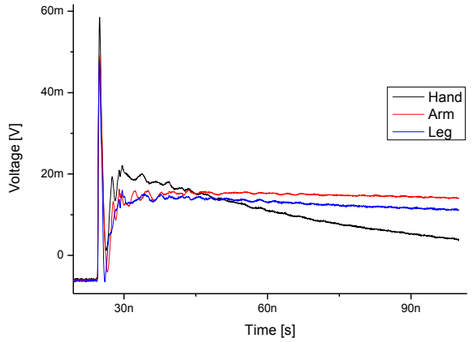

b)

Fig. 8 Transmitted waves measured by biosignal electrode at three different positions (a) and detail (b)

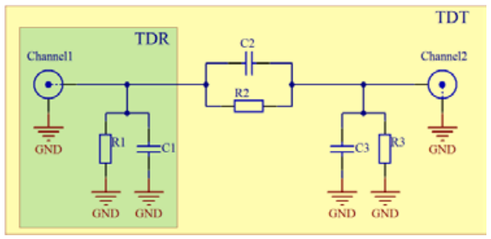

Fig. 9 Equivalent circuit of skin measurement by TDR and TDT methods

Conclusion

In conclusion, we have found that TDR is a reliable technique for characterization of different skin properties at different places of a human body. In addition to other techniques it allows direct observation and quantification of transient phenomena related to charging-discharging cells in a skin and underneath layers. In conclusion, TDR offers new insight into the characterization of skin properties using biosignal electrodes.

Acknowledgement

This work was supported by the Slovak Research and Development Agency under the contract No. VMSP-II-0018-09 and under the contract No. VMSP-II-0016-09.

References

[1] Strickland, J., A., Zimmerman, H., A., Long, G., Frye, G., *Time-domain reflectometry measurements,* Tektronix, Inc., 1970

[2] *"Time Domain Reflectometry Theory",* Application Note 1304-2, Agilent Technologies, Inc., May 10, 2006, 5966-4855E

[3] *"Signal Integrity Analysis Series"*, Application Note, Agilent Technologies, Inc., February 21, 2007, 5989-5763EN

[4] Andrews, J., R., *Step Response and "S" Parameter Measurements in the Time Domain*, Picosecond Pulse Labs, Application Note AN-3044, Revision 1, 5/89, May, 1989

[5] Vavrinský, E., Stopjaková, V., Brezina, I., Majer, L., Soláriková, P., Tvarožek, V., *Electro-Optical Monitoring and Analysis of Human Cognitive Processes.* In: Semiconductor Technologies. - Vukovar : InTech, 2010. ISBN 978-953-307-080-3

[6] Vavrinský, E., Daříček, M., Donoval, M., Rendek, K., Horínek, F., Horniak, M., Donoval, D., *Design of EMG Wireless Sensor System.* In: Applied Electronics 2011: International Conference on Applied Electronics. Pilsen, 7-8 September 2011. Pilsen, University of West Bohemia, 2011. ISBN 978-80-7043-987-6

[7] Horínek, F. - Daříček, M. - Horniak, M. - Donoval, M. - Vavrinský, E. - Rendek, K. - Donoval, D.: Modulárny systém pre rýchlu diagnostiku ochorení a zvyšovanie kvality zdravotnej starostlivosti. In: EE Journal: Journal of Electrical Engineering and Energy. Vol. 16, p. 165-167, 2010. ISSN 1335-2547

REAL-TIME PROCESSING OF MULTICHANNEL ECG SIGNALS USING GRAPHIC PROCESSING UNITS

Peter Kaľavský, Milan Tyšler

Institute of Measurement Science, Slovak Academy of Sciences, Bratislava, Slovak Republic

Abstract

A novel approach to real-time processing of tens to hundreds of measured ECG signals is proposed. For multichannel ECG signal processing we utilized computing capabilities of current heterogeneous computing systems consisting of CPUs and GPUs. Specifically we analyzed the potential of parallel hardware and software platform named CUDA that supports general purpose computation on GPUs. Three typical tasks were selected from the real-time ECG signal processing chain and distributed between the CPU and GPU according to their suitability and computational demands. Computationally less intensive task – data formatting and typical sequential task – data saving were executed on CPU and computationally more intensive task – data filtration was executed on the GPU using thousands of CUDA threads running in parallel. Furthermore, parallel execution on the GPU was also supported by parallel execution between the CPU and GPU using asynchronous function calls. Special attention was paid exactly to the parallelization of data filtration. A digital high-pass FIR filter for continual parallel filtration of tens of measured ECG signals was designed. The filter was realized in frequency domain using fast convolution and the overlap-save method. The CUDA platform enabled a 5.3-fold speedup of the application in comparison to its serial implementation and represents promising alternative for data-parallel signal processing algorithms.

Keywords

Real-time signal processing, multichannel ECG, heterogeneous computing systems, CUDA platform, general purpose computing on GPU, data-parallelism, parallel digital filtration, fast convolution

Introduction

Real-time measurement and processing of multichannel electrocardiographic (ECG) signals is a prerequisite for body surface potential (BSP) mapping. BSP mapping is a non-invasive ECG method enabling more precise diagnostic of cardiac diseases based on detailed registration of surface cardiac potentials using high number of sensing electrodes [1]. Forty years of experience with several mapping lead sets showed that information content in maps constructed from 24 to 240 leads is greater than that of standard 12-lead ECG .

However, the processing of large number of measured ECG signals, using traditional single threaded serial algorithms, imposes increased performance requirements on the computing system. Together with the growing number of processed signals also the demands on the basic ECG signal processing are growing, thus the demands on data formatting, digital filtration, computation of lead signals, displaying of ECG curves or saving the data (see Fig. 1). The high number of measured channels also complicates the possibility to implement advanced methods of ECG signal processing (like BSP mapping) in real-time. One possible way how to overcome the mentioned obstacles could be the use of new heterogeneous processor systems and programming models.

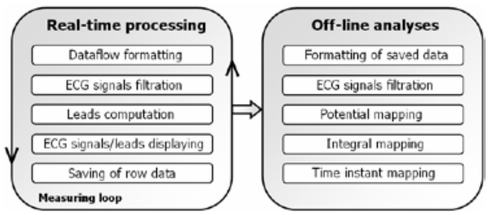

Fig. 1: Block diagram showing basic program modules of BSP mapping system.

Today, even more frequently the combination of a multi-core central processing unit (CPU) and a many-core graphic processing unit (GPU) is used to perform high-performance computations. Heterogeneous CPU-GPU based system enables to exploit the different

capabilities of its individual processors. Serial parts of algorithms could be effectively processed on the CPU and parallel parts on the GPU. The significant speedup of many scientific applications is possible mainly due to the hardware and software architecture of current modern GPUs that allows also realization of non-graphical, so called general purpose computations on GPUs (GPGPU) [2]. GPUs have evolved into processors with unprecedented floating-point performance and programmability. Today's GPUs greatly outpace CPUs in arithmetic throughput and memory bandwidth. The peak performance of the newest GPUs attacks almost 6 TFLOPS, whereas the newest desktop CPUs don't reach even the 200 GFLOPS boundaries. Anyway, GPUs are designed specifically to accelerate a variety of data-parallel problems. Because the processing of multichannel ECG signals shows considerable data-parallelism, the involvement of the GPU into the signal processing chain is considered a reasonable step.

The goal of the present study is to introduce and demonstrate a possible concept of real-time multichannel ECG signal processing speedup using one of the currently popular and heavily used heterogeneous CPU-GPU computing platform named CUDA. The speedup will be achieved through the parallelization of computationally most expensive programming modules of the ECG signal processing chain and by subsequent distribution of the workload between the CPU and GPU. In this study ECG filtration module will be parallelized and processed on the GPU.

Methods

CUDA platform

Compute unified device architecture (CUDA) is a parallel hardware and software platform supporting GPGPU on NVIDIA GPUs.

CUDA hardware is organized into an array of several unified streaming multiprocessors (SM), each consisting of many cores (the latest CUDA based GPU with codename Kepler consists of 16 SM and 192 cores in each of them). Important parts of the GPU are various types of memory spaces with different bandwidth and capacity. Managing the significant performance differences between the slow on-board (tens of GB/s) and fast on-chip memories (hundreds up to thousands of GB/s), as well as the data transfers between the CPU and GPU through the PCIe bus (8 GB/s), is the primary concern of a CUDA programmer [3].

The CUDA software enables to call parallel functions, called kernels. When a kernel function is invoked, the program execution is moved from the CPU to the GPU, where typically thousands of parallel threads are generated. These threads are organized into thread blocks and grids of thread blocks and may access data in multiple memory spaces during their execution. The hierarchy of CUDA threads is mapped to a hierarchy of processors on the GPU. A GPU executes one or more kernel grids, a SM executes one or more thread blocks, and CUDA cores and other execution units in the SM execute threads [2], [3]. For this mapping is essential that thread blocks are mutually independent, so they can be scheduled in any order across any number of SM, enabling programmers to write a code that scales with the number of cores.

Data parallelism and multichannel ECG

When a data-parallel problem is being solved, it can be partitioned into coarse sub-problems that can be solved in parallel by block of threads, and each sub-problem can be divided into finer pieces that can be solved cooperatively in parallel by all threads within the block.

If we look closer into the program modules shown in Fig. 1, we can see that they have one common characteristic. The input to these modules represents signal matrix of size *R x S*, where the number of rows *R* corresponds to the number of ECG signals processed, and the number of columns *S* corresponds to the number of samples in one individual ECG signal (see Fig. 2). Usually, in all *R* rows, eventually also in all *S* columns it is necessary to perform the same operations. It is evident that multichannel ECG signal processing might be considered as a data-parallel task. The signal matrix can be partitioned into smaller independent parts that can be mapped onto CUDA blocks and consequently the blocks can be executed on SMs.

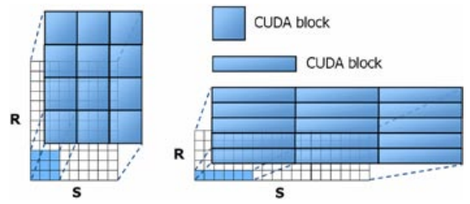

Fig. 2: Mapping of the signal matrix of different sizes to CUDA blocks.

Workload distribution between the CPU and GPU

In order to facilitate parallel execution between the CPU and GPU, some CUDA function calls are asynchronous. The control is returned to the CPU thread before the GPU stream has completed the requested task [2], [3], as shown in Fig. 3b. Thus we can exploit both, data parallelism inside the GPU and task parallelism between the CPU and GPU for a further reduction of the application runtime. This is a very valuable feature especially in conjunction with real-time applications.

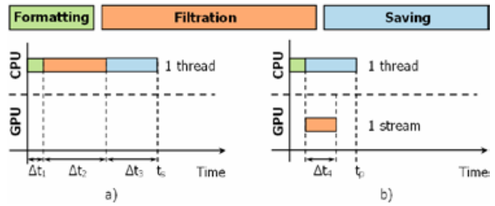

Fig. 3: Time diagrams of program modules: a) serial algorithm; b) parallel algorithm exploiting the data parallelism inside the GPU as well as the task parallelism between the CPU and GPU.

Experiments

In order to test the speed of processing multichannel ECG signals in real-time, three program modules named formatting, saving and filtration were designed (see Fig. 3). All three modules were written in C language and can be executed on CPU. The parallelized version of the filtration module was written in CUDA C and can be executed on GPU. Modules were intended specifically for high resolution multichannel ECG mapping system ProCardio-8 that was developed at the Institute of Measurement Science, SAS. Regarding the maximal data throughput of the system, 67 channels were measured using sampling frequency of 2000 Hz and 22-bit sample resolution. In the next section the inner realization of individual modules is briefly described.

The formatting module reads every 16 ms a block of 32 3-byte data from the FT245R USB chip of the ProCardio-8, converts the data into 16-byte samples (samples are of double precision, floating-point complex data type that consists of interleaved real and imaginary components) and saves the samples into the signal matrix SM_A of size 67 x 32. Each row of SM_A represents an individual input sequence *x(n)* of length $N = 32$.

The saving module removes control bytes from the input stream and saves the blocks of 3-byte raw data to the disk.

The filtration module eliminates the ECG baseline wander using a high-pass finite impulse response (FIR) filter with impulse response *h(n)* of length $M = 4065$. The filter cutoff frequency respects recommendations for low-frequency noise reduction ($f_{-3dB} = 0.67\ Hz$) [4]. The filtration is realized in the frequency domain using the convolution theorem of the discrete Fourier transform (DFT) that enables to compute output sequence *y(n)* of the length L ($L = N + M - 1$) as

$$y(n) = x(n) * h(n) \quad \underset{IDFT}{\overset{DFT}{\rightleftarrows}} \quad X(k) \cdot H(k) \qquad (1)$$

where *X(k)* and *H(k)* are DFTs of *x(n)* and *h(n)* respectively, *n* represents the time-domain index of the input samples and *k* the index of the DFT output in the frequency domain [5]. To ensure continual ECG filtration we used the well-known "overlap-save" block filtering algorithm [5]. The resultant configuration of the signal matrix SM_B of size 67 x 4096 destined for the data filtration is depicted in Fig. 4.

Two versions of filtration module were created. Both versions use optimized fast Fourier transform (FFT) libraries for DFT computation. The serial version uses the efficient FFTW CPU-based library while the parallelized version uses the CUFFT GPU-based library.

Parallelized filtration module allows for parallel processing of samples of SM_B. Using the CUFFT, 67 forward FFTs and consequently 67 inverse FFTs are computed in parallel. Moreover, the elementwise multiplication of *X(k).H(k)* uses a handcoded kernel. When a kernel is invoked, 67 x 4096 threads running in parallel are generated and every thread computes one element of the output matrix.

The processing of parallelized filtration module was assigned to one CUDA stream. In order to support the parallel execution between the filtration module running on the GPU and the saving module running on the CPU (see Fig. 3b), partial tasks of the parallelized filtration module (the CPU to GPU transfer, the FFT computation, the elementwise multiplication X(k).H(k), the IFFT computation and the GPU to CPU transfer) were designed using asynchronous functions.

The experiments were realized using one CPU core of the Intel core i7-875K (4 cores, 2.93 GHz, 4 GB DDR3) and NVIDIA GeForce GTX 480 GPU (480 cores, 1.4 GHz, 1536 MB GDDR5). The electrodes of the ProCardio-8 measuring unit sensed 67 simulated ECG signals from a signal generator.

We measured the total runtimes of the serial and parallel algorithms, t_s and t_p, the runtimes of individual program modules Δt_1, Δt_2, Δt_3, Δt_4 and also the runtimes needed to compute the FFT, the elementwise multiplication X(k).H(k) and the IFFT on CPU as well as on GPU (see Fig. 3). Results are shown in graphical and numerical form in Fig. 5. Measured values represent averaged values of corresponding runtimes over a 60 second time interval (or over 3750 runs of the 16 ms measuring loop).

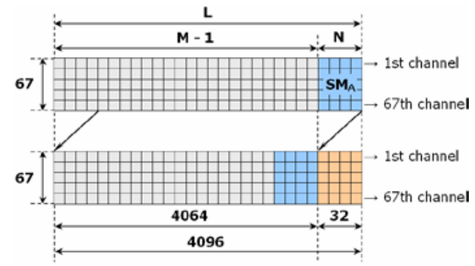

Fig. 4: The configuration of samples in the signal matrix SM_B. The signal matrices from two consecutive runs of the measuring loop are depicted.

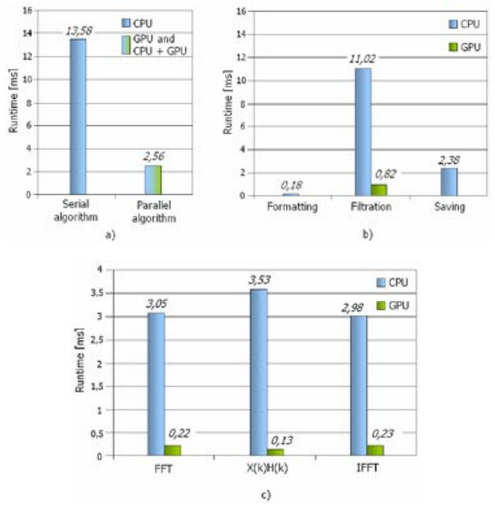

Fig. 5: Runtimes of a) serial and parallel algorithm, b) individual program modules of the serial and parallel algorithms, c) individual tasks of the filtration program module.

Results

The results depicted in Fig. 5 indicate the enormous computing power of the GPU. Using the combination of data parallelism inside the GPU and the task parallelism between the CPU and GPU, the total runtime needed to process all three program modules was reduced from 13.58 ms to 2.56 ms (see Fig. 5a). We achieved a 5.3-fold speedup and saved 81% of the total runtime when compared with the serial CPU version. As a consequence, an idle time interval of 13.44 ms has arisen in the 16 ms measuring loop. This relatively long time interval can be used for implementation of additional program modules into the ECG signal processing chain.

The major impact on the total runtime reduction had the movement of the digital filtration execution (initially the computationally most intensive task) from the CPU to the GPU. Thanks to thousands of CUDA threads running in parallel, the total runtime needed for multichannel filtration decreased from 11.02 ms to 0.82 ms (see Fig. 5b) what represents 13.4-fold speedup and 91% saving of runtime in comparison to the serial implementation.

Because also the parallel execution between the CPU and GPU was utilized and the runtime of the parallelized filtration module (0.82 ms) was shorter than the runtime of the saving module (2.38 ms), the total runtime of the parallel algorithm (2.56 ms) is given only by the sum of the formatting module runtime (0.18 ms) and the saving module runtime (2.38 ms).

Discussion

Thanks to the parallelization of the filtration module and the distribution of the workload between the CPU and GPU we speeded up the real-time ECG signal processing. As in many others GPGPU applications, the overall speedup of the parallel algorithm was limited by the serial portion of the application (in our case mainly by the saving module). For the sake of completeness it is important to say that the design and implementation of a high-order (4065) digital filter mentioned in this paper has more or less illustrative character because the time delay of this filter is approximately 1 second and displaying of ECG signals with such a long delay can be debatable.

Finally, we would like to point out that throughout the development of massive multithreaded applications we should beware of divergence of threads inside warps or deadlocks among the threads and also we should ensure the communication and synchronization among the threads, especially when they access shared resources. It is also important to be fair when making benchmark comparisons between the CPU and GPU by optimizing the application to achieve the highest performance on the CPU as well as on the GPU.

Acknowledgement

The work has been supported by research grant No. 2/0210/10 from the VEGA Grant Agency and by grant No. APVV-0513-10 from the Slovak Research and Development Agency.

References

[1] Tyšler, M. et all. *Non-invasive Assessment of Local Myocardium Repolarization Changes using High Resolution Surface ECG Mapping*. Physiological Research, 2007, vol. 56, suppl 1, S133-S141.

[2] Kirk, D. B., Hwu, W. W. *Programming Massively Parallel Processors*. Burlington: Morgan Kaufmann, 2010. 251 p.

[3] Farber, R. *CUDA Application Design and Development*. Waltham: Morgan Kaufmann, 2011. 311 p.

[4] Kligfield, P. et al. *Recommendations for the Standardization and Interpretation of the Electrocardiogram*. In Journal of the American College of Cardiology, 2007, vol. 49, no. 10, p. 1109-1127.

[5] Vijay, K. M. *The Digital Signal Processing Handbook – Digital Signal Processing Fundamentals*. Boca Raton: CRC Press, 2010. 904 p.

Ing. Peter Kaľavský
Department of Biomeasurements
Institute of Measurement Science
Slovak Academy of Sciences
Dúbravská cesta 9, 841 04 Bratislava

E-mail: peter.kalavsky@savba.sk
Phone: +421 259 104 551

MATLAB AND ITS USE FOR PROCESSING OF THERMOGRAMS

Martin Šarik[1], Jozef Živčák[2]

[1,2]Department of Biomedical Engineering and Measurement, Faculty of Mechanical Engineering,

Technical University of Košice, Slovakia

Abstract

Thermograms or better said images from thermal cameras belong to the outputs which are useful for analysis and evaluation of biological or technological systems, which have their own heat radiation. It can be used in many areas, mainly either in industry, army, architecture or and what is important in our case in medicine. This data outputs are carrying the information, which are in next phases analyzed and processed to a final or expected form. This processing can be done in more software applications, which are not only for thermograms. One of these suitable and significant applications is MATLAB. This program working on a base of matrix algorithm and with required toolbox can analyze and process the images. The main goal was to fill the problematic of processing thermograms in MATLAB and the related methodology of experiment design and its verification on a practical base. Also this methodology can be used like a guide for less or more advanced end users of MATLAB, which are working concretely with image processing toolbox.

Keywords

thermal camera, thermovision, thermograms, image analysis, software applications, image processing

Introduction

In this work was main issue based on the proposal of methodology of processing thermograms within which it was performed a series of verification tests. These checking tests were necessary for correct and independent working of whole process. MATLAB is not free application so there was also important to buy a license for next work in this program. The main target audiences which can derive from this research are people who are working with images not only with thermograms. In case of big popularity of MATLAB was purpose of article very simple and it was, to give the readers closer look at analyzing and processing the thermograms in MATLAB environment.

Material and methods

Image processing toolbox

This toolbox is one of most commonly used toolboxes in MATLAB. It allows work with images including editing and analyzing them. Main and significant functions of toolbox are [1][2][3]:

- the spatial transformation of image
- morphological operations
- adjoining and block operations
- linear filtering and filter design
- transformation
- image analysis and improvement

Design of methodology for processing of medical thermograms with using the MATLAB

For purposes of designed methodology, there are four major points or steps which are very important in whole process of analyzing and processing of thermograms:

A. Import of medical thermograms into the MATLAB workspace.
B. Analysis of imported thermograms
C. Processing of thermograms with using the functions of image toolbox.
D. Export of analyzed and processed images into statistical and graphical process.

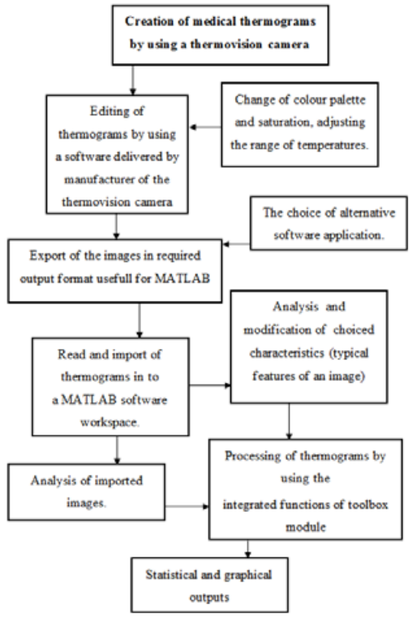

Fig. 1: Sequential layout of the blocks of methodology

Description of the four main points from the methodology

A.
- read and show of the image
- check of shown image in MATLAB workspace
- writing image like a file to the disc
- content check of a newly registered file

B.
- uses of morphological opening to estimate background
- subtract the background from the original image
- determination of the threshold images
- identification of objects in the image
- inspection of a one object
- view all objects
- calculation of the surface area of each objects

C.
- histogram equalization
- segmentation, thresholding
- edge detection
- noise reduction
  - · linear filter
  - · median filter
  - · adaptive filter

D.
- save of processed image to the disc

Examples of practical testing of designed methodology.

Background subtraction

After using *I2 = I - background*, we highlight a body over the background but before that we had define the background with using command:
- *background = imopen (I,strel('disk',15))*
- *imshow(background)*

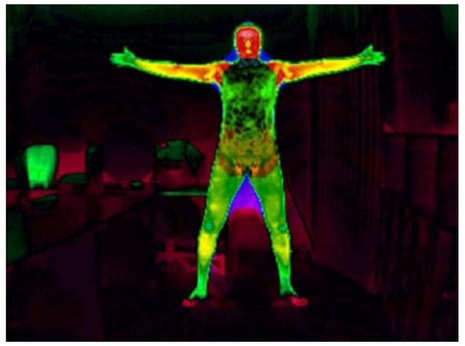

Fig. 2: Subtract of the background from the original image.

Identification of objects in the image

After use of the command *cc = bwconncomp (bw, 4)*, we found all the objects in the binary image. Using the parameter "4" was detected 39 objects. If there were some objects in contact, they were labeled as one.

```
>> imshow(bw)
>> cc = bwconncomp(bw,4)

cc =

    Connectivity: 4
       ImageSize: [240 320]
      NumObjects: 39
    PixelIdxList: {1x39 cell}

fx >>
```

Fig. 3: Identification of objects in the image

Inspection of one or more objects

When viewing a single object, a sequence of objects in the numerical order as they are pictured. In this treatment were displayed objects in the following order (2, 5, 10, 15, 20, 25, 30, 35, and 39).

Fig. 4: Check of one or more selected objects

View all objects

In view of all objects, we used one of the ways that visualize the connected objects. Following the establishment of label matrix, we then show it as a pseudo - indexed color image

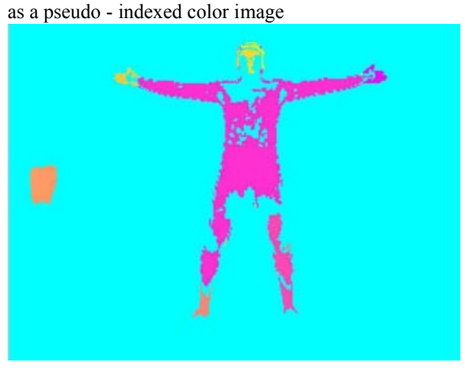

Fig. 5: View of the all objects

Edge detection

This function is used to find the overall boundaries of the object. The edges of the object are manifested as a rapid brightness changes. Image should be conducted in an area in which are no other objects that do not cause the various anomalies which reduce predictive value.

Fig. 6: Application of edge detector „Sobel“

Noise reduction

After applying of a salt and pepper filter we simulated, the noise, which can be caused by the same background temperature and the measured object, poor calibration or interference of TIC device certain external influences.

Fig. 7: Application of a“Salt and Pepper “noise

Fig. 8: Removal of noise by median filter

Conclusion

After the practical testing we have reached these conclusions. Like most suitable functions from all of tested significantly are:

- identification of objects in the image
- inspection of a one object
- calculation of the surface area of each objects
- segmentation, thresholding
- edge detection

and

- noise reduction

Some filters, such as "average" filter or "Gaussian" filter suitable for removing noise. For example, "average" filter is useful for removing noise from images, because each pixel is set to average neighboring pixels and they are reduced due to local differences in grain size.

Other of tested functions weren't suitable for thermograms but only in cases of processing classical images, because there were no important benefits, which would be helpful for medical sector.

According to comparison with other software applications we give a proposal to compare MATLAB with other similar programs which allows image or video processing, for example Scilab etc.

Considering usefulness and relevance of appropriate functions, we can declare, that they can bring the quality outputs from application like is the MATLAB.

Acknowledgement

This work was supported by research grant No. 26220120066 Centrum excelentnosti biomedicínskych technológií „Centre of Excellence for Biomedical Technologies“ 11/2010-10/2013

References

[1] Wikipedia: MATLAB. [cit.2012-05-25]. Available on the internet: http://sk.wikipedia.org/wiki/MATLAB

[2] ZAPLATÍLEK, K – DOŇAR, B.: (translated from original), MATLAB for beginners, 2.edition Praha: BEN, 2005. 152 s. ISBN 80-7300-175-6.

[3] GOMBÁR, M.: (translated from original), MATLAB – effective resource for teaching technical subjects. Prešov. [cit.2012-05-26]. Available on the internet: http://www.pulib.sk/elpub2/FHPV/Pavelka1/5.pdf

[4] Mathworks Homepage for MATLAB [cit.2012-05-25]. Available on the internet: http://www.mathworks.com/

[5] Full Online Manuals [cit.2012-05-25]. Available on the internet: http://www.ee.duke.edu/Documentation/Matlab/ReferenceTOC.html

[6] KOVÁŘÍK, M.: (translated from original), Programming and production of graphics in MATLAB I., vyd. Zlín 2008. 130 s. ISBN 978-80-7318-754-5.

Martin Šarik.
Jozef Živčák, Ph.D.
Department of Biomedical Engineering and Measurement
Faculty of Mechanical Engineering
Technical University of Košice
Letná 9, SR-040 01 Košice

E-mail: martin.sarik@tuke.sk
jozef.zivcak@tuke.sk
Phone: +421 915 875 024

IDENTIFICATION OF MAGNETIC NANOPARTICLES BY SQUID BIOSUSCEPTOMETRIC SYSTEM

M. Škrátek, I. Šimáček, A. Dvurečenskij, A. Cigáň

Institute of Measurement Science, Slovak Academy of Sciences, Bratislava, Slovakia

Abstract
A method of non-invasive localization of magnetic nanoparticles injected in living animal is presented. Measuring the magnetic response of magnetic nanoparticles to AC magnetic field by using SQUID biosusceptometric system is investigated. Experimental measurements in vivo and in vitro show possibility of using this method as a non-invasive method of identification and distribution of magnetic nanoparticles in biological tissues of small animals.

Keywords
magnetic nanoparticles, SQUID, superparamagnetism, experimental animal

Introduction

In recent years the use of magnetic nanoparticles in medicine has been risen. There are attempts to use them in cancer diagnostics, direct treatment like hyperthermia or the use of nanoparticles for targeted drug delivery. Magnetic nanoparticles (MNP) with appropriate properties, which are focused to the treated organ by external magnetic field, seem to be very useful carriers for various genes [1, 2, 3]. For biocompatibility these MNP should be covered by appropriate polymers, such as polyetylenglycol, polyetylenimin, heparin. The covering, shape and size of MNP is crucial from the view of transport properties in the cells and their toxicity. Unsuitable MNP may cause inflammatory reaction in various organs and tissues.

Determination of the distribution of MNP in living organism is the first important issue to confirm the effects of magnetic nanoparticles and also to evaluate the possible untoward effects. In this study, SQUID biosusceptometric system (SBS) was used for magnetic nanoparticle detection test, performed by *in* and *ex vivo* scanning of Wistar rats to clarify the distribution of MNP in living organism for the pharmacokinetics analysis, like drug delivers.

Methods

SBS consists of the RF SQUID, 2nd-order gradiometer, electronic modules, movable bed and the magnetization system with Helmholtz coils generating the magnetic field in the direction of gradiometer axis. AC magnetic field has the intensity of 240 A/m and the frequency of 2.8 Hz.

This frequency enables to achieve a low level of the disturbing signal, as the most significant disturbing components are the fluctuations of the DC geomagnetic field component and the low-frequency band components below ~ 1 Hz, and also enables to minimize the effects of eddy currents (induced in the walls of the shielded chamber - Faraday cage) influence. The gradiometer sensor is placed close (~1 cm) to the surface of measured object. The spectral sensitivity of the measuring system (for the gradiometer pickup coil with the diameter of 2.8×10^{-2} m) is ~ 2×10^{-14} T $Hz^{-1/2}$.

Magnetometric measurement of MNP solution was performed with the same SQUID gradiometric system, by using different magnetization system and compensation coil [4].

Results

Studied Fe_3O_4 nanoparticles were prepared by microemulsion method at Polymer Institute of SAS by prof. Ignác Capek. These superparamagnetic Fe_3O_4 MNP were coated with citric acid and the mean hydrodynamic particle diameter was ~ 35 nm. From the magnetization measurement, fig. 1, the mass magnetic susceptibility was determined, which was later used to determine the concentration of this MNP in the organs of the tested animal.

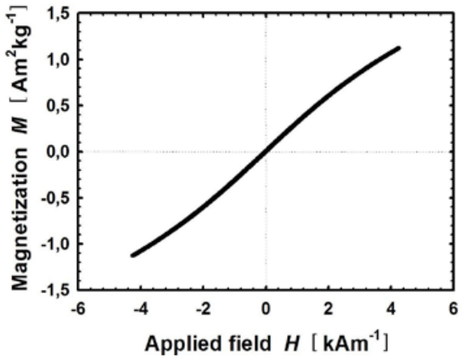

Fig. 1: Magnetization characteristics of the 35nm MNP solution.

Fig. 2 documents the measured values of the output signal U_{pp}, depending on the distance d of the cylindrical surface of the model, where c_F is the concentration of MNP in the water filled model.

i) From the characteristics is clear that the active area of the measured object is located near the surface.

The level of the magnetic signal decreases with a ratio of approximately $1/d^3$, so it can be assumed that the effective detection of MNP will be in ~ 5 cm depth. Sensing characteristic of the 2nd-order gradiometer is narrow, so effective detection field has a shape of cone with a base diameter of 5 cm and a height of 5 cm. On the other side, this narrow sensing characteristics allows better determining of different c_F in various locations of the measured object.

ii) Living biological tissue is diamagnetic and this is presented on figures with negative values of output signal U_{pp}. This means that at low values of c_F, the measured object still will appear as diamagnetic. Specifically, for our SBS and the object with used 35 nm MNP solution, the transition from paramagnetic to diamagnetic state is expected when the value of c_F is in the range 13 - 20 μg_{Fe3O4} cm^{-3}. Relationship U_{pp} and c_F is influenced mainly by contribution of diamagnetic biological tissues, which in terms of susceptibility appears to be water, paramagnetic MNP and also paramagnetic air layer between the sensor and the surface of the measured object.

Results of measurements of U_{pp} in experimental animal, which was injected to tail with 1 cm^3 solution of MNP and after 5 minutes measured, could be seen in fig. 3.

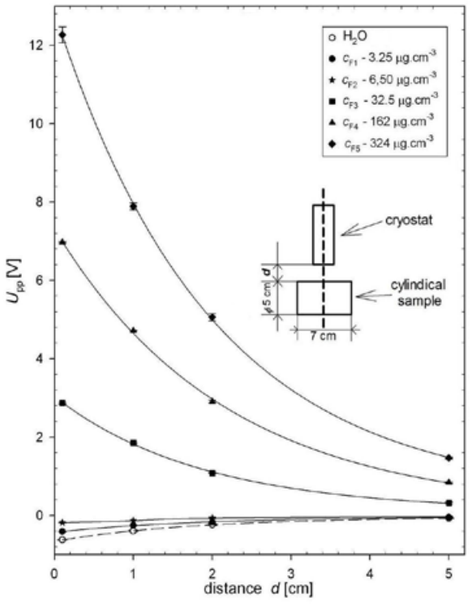

Fig. 2: Dependence of the measured signal U_{pp} on the distance d and the concentration c_F of MNP in the measured object.

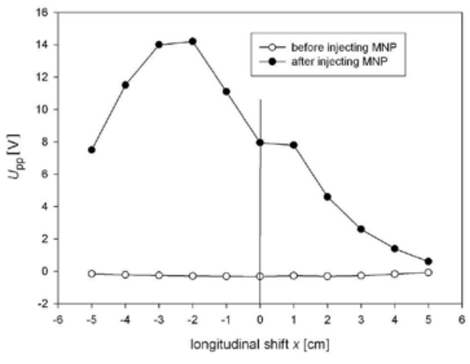

Fig. 3: The measured output signal U_{pp} of sleeping rat before and after injecting of MNP.

Measured U_{pp} values clearly show the difference between the magnetic response before and after injection of the MNP solution. Plotted values of U_{pp} correspond to c_F obtained during movement of the animal under the SQUID sensor along the torso (left part) and upper part of the tail (right side). From the measured values, the accumulation of MNP in the region of heart and liver could be assumed.

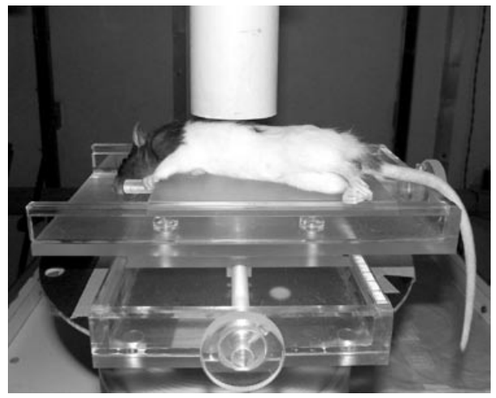

Fig. 4: Asleep rat placed on a movable acrylic bed under SBS.

Subsequently, the animals were sacrificed and selected organs were removed to be measured with the SBS. Obtained data were used to determine the magnetic susceptibility of tissues, or c_F of MNP in the tissue. From the results shown in fig. 5, MNP are mostly accumulated in the liver.

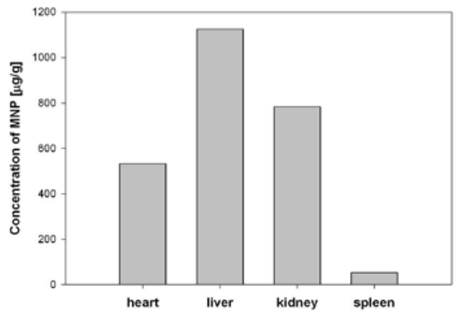

Fig. 5: c_F in organs of rat measured by SBS.

Conclusion

In the paper SBS and the method for measurement of magnetic response of Fe_3O_4 MNP to the AC magnetic field in the samples and also of injected MNP to tissues of the living animal are presented. Dependences between measured output signal, the concentration and distance of the sensor from magnetized MNP were obtained. Experimental measurements on living rat showed a possibility of using this method as an non-invasive method of identification and distribution determination of MNP in biological tissues of small animals. It can be assumed that by focusation of MNP with the external magnetic field, MNP could be accumulated in other areas of the animal body.

Acknowledgement

This work was supported by Agency of the Ministry of Education of the Slovak Republic for the Structural Funds of the EU, Operational Programme Research and Development (OPVaV-2009/4.1/02-SORO), Project Code 26240120019 (0.7) and by VEGA grant 2/0160/10.

References

[1] M. L. Tan, P. F. Choong, C. R. Dass: *Cancer, chitosan nanoparticles an catalytic nucleis acids*, J. Pharm. Pharmacol. , 2009, vol. 61, p. 3-12.

[2] M. Koneracká, P. Kopčanský, P. Sosa, J. Bageľová, M. Timko: *Interliposomal transfer of crystal violet dye from DPPC liposomes to magnetoliposomes*, Journal of Magnetism and Magnetic Materials, 2005, vol. 293, p. 271-276.

[3] M. Koneracká, P. Kopčanský, M. Timko, C. N. Ramchand: *Direct binding procedure of proteins and enzymes to fine magnetic particles*, Journal of Magnetism and Magnetic Materials, 2002, vol. 252, p. 409-411.

[4] V. Zrubec: *Improved system for measurement of the magnetization characteristics of the high-temperature superconductors by the compensation method in weak magnetic fields*, Review of scientific instruments, 2001, vol. 72, no. 6, p. 2653-2660

Mgr. Martin Škrátek, PhD.
Institute of Measurement Science
Slovak Academy of Sciences
Dúbravská cesta 9, SK-841 04 Bratislava

E-mail: martin.skratek@savba.sk
Phone: +421 259 104 528
Fax: +421 254 775 943

EXPORT OF INFORMATION FROM MEDICAL RECORDS INTO DATABASE

Liuba Grama [1]

[1]Czech Technical University in Prague, Prague, Czech Republic

Abstract

Automatic analysis of medical records can help to improve our understanding of all diseases, their development and treatment. Main problem with it is that most medical records nowadays are stored in a semi-structured text, which makes automatic classification and analysis more difficult. One of the possible approaches towards process simplification is to export all relevant data from semi-structured health records into a database. We propose to use semantics-oriented approach for this, as it provides relative freedom in portability. With this aim disease ontology is used for intermediate representation of the domain. Ontology can be modified and expanded at any moment to adjust the system for another disease or medical area. Our contribution describes an experiment run on a set of medical records, which have already been exported to a database manually, and compares the obtained results to estimate efficiency of the method.

Keywords

medical records, export, database

Introduction

In the biomedical domain the growth of electronic health records popularity raises the need for formal representation of information stored in medical records. Most of the available health records are stored in form of semi-structured text files, which is convenient for human perception, but causes problems with structuring, searching, classification, analysis and other automatic tasks concentrated on patients' data processing. It will also make it more difficult to apply different data mining techniques on this data, as most of techniques are designed to work with data stored in form of a table or a relational database and are not able to work with free-form text.

One of the possible approaches towards process simplification is to export all relevant data from semi-structured health records into a database automatically. This approach is rather challenging, because it is difficult to create a software that understands natural language in the same extent as humans. In general, current state of art suggests to start the process by extensive pre-processing of the input text using spell-checking, sentence splitting, tokenization, part-of-speech tagging in some cases. Medical records in most cases contain lots of abbreviations that should also be resolved during pre-processing stage. We will try to design a dedicated tool that will automate significant part of the export process for specific type of real life medical records – see Fig. 1 for a characteristic example. All over full automation of such a process is not yet achievable, because it requires preparation of knowledge domain model, database model and thesaurus with some manual adjustments, even the partial solution can bring value to the health records analysis.

Our intention is to use semantics-oriented approach to natural language analysis. The described method is based on semantics-oriented approach to natural language analysis proposed by Narinyani, 1980. In semantics-oriented approach the lexical units of the language are matched to certain semantic classes, which express meaning of the given lexical unit in the database. Semantic classes system and process of analysis are designed in such a way, that during analysis itself those combinations of semantic classes, which have meaning of the largest semantic structure, are distinguished. Semantic orientations make possible mutual precisions of the lexemes sense based on their context. For example, we meet in text phrase “aged 29”. Word “aged” will be referred to AGE semantic class. Determination of semantic class for “29” will not be straightforward, because digits met in text can refer to any of age, medicine dose, phone number, date, etc. Some certainly wrong orientations can be removed if constraints are applied (e.g. age can not be more than 100), but ambiguity will still be present. In this case context comes for help – nearest neighbor of “29” has semantic class AGE, and “29” among other classes has AGE class as well. This leads to conclusion that AGE is the most probable semantic orientation for “29”.

447995	dělnice, 29 let, rozvedená, druh Roman Hirtel 1966, bydlí s druhem RA: bezvýznamná OA: běžné dětské choroby, v 15 letech inf. mononukleóza 1999 - tularemie, 2000 vyřezena z evidence dispenzarizace s ničím se neléčí Léky v grav.: Paralen tbl. d.p., Alergie: 0 Transfuze: 0 Úrazy: ve 13 letech - fr. pravého zápěstí Operace: 1995 - cholecystektomie per LSK Abůzus: 0 GA: menses od 12 let, 35/7 pravidelné, občas bolestiví, antikocepce: neguje, záněty neguje, oeprace gyn. neguje	12	35	7	pravidelné	0	1	1	2003-03-30	2004-01-05

Fig. 1: Characteristic example of a medical record used in experiment

Method Description

Paper medical records are still most popular way of recording patient information for most medical institutes. In order to have complete patients' medical history in electronic form all existing paper records should be scanned and processed by some OCR software. Pure recognition system is not enough for this goal, as it would not effectively reduce efforts. This limitation occurs due to the fact that medical records usually follow different kinds of formats, so it is difficult to extract content using a uniform template.

A number of medical records scanning solutions have been developed lately. Among them can be named MedicScan, InfoMedix, FileScan, ExperVision, etc.

[1] provides a review of recent research and achievements in information extraction from medical records, it also mentions different approaches that were used in similar systems. They include pattern-matching, shallow and full syntactic parsing as well as semantic parsing, use of ontologies and sub-languages. Each approach has its own advantages and disadvantages (like lack of generalizability, non-robust performance, expensive prerequisites) and the particular choice should be made according to the pursued goals.

Our system is using semantics-oriented oriented approach to natural language analysis. According to it lexical semantics of words and phrases is represented by the so-called “orientation” [2], which is linked to a number of domain model concepts that could represent these words and phrases. In ambiguous cases the strongest orientation is selected.

Our method of data extraction from medical records will proceed in several phases: text processing, ontology mapping and database mapping. All these phases utilize specific structure of the textual documents we are considering.

The test processing stage is responsible for extracting meaningful entities from original text. Careful analysis of the 70 available medical records was done. It was noticed that each record has several distinct sections and it was decided first to divide each record. For example record shown in Fig. 1 will have 9 sections: RA, OA, Léky, Operace, Alergie, Transfuze, Úrazy, Abůzus, GA.

Each section is analyzed separately as they are not interconnected. Section consists of two parts – head and tail. Head will contain text before colon (or main notion if several words are there) - in most cases it will have direct link to some column in database tables.

Tail will contain rest of the section (text after the colon). It will be a list of several items in some cases. Comma is considered as a separator of the tail items.

Stop words should be removed from the tails. Each word in tail item should be brought to infinitive form (suppose that we can drop original form of the word off and insert in database only infinitive forms for a better

unification). Each abbreviation should be resolved to full form (or left as it is in some cases for unification).

Special treatment has to be applied to word negations. There is no general solution to this problem, yet. One possible approach can concentrate on those words that start with “ne-” that are not present in some list of words where “ne-” always goes with the word and doesn't have negative meaning. For these words, the “ne-” particle is removed and the negative flag applied to the word is changed to true. Negation treatment is left for a future direction for the moment, as it requires careful analysis.

The idea is to have at the end of text processing stage attribute/value pairs for each section, that can be easily mapped to ontology.

Ontology mapping. For the first experiments we used an ontology that was created manually to describe medical domain from the available records. Further applications of the system will be made using some existing disease ontologies (Mesh, Snomed, Disease Ontology, etc.). If existing ontologies do not fully describe the disease, or the area in question, custom ontology can be added. It is also expected that the tool will allow uploading some custom ontology by end-users. This will make it possible to use it for different other areas where transformation to formal representation may be needed.

Ontology mapping process by itself should be an easy one after text is properly processed. Each word should have one (or several in some cases) attributes from the ontology which allows straightforward mapping. In case several attributes can be applied to a single word, we are facing an ambiguous expression. Its main attribute is selected taking into account the current context represented by the context attributes. These attributes are analyzed and if some intersection appears with the ambiguous word, then it is resolved; otherwise statistical approach is used – most common attribute for this word within particular group of records is selected.

Database mapping. Database mapping is performed according to some database model, which will be elaborated for each database separately. Database model is created in strict correlation with ontology to reduce efforts on database mapping stage. Each column in database should have link with just one ontology attribute to prevent occurrenc ambiguity in this step.

It is planned to provide user with some tools for semi-automatic creation of database model in future. It will read database structure and create core model, which can be later broadened with additional fields and ontology links.

Usage of Ontologies

Ontologies are becoming more and popular way of representation of any domain semantics – concepts and entities in this domain, and their properties and relationships. This happens mostly due to ontologies' flexibility, which is particularly valuable nowadays, when information is constantly changing and growing. Ontologies can also join information from different domains, sources and create new relations based on this. It is very important that existing ontologies can be updated and extended with new knowledge very easily. This helps very much when several different domains are under research and they do not have common existing ontology.

Due to the limited Czech disease ontologies present, for initial experiments ontology was created manually. Fig. 2 represents main part of it. This ontology fully describes domain referenced in available medical records – information about diseases, medicines, other medical history and also general information, like concepts about age, gender, status, etc.

When creating the ontology we strictly followed structure and content of the available health records. That's why it contains 9 main classes – general_info, personal_disease_history, family_disease_history, medicine_history, surgery_history, allergy_history, transfusion_history, injury_history, abuse_history and gynecological_history. Each of these classes are further supplemented with detailed classification, additional properties and concepts.

Future experiment will be produced using Mesh-CZ ontology, as it seems to suitable for our goals. MeSH (Medical Subject Heading) thesaurus is a controlled vocabulary developed by the U.S. National Library of Medicine [3]. Current version of thesaurus includes concepts related to biomedical and health information that appear in MEDLINE/PubMed, NLM catalog database and other NLM databases. Czech translation of MeSH was done in 1977 by Czech National Medical Library, it is revised and updated periodically.

Results

Automated export of information from medical records brings value only if its result is reliable and precise. To prove effectiveness of the approach evaluation of the results is performed. We evaluated performance of the application using precision metric, which is a measure of the amount of true returned data compared to the amount of false exported data.

Due to the fact that all medical records, that were used in the experiment, were initially exported to the database manually, evaluation process was straightforward. We have compared fields from the two databases – one processed manually and another automatically, and counted number of miss-exports. Miss-exports were considered fields that were not matching. All the erroneous fields were selected and analyzed. A number of them was eventually considered as a correct export, since the error in automatically exported field consisted in different representation of the word. This gave us precision of 94% (2793 correct exports out of 2982 fields).

Our assumption is that errors were mainly made because of misspellings in original health records. For the moment some corrections were made manually. To avoid this in future we are planning to incorporate automatic spell-checking step in next experiments. Other possible source of errors could be lack of reliable context for some concepts, which led to mistakes in the process of ambiguity resolution.

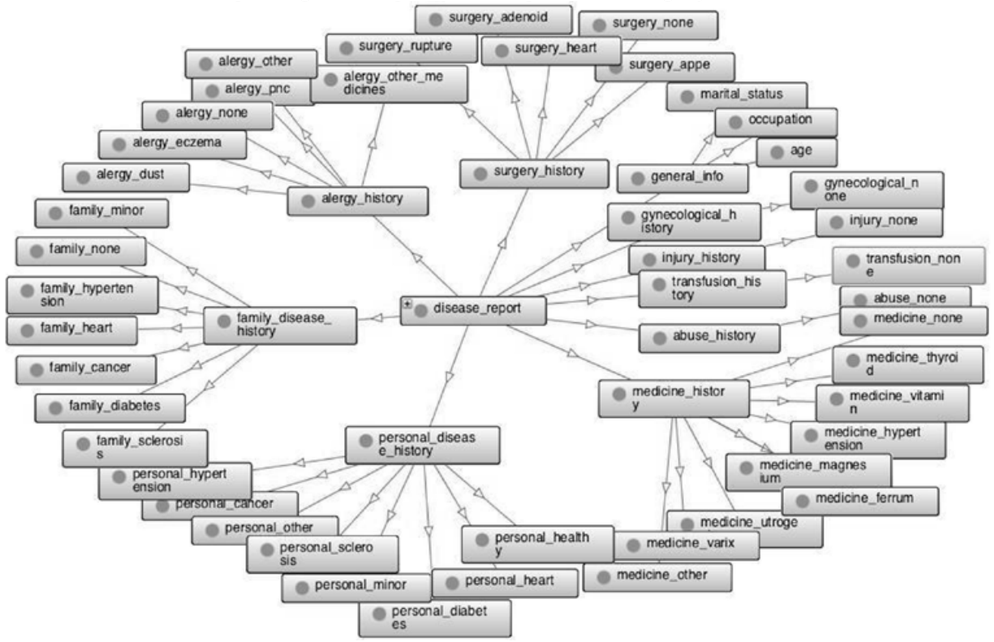

Fig. 2: Ontology used in the experiment

Conclusion

Export of data from a natural language source is a rigorous and complicated task, especially in biomedical domain. Medical text is harder to analyze, because it often contains multiple abbreviations, medical codes, latin concepts, etc. But the existence of a reliable automatic export tool would bring a lot of value to the domain, because its potential uses are numerous.

Our approach proved to be rather accurate with an ontology, restricted to the available medical records. We are planning to run a set of further experiments using general ontology, possibly sightly adjusted to meet our goal. It is expected that efficiency of the method will decrease during the first tests with a more general ontology. Results will be analyzed to define possible improvements in the method, and these improvements will be applied. Usage of restricted ontology still remains as an option for a reliable data export process, if general ontology causes vey low level of precision after all the improvements.

Acknowledgement

We thank BioDat Research Group for the provided database with the manually exported medical records and Prof. Olga Stepankova for her help in reviewing this paper.

References

[1] S.M. Meystre, G.K. Savova, K.C. Kipper-Schuler, J.F. Hurdle. *Extracting Information from Textual Documents in the Electronic Health Record: A Review of Recent Research*, 2008.

[2] M.A. Sasse, C.W. Johnson. *Human-computer Interaction, INTERACT '99*, 1999

[3] C.E. Lipscomb. *Medical Subject Headings (MeSH)*. Bull Med Libr Assoc. 2000 July; 88(3): 265–266

[4] M. Zakova, L. Novakova, O. Stepankova, T. Markova. *Ontologies in Annotation and Analysis of Medical Records*, 2008.

[5] D. Jurafsky, J.H. Martin. *Speech and Language Processing: An Introduction to Natural Language Processing, Computational Linguistics, and Speech Recognition*, Prentice-Hall, ISBN: 0-13-095069-6, 2000.

Liuba Grama, Mgr.
Department of Cybernetics
Faculty of Electrical Engineering
Czech Technical University in Prague
Karlovo nám. 13, CZ-121 35 Praha 2

E-mail: gramulka@gmail.com
Phone: +420 608 268 746

WIRELLES PROBE FOR HUMAN BODY BIOSIGNALS

Martin Daricek, Martin Jagelka, Lubomir Sladek, Frantisek Horinek, Peter Miklovic

Institute of Electronics and Photonics, Slovak University of Technology in Bratislava, Slovakia

Abstract

This paper describes in detail the multi-purpose device (probe) for wireless biosignal measurement. The proposed system uses two electrodes measurement of the potential and the measured data is sent in real time to user's computer for processing. It is possible to measure simultaneously at several places on the body, while single devices are time synchronized. At this time, designed system can measure two basic biosignals in the human body, EMG and ECG. There are also capabilities for EEG measurements, but it hasn't been implemented yet.

Keywords

Wireless biosignal probe, EMG, ECG

Introduction

There is a lot of existing equipment for measuring the biosignals. Most of them are not mobile enough to avoid affecting the measurement, particularly if investigated person is under physical load. This paper describes hardware of wireless bio-probe, which is part of our sensing network, dedicated to capture biosignals from human body using non-invasive application.

In general, EMG and ECG biosignal measurement includes electrical differential potential measurement captured from electrodes applied to skin of human body. There is also possibility of non-contact measurement, based on capacitive coupling, but in this case, we used contact method. EMG and ECG signals could by described as alternating voltage with bandwidth 1 to 300 Hz, with amplitude less than 10 mV. This range is also the strong source of interference, mainly due power line. This is the reason, why most of conventional systems use three electrode connection, where two of them are used for differential potential sensing and the last one serves as potential pre-bias and compensation for common mode interference rejection. We use only two electrodes, because there is no galvanic connection between different devices of the system and also electrodes are places very close to processing circuitry.

Description of device

This design is 4th device version, which was developed during last few years [1], [2], [3]. The entire device consists of several parts, including two main circuit boards (PCB), battery and casing with integrated electrodes (fig. 1). Casing is made from polyurethane and electrodes are made from aluminum coated by evaporated platinum.

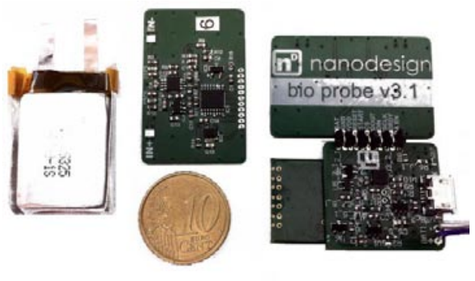

Fig. 1: Main parts of the device: battery (on the left), analog PCB (top side; on the middle) and configuration of digital and analog PCB with (analog from bottom side on top; on the right of the figure).

Power supply

The power supply is provided designed by integrated single cell Li-Po cell with a capacity of 120 mAh. Both, analog and digital PCBs are supplied from its own LDO and there is also separated ground. This is done due to proper insulation between sensitive analog circuitry and fast switched digital signals on digital PCB. Charging is handled by MCP73831T integrated circuit having a programmable charge current. Device can be charged from USB port or USB compatible wall/car charger. 250 mA charge current ensures full charge cycle in 30 minutes. Current consumption of the device is on average 20 mA, which designates up to 6 hours of working time. Each electronic component used in this device is able to operate from 2.7 V of supply voltage.

Analog circuitry

The analog frontend circuitry is essential for differential sensing of potential on the skin surface. Most signals in the human body are represented by low power differences between two points. We therefore designed a system whose block diagram is shown in Figure 2.

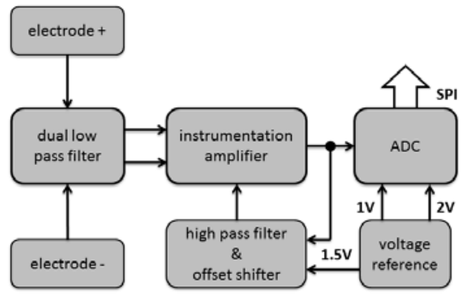

Fig. 2: Block diagram of analog frontend circuitry.

Low power signal, captured by two platinum electrodes, pass through the second order passive low pass filter to INA326, low noise, high precision instrumentation amplifier. The corner frequency of the low pass filter, which helps to suppress ineligible interference, is set to 1 kHz. To ensure correct function of instrumentation amplifier, both electrodes are through high impedance resistor pre-biased to virtual ground voltage level, because there is no third electrode, which usually provides this function.

Due to supply voltage is set to 3 V, reference or virtual ground voltage is set to 1.5 V. Input instrumentation amplifier is supplemented by high pass filter, which is used to eliminate offsets, thermal floating and other DC instabilities. The filter is designed as non-pass filter, which means that output signal does not pass through this filter, to avoid any additional distortion, but it is placed in INA326 reference bias circuit. Instrumentation amplifier gain is 10, which is set by external components.

The next signal processing provides analog to digital converter (ADC) represented by ADS1246, highly integrated and accurate 24-bit ΔΣ ADC. It has a low noise built-in programmable amplifier, internal oscillator and adjustable digital filter with differential input. Programmable amplifier is a low noise and low drift with adjustable amplification in range 1 to 128 in 8 steps. ADC input range is given by/between two reference voltage levels (1 V and 2 V). The frequency modulator can be varied from its value, then the sampling frequency is derived (Table 2). There is also integrated low pass digital FIR filter, whose cut-off frequency is given by actual sample rate, which can be set from 5 to 2000 SPS in 10 steps. For rates lower than 160 SPS filter is automatically configured to additionally suppress 50 Hz component from filtered spectra [4]. Two differential inputs of ADC are connected to instrumentation amplifier output signal and to 1.5 V virtual ground reference voltage.

We used integrated shunt reference IC to produce all three desired reference voltages. Class B of LM4040, provides high stability and accuracy of 2V voltage. All nets using any of reference voltages are high impedance types, so we were allowed to place an resistor divider as 1.5 and 1 V voltage sources.

Digital part

The core of the digital PCB is JN5148, 32-bit RISC microcontroller (MCU, 128 kB RAM, 4 MB FLASH), which includes digital radio transceiver working in ISM band (2.4 GHz) based on IEEE 802.15.4 standard. Standard ZigBee Pro network or Jennet type network can be used to set wireless system [5].

The probe is equipped with 14-bit digital accelerometer, which is used for motion sensing and for power management. There is no mechanical component used for switching the device on and off, therefore if there is any motion noticed, accelerometer will generate digital wake signal for MCU. Device is powered off, if there is no motion for defined time period. Accelerometer communicates with MCU through onboard TWI interface, while SPI interface is used for capturing data from ADC. RGB LED, driven by three PWM channels, is used as state indicator (fig. 4).

Up to 16 probes can be connected in wireless sensor network, which consists from USB dongle device, serves as network coordinator, and described probe devices, which are network slaves. All network devices are synchronized in time [6]. Data flow through USB interface to users PC, used for signal processing, storage, visualization and for measurement parameters set up.

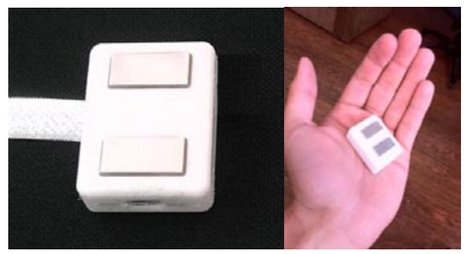

Fig. 3: Encased probe device.

Experimental results

To optimize the sensor smart system were carried out several experiments. This chapter lists only some of the recent experiments, proving system abilities. We used professional biomedical laboratory equipment (AD Instruments PowerLAB) for comparison. Experimental setup was installed (fig. 4) to capture the same EMG/ECG signals simultaneously by two independent sensing systems. While electrodes during AD Instruments ECG measurement were in Einthoven triangle configuration, wireless bio-probe was placed right under left breast with horizontally oriented electrodes. ECG measurement Figures 5 and 6, showing raw data, demonstrate a higher signal quality, greater stability, lower noise and greater suppression of undesirable artifacts in case of our wireless probe system (EMG_{MED}). Moreover there is no need of using conductivity gel. Another great advantage is that it provides a portable monitoring system, so exanimated person is not delimited by wiring.

Fig. 4: Encased device (top) and experimental setup (bottom).

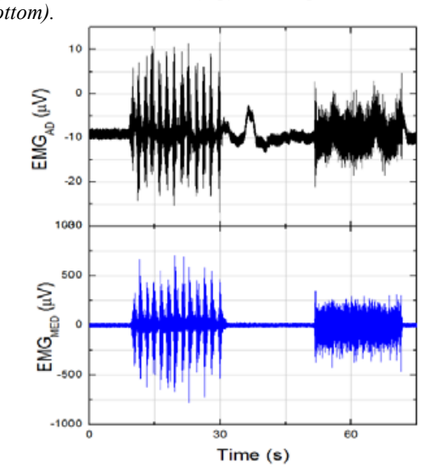

Fig. 5: Measured EMG signals used for sensor system verification.

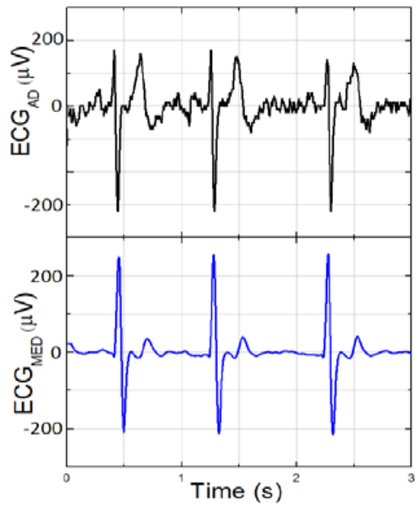

Fig. 6: Measured ECG signals used for sensor system verification.

The second experiment provides brief investigation of dependence between the amplitude of the EMG signal and the force exerted by EMG = f (F) (fig. 6). The results achieved by smart sensor system prove theoretical model, which suggest that the dependence should have a logarithmic shape. Most of the measurements, made by other research groups, result in linear dependence.

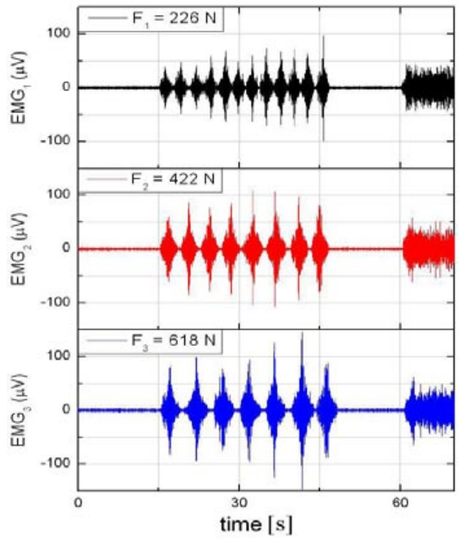

Fig. 7: Experimental data focused to muscle force investigation.

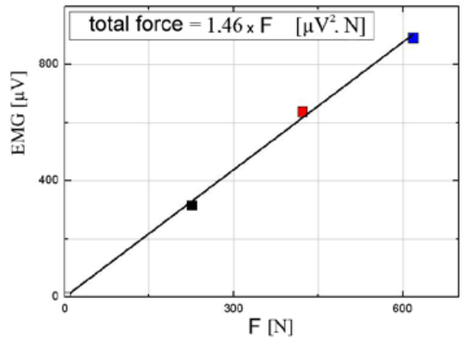

Fig. 8: Dependence between muscle force and total power of captured EMG signal.

Conclusion

Experimental results indicate high level usefulness for medicine and sport researches [7]. In the next version of the device, we will implement possibility of conductive measurements. Also PCB design will be optimized using a custom analog design of the radio antenna and the using physically smaller battery. Waterproof construction will be used, which needs implementation of wireless battery charging method. Using the proposed diagnostic system in practice is also strongly supported through the daily use of smart-phones with Android or iOS high computing power and functionality that will be compatible with next version of the sensor system.

Acknowledgement

This work was supported by NanoDesign, Ltd. company and the Slovak Research and Development Agency under the contract No. VMSP-II-0016-09 and by Competence Center for SMART Technologies for Electronics and Informatics Systems and Services, ITMS 26240220072, funded by the Research & Development Operational Programme from the ERDF. Also Slovak Grant Agency supported this work though grant no. 1/1177/12

References

[1] Rendek, K. - Daříček, M. - Vavrinský, E. - Donoval, M. - Donoval, D.: Biomedical signal amplifier for EMG wireless sensor system. In: ASDAM 2010. The Eighth International Conference on Advanced Semiconductor Devices and Microsystems. Smolenice, 25 - 27 October 2010. - Piscataway : Institute of Electrical and Electronics Engineers, 2010. - ISBN 978-1-4244-8572-7

[2] Vavrinský, E. - Rendek, K. - Daříček, M. - Donoval, M. - Horínek, F. - Horniak, M. - Donoval, D.: Electrode configuration for EMG measurements. In: ASDAM 2010. The Eighth International Conference on Advanced Semiconductor Devices and Microsystems. Smolenice, 25 - 27 October 2010. - Piscataway : Institute of Electrical and Electronics Engineers, 2010. - ISBN 978-1-4244-8572-7

[3] Vavrinský, E. - Daříček, M. - Donoval, M. - Rendek, K. - Horínek, F. - Horniak, M. - Donoval, D.: Design of EMG Wireless Sensor System. In: Applied Electronics 2011 : International Conference on Applied Electronics. Pilsen, 7-8 September 2011. - Pilsen : University of West Bohemia, 2011. - ISBN 978-80-7043-987-6. - S. 401-404

[4] ADS1246/47/48 datasheet, http://www.ti.com/lit/ds/symlink/ads1246.pdf

[5] JN5148-001-Myy datasheet, http://www.jennic.com/files/product_briefs/JN-DS-JN5148MO-1v4.pdf

[6] Daříček, M., „Synchronization Methods for Wireless Bio-sensing Network“, Proceeding of 22nd International Conference Radioelektronika 2012, Brno, pp. 157-160, ISBN 978-80-214-4468-3

[7] Vavrinský, E., Praktický monitoring biopotenciálov pomocou nízkošumového bezdrôtového senzora, Transfer, 1, 2012, str. 16-17, ISSN 1337-9747

Martin Daříček, Ph.D.
Institute of Electronics and Photonics
Faculty of Electrical Engineering and Information Technology
Slovak Technical University in Bratislava
Ilkovičova 3, SK-812 19 Bratislava

E-mail: martin.daricek@stuba.sk
Phone: +421 903 744 442

WRITTEN TESTS ON BIOPHYSICS AND MEDICAL BIOPHYSICS AT MEDICAL FACULTY, COMENIUS UNIVERSITY IN BRATISLAVA – A CONTINUOUS CHECK DURING TWO ACADEMIC YEARS

Katarína Kozlíková[1], Renáta Knezović[2]

[1]Institute of Medical Physics, Biophysics, Informatics and Telemedicine,

Faculty of Medicine, Comenius University in Bratislava, Bratislava, Slovak Republic

[2]Institute of Social Medicine and Medical Ethics,

Faculty of Medicine, Comenius University in Bratislava, Bratislava, Slovak Republic

Abstract

Written tests on Biophysics and Medical Biophysics devoted to physical units and to measurement and statistical evaluation of data were written in the winter term of the first study year with students studying in English language in two study programmes at Medical Faculty. The aim of this study is to analyse these tests, set an appropriate threshold for passing the test and propose how to improve the students' knowledge. Altogether 535 tests were written with the average result (66 ± 7) % of correct answers. Students of General Medicine (410 tests; (66 ± 6) %) achieved better results than those of Dentistry (125 tests; (64 ± 8) %, $p < 0.05$). Tests on statistics - lectured topics (272 tests; (68 ± 7) %) ended better than tests on units - individually studied (263 tests; (64 ± 6) %, $p < 0.05$). From the obtained results we can conclude that an appropriate threshold for passing the test could be set at different levels according to the way of evaluation and whether the questions are published in advance or not (ranging from 60 % to 75 %). Tests involving lectured topics ended better than those involving mainly secondary school knowledge. Therefore, more training of physical units and data evaluation during practical classes is needed as well as better supplementation with study literature. The overall success of the tests as well as the students' knowledge could be improved by the prepared lectures in electronic form as well as by introducing an entrance examination on Physics and/or preparatory courses as are done on Biology and Chemistry at our faculty.

Keywords

written test, biophysics, physical units, measurement, statistical evaluation, e-learning

Introduction

Biophysics and Medical Biophysics are compulsory courses integrated in the study programme of General Medicine and of Dentistry, respectively, at Faculty of Medicine, in the first semester. Biophysics is taught in form of 42 hours of lectures and 36 hours of practical training and Medical Biophysics in form of 28 hours of lectures and 24 hours of practical training. Both courses end with an examination.

To support critical scientific thinking of students, an important part of the content of these courses is devoted to the measurement of physical quantities in medicine, evaluation of the measurement results and basic statistical methods in medicine. The measurement of the physical quantities as well as the evaluation of the results is connected with the utilisation of correct physical units according to the International System of Units that was established in 1960 and is based on seven base units and the convenience of the number ten [1].

As both, the physical units and the statistical and numerical evaluation represent serious problems for all students, but especially those from foreign countries studying medicine in English language, we have introduced a current check in form of written tests to help the students to evaluate their knowledge continuously.

The aim of this paper is to analyse these tests, set an appropriate threshold for passing the test and propose how to improve the students' knowledge.

Methods

Each written test consisted of twenty questions with multiple choices. Any of the four answers could be correct or incorrect. Every partial answer was evaluated and to pass, the student has to reach 75 % of correct answers. The same tests were used in the academic years 2010/11 and 2011/12 for both courses and were written with students studying in English language only. Neither the questions nor the answers were disclosed to the students in advance. All students participated in the tests optionally.

In the test concerning basic terminology of physics and physical units ("units"), ten questions dealt with terminology of units (which units are basic, derived and secondary) and their assignment to corresponding quantities. The students had to express a derived unit in form of basic SI units in two questions. Four questions were devoted to unit conversion. The last four questions dealt with basic operations of vector calculus (addition, subtraction, scalar and vector product).

The test on medical statistics and measurement evaluation ("statistics") involved five questions concerning basic statistical terminology (population, sample, experiment, observation, sorting and classes). Graphs (polygon, histogram), probability in the normal (Gaussian) distribution and prediction of values (linear regression) were evaluated per one question. Six questions dealt with basic sample characteristics of location and variability, four questions dealt with measurement errors and their propagation. The last two questions were devoted to significant figures and correct rounding off of the result. If any calculation in any question was involved, this was available in the answers of both tests except for multiplication or division by multiples of ten.

Students were informed about the topics of the test at least three weeks in advance. As the topic of the first test comprised mainly repetition from the secondary school, they had to study by themselves. Tables of units were available in more recommended textbooks, for example [2; 3], as well as on the internet, for example [1]. The topic of the second test was lectured, repeated at practical classes and is available in their textbook [2]. After evaluating the tests by the teacher, the students were informed about the results and each question and answer was explained. The test results were announced anonymously, using code numbers identifiable only by individual students.

Results

During the two academic years, altogether 535 test were written with the average result (66 ± 7) % of correct answers, ranging from 46 to 84. The results of the test for both study programmes are summarised in Table 1. N is the number of students writing the test. The test results are expressed as percentage of correct partial answers in form of averages and standard deviations. The range of correct answers is given in the parentheses.

Tab. 1: Test results of all tests for both study programmes.

Test	N	Average ± SD (range) [%]
General Medicine – Biophysics		
Units 2010/11	48	65 ± 6 (54; 79)
Units 2011/12	152	64 ± 6 (51; 81)
Units total	200	65 ± 6 (51; 81)
Statistics 2010/11	58	66 ± 7 (48; 80)
Statistics 2011/12	152	69 ± 6 (54; 84)
Statistics total	210	68 ± 6 (48; 84)
Dentistry - Medical Biophysics		
Units 2011/12	17	64 ± 6 (55; 78)
Units 2011/12	46	59 ± 6 (46; 68)
Units total	63	60 ± 6 (46; 78)
Statistics 2010/11	16	62 ± 7 (53; 71)
Statistics 2011/12	46	69 ± 8 (53; 83)
Statistics total	62	67 ± 8 (53; 83)

The overall test results were statistically significantly better for General Medicine than for Dentistry (GM: 410 tests (66 ± 6) %; D: 125 tests (64 ± 8) %; $p < 0.05$) and better for the statistics than for the units (statistics: 272 test (68 ± 7) %; units: 263 tests (64 ± 6) %; $p < 0.05$). The test results were slightly but not significantly better in the academic year 2011/12 than in 2010/11 (2011/12: 396 test (66 ± 7) %; 2010/11: 139 tests (65 ± 7) %). None of the questions in any test was answered correctly to 100 % (at most 93 %, two questions). Any of the partial answers was correct neither to 100 % nor to 0 %.

We were also interested in four questions, which were answered correctly in less than 50 %. In the "units" test, this concerned the conversion of volume given in cubic decimetres to litres and its multiples

(42 %) as well as properties of vector product of two vectors (47 %) that is applied, for example, in the definition of the Lorentz force. In the “statistics” test, this concerned the properties of population (38 %) and identification of ordinal data from given examples (47 %). For all other questions, at least 50 % of correct answers were given.

Discussion

According to the test results, the average value of correct answers around two thirds with the maxima slightly exceeding 80 % is relatively low. This may be caused by more reasons. The first one could be the fact, that the English language is not the mother language of the students except for 2 – 3 % of them. The second reason could be caused by decreased number of hours or even no Physics (and no Mathematics) in the secondary schools. The third and probably the most important reason is the fact that the entrance examination to the Faculty of Medicine, Comenius University in Bratislava, involves only Biology and Chemistry. Therefore, many students pay no attention to Physics at all. This could be supported by better results from statistics test (lectured and trained at the university) compared to the units test based mainly on the secondary school knowledge.

From the other side, the worst test results for partial answers were close to 50 %, what can be regarded positively, although some ”random” correct answers cannot be excluded. The distribution of the count of correct answers in each test approached the normal distribution according to the normality test based on skewness and kurtosis [4]. Therefore, we can assume that the test questions were chosen with appropriate difficulty.

It is worth mentioning that similar analysis was done several years ago for tests at final biophysical examination [5]. Eleven tests comprising all topics on Biophysics involved in 275 different questions and written in average by twenty six Slovak students were analysed. Almost 37 % of the questions were answered correctly in less than 50 % although the students knew the questions with correct answers at least one month in advance. Over six hundred questions with six possible answers were available. It is possible, that knowing the questions with answers in advance led to underestimation of the preparation for the exam.

The analysis of the continuous tests followed by the explanation of the problematic questions is very helpful for the teacher as well as for the students. In any case, it improves the interaction and communication between them and offers better feedback to the teacher. From the other side, it can help students to complete and update their knowledge and to motivate them to achieve better results. From the results of our tests follows that more training of physical units and data evaluation during practical classes is needed as well as better supplementation with study literature.

For lack of identical or at least comparable study literature in both Slovak and English language, in which the courses are given, the students had to study either from the given lectures or from several textbooks predominantly in English language (mainly foreigners) or in Czech language (mainly Slovaks). Unfortunately, almost all of them are in a summarising (encyclopaedic) form without explanation and neither textbook covers the whole content of the course. To avoid this drawback, we have prepared parts of the courses in electronic form (e-learning), supported by the project KEGA 004UK-4/2011. The first lectures are nowadays available at the MEFANET Portal of the FM CU in Slovak as well as in English language with identical content (http://portal.fmed.uniba.sk/).

What concerns the test evaluation, we have to consider that almost all students of medicine, regardless which study programme, have in general more difficulties with Physics and Mathematics that students of universities oriented toward sciences or engineering. From the obtained results we can conclude that an appropriate threshold for passing the test could be set at 60 % to 66 % if each question involves four partial answers that are separately evaluated. The level 75 % can be acceptable only if the test questions (without answers) are known in advance [6]. We assume that open question would lead to worse results [7].

Conclusion

From the obtained results we can conclude that an appropriate threshold for passing the test could be set at different levels according to the way of evaluation and publishing the questions. Tests involving lectured topics ended better than those involving mainly secondary school knowledge, although repeated. Therefore, more training of physical units and data evaluation during practical classes is needed as well as better supplementation with study literature. The overall success of the tests as well as the students' knowledge could be improved by the prepared lectures as well as by introducing an entrance examination on Physics and/or preparatory courses similar to those that are done on Biology and Chemistry at our faculty.

Acknowledgement

The work has been supported by grant KEGA No. 004UK-4/2011 of the Ministry of Education, Science, Research and Sport of the Slovak Republic.

References

[1] International System of Units. [Cit. 2012-05-10] Available at: http://en.wikipedia.org/wiki/International_System_of_Units.
[2] Kozlíková, K., Martinka, J. *Theory And Tasks For Practicals On Medical Biophysics.* Brno : Librix, 2010. 248 pp. ISBN 978-80-7399-881-3
[3] Rontó G., Tarján I. (Eds.) *An Introduction to Biophysics with Medical Orientation.* Budapest : Akadémiai Kiadó, 1999. 447 pp. ISBN 963-05-7607-4
[4] Kozlíková, K., Martinka, J. *Základy spracovania biomedicínskych meraní II.* Bratislava : Asklepios, 2009. 204 pp. ISBN 978-80-7167-137-4
[5] Kozlíková, K., Kráľová, E. *Písomné testy na skúške z biofyziky.* Plzeňský lékařský sborník. 2001, vol. 67, p. 15-17.
[6] Study Regulations, Faculty of Medicine, Comenius University in Bratislava. Internal provision No. 5/2008 [Cit. 2012-05-10] Available at: http://www.fmed.uniba.sk/index.php?id=3928.
[7] Burjan, V.: *Tvorba a využívanie školských testov (5.).* EXAM-Info 2003, vol. 5, p. 8-117

Katarína Kozlíková, Assoc. Prof., RN, Ph.D.
Institute of Medical Physics, Biophysics, Informatics and Telemedicine,
Faculty of Medicine,
Comenius University in Bratislava,
Sasinkova 2, SK 813 72 Bratislava, SR

E-mail: katarina.kozlikova@fmed.uniba.sk
Phone: +421 2 593 57 533

VALUATION METHODOLOGY FOR MEDICAL DEVICES

Šárka Čížková[1], Zuzana Heinzová[1], Vladimír Rogalewicz[1]

[1]CzechHTA, Faculty of Biomedical Engineering, Czech Technical University in Prague, Czech Republic

Abstract

No medical devices valuation methodology has been published in the Czech Republic yet. Such a methodology is important for valuation in the case of public procurements, auctions, sales or purchases of used equipment, valuation of assets for accounting purposes, e.g. in the case of gifts, etc. The Property Valuation Act defines valuation methods to be used in determining the normal value of items. In the case of medical devices, the cost method and the comparison method seem to be suitable movable property valuation methods. A detailed description and examples of calculations for selected mechanical ventilators are provided.

Keywords

Property valuation, movable property, cost valuation method, comparative valuation method

Valuation of medical devices

Situations when it is necessary to appraise medical equipment are quite frequent. A valuation is required in the case of public procurements, auctions, sales or purchases of used equipment (which is connected with a possible opening of the commodity market), valuation of assets for accounting purposes, e.g. in the case of gifts, etc. Valuation methods are well developed and described for industrial property. In the Czech Republic, the basic norm is the Property Valuation Act No. 151/1991 Coll., where valuation methods are defined and explained. A detailed description of appraisal can be found in [1, 7, 8]. Valuation of medical devices will follow the same patterns as in the case of any other equipment; however, there will be some specifics due to a special character of the medical devices market. Out of the valuation methods, the cost method and the comparison method will be most useful for medical devices valuation. It is still questionable, whether the yield method can be used as well. It expresses the ability of the device to create yield. As renting medical equipment is not a common business and it is very difficult to find a company that would do it, the yield method seems rather impractical, despite of the fact that renting is possible in the case of a host of devices, such as ultrasonic devices. Hence, the cost method and the comparison method applied for medical technology are studied in this paper.

The cost method

The cost method is based on a conversion of costs incurred to acquire the item, and/or from statistical data concerning transactions realized. The aim is to determine the reproduction cost, subsequently reduced by the wear and tear, i.e. by depreciations[1]. The calculation follows the formula:

$$OC = \frac{\frac{PC * C * \Pi K * VTH * (100 - ZA) * (100 \mp PS)}{10^4}}{100} * Kp, \qquad (1)$$

where OC is the general price, called also the usual price, which the device could be bought or sold for in an open market in the given time and place; PC is the purchase price, i.e. the price, which the device was purchased for; C is the resulting price index of the machine class (according to formerly valid Decree No. 586/1990 Coll. on depreciation of fixed assets); ΠK is the product of price indices according to the Czech Statistical Office; VTH is the technical default value (the technical value of the machine over the value of a new factory produced machine); ZA is basic amortization; PS is a margin or deduction (correcting the amortized value); Kp the sale rate coefficient (a price coefficient corresponding to the supply and/or demand of the device in the market in a given place and time).

[1] Decrease in value (price) of the item depending on the age, technical state, and other factors. [1]

Fig. 1: Exponential depreciation - the choice of parameters P [5]

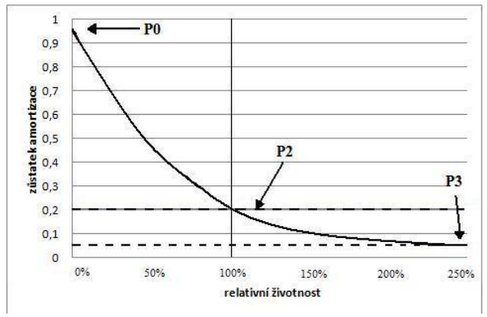

The values of individual variables are primarily obtained during a personal inspection, from information provided by the client, from data on past transactions, from other expert opinions, and/or one´s own expertise and knowledge of the market. Most problematic part of the formula (1) is a suitable choice of the calculation of depreciations. There are more methods and models representing the wear and tear. In this paper, we present 3 basic types – linear, tabular, and exponential – that can give a clear image of the function shape over the entire length of the device lifetime. The linear model assumes a uniform reduction in useful life expectancy up to a 10% limit of the original value. The tabular amortization is based on 5 basic waveforms and scales, divided by the assumed age of the machine of 5, 10, 15, 20 and/or 25 years. It is governed by several rules, for example by a faster decline in value in the first years, a milder decline to about 10-30 % of the equipment technical value[2] reflecting the age and normal wear and tear under good maintenance; the 10% value of the machine is generally considered as a limit, and a machine in operation should not breach this limit. The exponential depreciation is a non-linear method that relatively truly simulates wear and tear in relation to the age and the lifespan. The main difference from the tabular and linear methods is a more accurate determination of values in 3 areas that are shown in Fig. 1.

[2] The technical value is the device´s technical life expectancy at the date of evaluation, in comparison with a completely new device and its expected lifetime.

Fig. 2: Amortization: linear, tabular, exponential

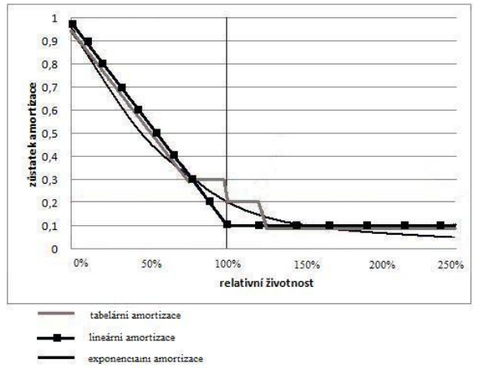

As shown in Fig. 2, the amortization is most problematic in the range of 70-130 % of the lifespan. Values from this range affect the final price of the valuated device so much that the final general price can vary by tens of percent. Hence, the appraiser must select a proper model of amortization. We show the effect of the model chosen to the final valuation in Tab. 1.

Tab. 1: General prices and representation depending on the choice of depreciation model

	linear depreciation	tabular depreciation
Basic amortization (ZA)	0.26	0.6
=1-ZA	0.74	0.4
Conversion of the depreciation	**185 037**	**274 129**
Time price	137 905	229 841
General price	**436 698**	**344 761**

We have experimentally applied the calculation of the general price to artificial ventilation devices. The data were taken from data bases of public tenders for deliveries to various medical facilities in the Czech Republic over the past 5 years. We want to find out the price of an item, whose purchase price was

CZK 685 322, whose age at the date of calculation is three years, and the life expectancy is 10 years. The results are shown in Tab. 1. The actual difference between the two resulting general prices is more than CZK 90 000, which is really a considerable price range comparing with the purchase price level.

The comparative method

The comparative (comparison, or comparable) method is based on the comparison and evaluation of certain parameters of devices that have the same or similar character. An important role is played by the method of paired comparisons and regression index of usability, published in [11]. The method is a combination of the multi-criteria decision analysis and the regression analysis. An important part of the method is the selection of suitable devices and their parameters or criteria to be considered. After the selection is finished, and criteria have been transferred maximization or minimization ones, we can proceed to assigning weights to individual items. This assigning is carried out only by experts in the field, who can rely on methods used in decision-making processes (regression analysis, the Saaty matrix), or on the basis of their own opinion. After that the definition of variables follows, and then paired comparisons of individual devices with the evaluated device. As a result we get indices of utilities of individual compared devices; consequently we perform a regression analysis. As a result we get a function, and we appoint the evaluated device into it. Hence, we have compared parameters of the device with themselves, the result being default price of the machine.

Conclusion

The paper presents partial results of a project investigating valuation of medical devices. However the methods mentioned are based on general valuation principles, medical devices require more care and some special considerations. The results find immediate application in expert analyses of medical technology purchases.

Acknowledgement

The work has been supported by a grant of Ministry of Health Services of the Czech Republic No. NT11532-5/2010 “Health Technology Assessment”.

References

[1] Bradáč, A., Kledus, M., Krejčíř, P. et al.. Introduction to witness expertize [Úvod do soudního znalectví]. (In Czech.) Brno: Akademické nakladatelství CERM, 2004, 220 pp.
[2] Bradáč, A., Kledus, M., Krejčíř, P. et al. Witness expertize. [Soudní znalectví.] (In Czech.) Brno: Akademické nakladatelství CERM, 2010, 242 pp.
[3] Dohányos, Michal. Movable assets valuation – a practical view. [Oceňování movitého majetku - pohled z praxe.] (In Czech.) Odhadce a oceňování majetku, 2007, No. 3-4.
[4] Dohányos, M. New aproaches to movable assets valuation. [Nové přístupy oceňování movitého majetku.] (In Czech.) Odhadce a oceňování majetku, 2008, No. 3-4.
[5] Dohányos, M. Public lecture, Movable assets valuation. [Oceňování movitého majetku.] (In Czech.), Praha, 2009.
[6] Drozen, F. Price – value – model. [Cena – hodnota – model.] (In Czech.) Praha: Oeconomica, 2003, 126 pp.
[7] Knoflíček, R. Methodical handbook: Valuation of machines and machinery for the purpose of Technological expertize. [Metodická pomůcka: Oceňování strojů a strojního zařízení pro účely Technického znalectví.] (In Czech.) 2nd revised ed.. Brno: VÚT, 1997.
[8] Makovec, J. Valuation of machines and production equipment. [Oceňování strojů a výrobních zařízení.] (In Czech.) Praha: Oeconomica 2007. 92 pp.
[9] Mařík, M. Standards of value – a formal issue? [Standardy hodnoty – formální záležitost?] (In Czech.) Odhadce a oceňování majetku, 2006, No. 4., p.5-14.
[10] Němeček, Alojz. Determination of the initial price of a device. [Určení výchozí ceny stroje.] (In Czech.) Odhadce a oceňování majetku, 2007, No. 2.
[11] Němeček, A., Janata, J. Property valuation for the insurance industry. [Oceňování majetku v pojišťovnictví.] (In Czech.) Český Těšín: C.H.Beck, 2010.

Bc. Šárka Čížková
Ing. Zuzana Heinzová
Katedra biomedicínské techniky
Fakulta biomedicínského inženýrství
České vysoké učení technické v Praze
nám. Sítná 3105, CZ-272 01 Kladno

E-mail: sarka.cizkova@fbmi.cvut.cz

SETTING EMG STIMULATION PARAMETERS BY MICROCONTROLLER MSP430

Martin Nováček, Peter Fuchs, Daniela Ďuračková, Elena Cocherová

Slovak University of Technology, Bratislava, Slovak Republic

Abstract
This article deals with basic techniques of neurophysiologic monitoring and stimulation. The described practices are used in medical diagnosis, surgery and treatment. Different devices with many functions and properties are used in stimulation. A system for electromyographic monitoring (EMG) and stimulation is proposed. The stimulating part of the prepared device described in this article is based on signal processing using an MSP430 microcontroller. This should certainly prove to be beneficial for future use, in a similar manner to the benefits bestowed by some current parts of modern, smaller and cheaper medical devices related to EMG.

Keywords
EMG, stimulation, monitoring, PWM, microcontroller

Introduction

Modern medical practice is based on high-tech technology utilization. To this end, the most modern technology is required to ensure continued progress in the development of medical devices. Many forms of bio-electric phenomena can be recorded with relative ease. These include measurement, stimulation and recording such as in the neurophysiologic intra-operative monitoring (NIOM) used in medical monitoring, treatment and surgery.

Techniques based on monitoring include: electromyography (EMG), somato-sensory evoked potentials (SEPs), motor evoked potentials (MEPs), brainstem auditory evoked potentials (BAEPs), electroencephalography (EEG), electrocardiography (ECG) and electroneurography (ENG). Electrical stimulation is required to record some of these signals, with the stimulating and recording device parameters dependent on the expected frequency range and signal intensity [1]-[4] (Tab. 1,Tab. 2).

This paper proposes a system for stimulation and EMG signal recording based on the MSP430 microcontroller, which is currently one of the most advanced, fastest, ultra-low-power and most compact processors.

The first two sections of this article discuss medical measurement techniques for selected bioelectric phenomena, and the design of the proposed system is then described

Intra-operative electromyography

Intra-operative electromyography (EMG) provides useful diagnostic and prognostic information in spinal and peripheral nerve surgery [1]. Basic techniques include free-running EMG, stimulus-triggered EMG and intra-operative nerve conduction studies. These techniques can be used to monitor the following; (1) nerve roots during spinal surgery; (2) the facial nerve during cerebellopontine angle surgery and (3) peripheral nerves during brachial plexus exploration and repair. However, there are a number of technical limitations which can cause false-positive or false-negative results, and these must be recognized and avoided wherever possible [2].

EMG can be monitored in any muscle accessible to a needle, wire, or surface electrode, so that mechanical irritation of peripheral nerves or nerve roots results in muscle activity in the corresponding musculature.

Tab. 1: EMG recording parameters [2]

	Filters (Hz)	Filters (Hz)	Typical amplitude (μV)	Typical latency (ms)
	Low Freq.	High Freq.	Low-High	Low-High
Free-running EMG	10	2000–5000	20–1000	n/a
MEPs	10-40	2000–5000	25–2000	15–75

Tab. 2: EMG stimulation parameters [2]

	Stimulation intensity	Stimulation duration (ms)	Stimulation rate (Hz)
	Low- High	Low- High	Low- High
SEP– median cortical nerve	20 mA-35 mA	0.2–0.5	1.3–4.7
Motor evoked potentials	200 V–1000 V	0.05–1	n/a

MEPs Techniques

Recording and Stimulation

Trans-cranial stimulation activates spinal cord motor fibers. It is important to localize motor tract deficits by choosing appropriate muscles to record. The most convenient recording is performed from at least two muscles on either side below the surgical level, and from one muscle above it which serves as a control signal. The precise methodology involved in the choice of stimulated muscles and instigated medical processes is beyond the scope of this article [2].

Trans-cranial activation of subcortical motor tracts is elicited most efficiently by anodal stimulation. Figure1 shows a typical electrical recording from a single nerve fiber, including the dc offset potential (resting potential) which occurs on membrane penetration. It also shows the transient disturbance of membrane potential (the action potential) when an adequate stimulus is applied.

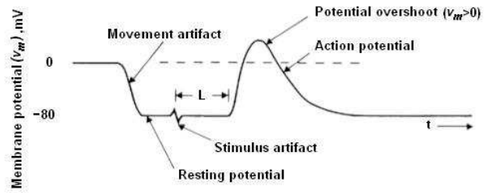

Fig. 1: Recording of action potential in an invertebrate nerve [3].

Conduction velocity in a peripheral nerve is measured by stimulating a motor nerve at two points a known distance apart along its course [3]. Subtraction of the shorter latency from the longer one gives the conduction time along the segment of nerve between the stimulating electrodes (Fig. 2). The conduction velocity of the nerve can be determined when the separation distance is known. This has great potential clinical value, especially where conduction velocity in a regenerating nerve fiber is slowed following nerve injury.

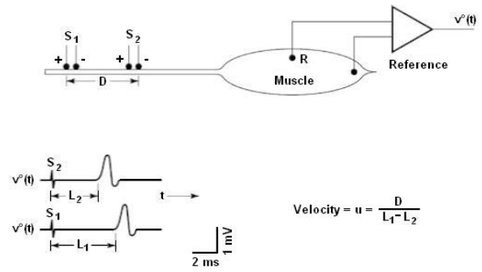

Fig. 2: Measurement of neural conduction velocity via measurement of latency in the evoked electrical response of a muscle. The nerve was stimulated at two sites with separation distance "D" [3].

Characterization and Interpretation

In order to understand the level of clinical significance represented by a pattern of EMG activity, the activity must be characterized beyond a simple burst or train description [3]. The most important feature suggesting significance is its relationship to the surgical events at that time. In addition, a number of electrical features of EMG activity can suggest greater or lesser degrees of irritation and therefore greater or lesser clinical significance.

The following EMG patterns are highlighted in Figure 3: (A) a minor burst of activity occurring as a lumbar root is manipulated; (B) a more intense burst occurring on the background of an ongoing train of activity; (C) intense ongoing trains of activity from multiple motor units, denoting asynchronous activity. (D) a residual train of activity as the effect of nerve root irritation wanes and (E) an interference pattern in the left gastrocnemius muscle after inadvertent trauma to the corresponding nerve root.

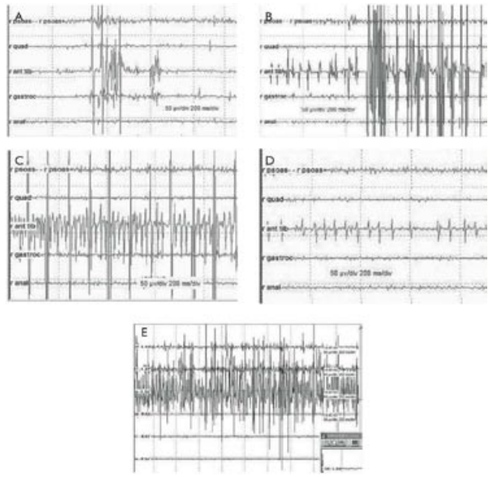

Fig. 3: EMG screens in a variety of patterns of burst activity during lumbar root manipulation [2].

System Design

The proposed EMG system comprises recording and stimulating parts. The digital part of the system is based on MSP430 microcontroller utilization. Here, a pulse width modulation (PWM) signal generated by a timer and D/A converter in the microcontroller is used for stimulation.

Theory of PWM signals

Pulse width modulation (PWM) is a powerful technique for controlling analog circuits with processor digital outputs. PWM is employed in a wide variety of applications, ranging from measurement and communication to power control and conversion.

Pulse-width modulation uses a square wave with a modulated duty cycle which results in variation in the average waveform value. When a square waveform $f(t)$ with a low value y_{min}, a high value y_{max} and a duty cycle D is considered the resultant average value of the waveform is given by:

$$\bar{y} = \frac{1}{T}\int_0^T f(t)dt \,. \qquad (1)$$

As $f(t)$ is a square wave, its value is y_{max} for $0 < t < D.T$ and y_{min} for $D.T < t < T$. Expression (1) then becomes:

$$\bar{y} = \frac{1}{T}\left(\int_0^{DT} y_{max}\,dt + \int_{DT}^{T} y_{min}\,dt\right)$$

$$\bar{y} = \frac{D\cdot T\cdot y_{max} + T(1-D)y_{min}}{T} \qquad (2)$$

$$\bar{y} = D\cdot y_{max} + (1-D)y_{min}$$

The duty cycle "D" is the time an entity spends in an active state as a fraction of the total time considered.

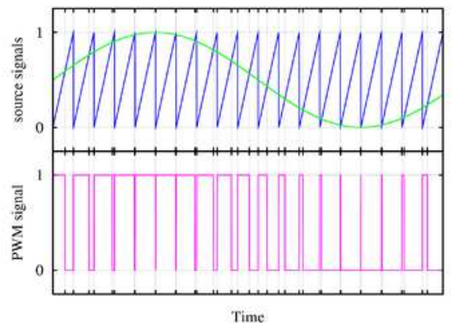

Fig. 4: A simple method of generating the PWM pulse train corresponding to a given signal is the intersective PWM: the signal is compared with a sawtooth waveform. When the latter is less than the former, the PWM signal is in high state (1). Otherwise, it is in the low state (0).

Microcontroller MSP430

The microcontroller is used as a PWM signal generator. This signal is fully programmable, so that the frequency range, amplitude, and target signal latency are easily set.

MSP430 Microcontrollers (MCUs) from Texas Instruments (TI) are 16-bit, RISC-based, mixed-signal processors designed specifically for ultra-low-power. MSP430 MCUs have the right mix of intelligent peripherals, ease-of-use, low cost and the lowest power consumption for many applications [4].

Since the MSP430 MCU is designed specifically for ultra-low-power applications, its flexible clocking system, multiple low-power modes, instant wakeup and intelligent autonomous peripherals enable true ultra-low-power optimization which dramatically extends battery life.

The MSP430 MCU clock system has the ability to enable and disable various clocks and oscillators which allow the device to enter various low-power modes (LPMs). This flexible clocking system optimizes overall current consumption by enabling the required clocks only when appropriate [6].

The architecture, combined with five low power modes is optimized to achieve extended battery life in portable measurement applications. The device features a powerful 16-bit RISC CPU, 16-bit registers, and constant generators that contribute to maximum code efficiency. The digitally controlled oscillator (DCO) allows wake-up from low-power modes to active mode, typically within 3 µs.

The MSP430F563x series are microcontroller configurations with a high performance 12-bit analog-to-digital (A/D) converter, comparator, two universal serial communication interfaces (USCI), USB 2.0, hardware multiplier, DMA, four 16-bit timers, a real-time clock module with alarm capabilities and up to 74 I/O pins.

Typical applications for this device include analog and digital sensor systems, digital motor control, remote controls, thermostats, digital timers and hand-held meters. The MSP430F5638 is used as a generator of PWM signals where the amplitude, latency and frequency of the EMG stimulating signal can be set.

Timer

Timer_A is a 16-bit timer/counter with up to seven capture/compare registers [5]. This timer can support multiple capture/compares, PWM outputs, and interval timing, and it also has extensive interrupt capabilities. Interruptions can be generated from the counter in overflow conditions and from each capture/compare register.

Timer_A features include:

- A synchronous 16-bit timer/counter with four operating modes
- A selectable and configurable clock source
- Up to seven configurable capture/compare registers

- Configurable outputs with pulse width modulation (PWM) capability
- Asynchronous input and output latching
- An interrupt vector register for fast decoding of all Timer_A interrupts

D/A Converter

The DAC12_A module is a 12-bit, voltage output DAC, which can be configured in 8-bit or 12-bit mode and can be used in conjunction with the DMA controller. When multiple DAC12_A modules are present, they can be grouped together for synchronous update operation.

Features of the DAC12_A include:

- 12-bit monotonic output
- 8-bit or 12-bit voltage output resolution
- Programmable settling time vs power consumption
- Internal or external reference selection
- Straight binary or 2's complement data format, right or left justified
- Self-calibration option for offset correction
- Synchronized update capability for multiple DAC12_A modules

Results of System Testing

Figure 5 depicts an example of a PWM signal where the amplitude can be set by a D/A converter. The frequency and latency of generated pulses are set in the time-interrupt routine. There is some noise problem when the device is powered by the USB cable. Although there is no apparent problem when the amplitude is 200 mV, the absolute noise destroys all useful signals at less amplitude.

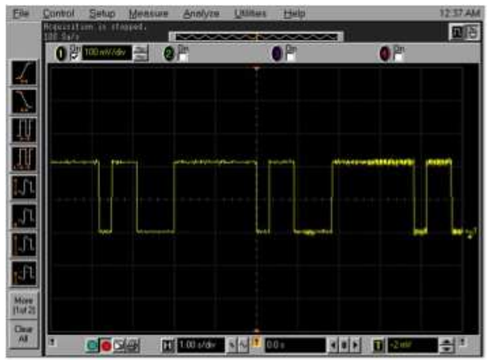

Fig. 5: PWM signal with 200 mV amplitude.

The comparison of noises for different power supplies at low signal amplitudes is shown in Figure 6.

For further stimulations and measurements, it is necessary to use a battery powered device.

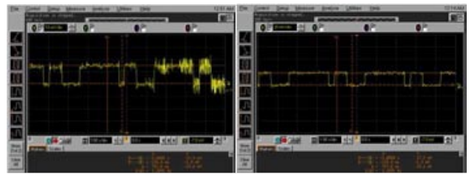

Fig. 6. Screens showing the PWM signal at 20 mV amplitude. The device is powered by USB cable in the left screen and by battery in the right screen.

Conclusion

An EMG system for recording and stimulation is proposed in this article, and the stimulating device was developed and tested. For this stimulation, a modern MSP430 microcontroller was used to generate stimulation pulses with the configurable parameters of pulse width and amplitude, the number and frequency of pulses in the burst and the latency between bursts.

Our future task is to develop a wearable neuro-stimulator based on EMG technology, including an adaptive output control based on on-line signal DSP processing.

Acknowledgement

This material, and the MSP-TS430PZ100USB 100-Pin Socket Target Board and USB Programmer were financially supported by the: AV 4/0012/07 FEI.

The research described in the paper was financially supported by the Slovak Ministry of Education under VEGA Grant No. 1/0987/12.

References

[1] Holland, N. R. *Intraoperative electromyography*. Journal of Clinical Neurophysiology, 2002, vol. 19, no. 5, p. 444–453.
[2] Minahan, R. E., Mandir, A. S. *Basic neurophysiologic intraoperative monitoring techniques*. In: Husain, A. M. *A practical approach to neruophysiologic intraoperative monitoring*. 2008, Demos Medical Pub., p. 21–44, ISBN: 978-1-933864-09-9.
[3] Webster, J. G. *Medical instrumentation: Application and design*. Fourth edition, 2010, Madison, Wiley, ISBN 978-0-471-67600-3.
[4] http://www.ti.com/lit/sg/slab034v/slab034v.pdf
[5] Datasheet MSP430F5638 by Texas Instruments
[6] Fuchs, P., Lojko, B.: Mikroradiče MSP430. Nakladateľstvo STU v Bratislave FEI, 2012. 297 s. ISBN 978-80-227-3660-2.

Ing. Martin Nováček
Institute of Electronics and Photonics
Faculty of Electrical Engineering and Information Technology
Slovak University of Technology in Bratislava
Ilkovičova 3, SK-812 19, Bratislava
Slovak Republic

E-mail: martin.novacek@stuba.sk
Phone: +421-2-602 91 213

SOFTWARE PACKAGE FOR ELECTROPHYSIOLOGICAL MODELING OF NEURONAL AND CARDIAC EXCITABLE CELLS

Elena Cocherová[1,2], Jozef Púčik[1], Martin Nováček[1]

[1]Institute of Electronics and Photonics, FEI STU, Bratislava, Slovak Republic

[2]Institute of Measurement Science, Slovak Academy of Sciences, Bratislava, Slovak Republic

Abstract
The software package described in this article is dedicated for educational and research purposes in the area of electrophysiological cell membrane properties modeling. The designed and created software package offers a selection of several models of nerve fibre membrane, cortical neuron models and various models of heart cells. The model properties and simulation conditions can be set interactively. Consequently, generation of an action potential (AP) on a particular membrane can be observed. The software allows computation and graphical visualization of actual time courses of model state variables, particularly the membrane potential, membrane currents and other model variables. Eventually, additional important characteristics are evaluated from the output data, such as AP duration (APD) of heart cells or AP frequency of cortical neurons.

Keywords
electrophysiological modeling, software package, neuron, heart cell, cell membrane models, action potential

Introduction

Computational cell models are a very useful tool for better understanding of cell function, furthermore, they create powerful ability to predict cell behavior under different conditions. Models of excitable nerve, heart and muscle cells have been developed for more than half a century. This began with the well-known Hodgkin-Huxley model of the giant squid axon [4], and other cell type models then followed.

System description

Various models of nerve fibre membrane [1], [3], [4], [10], [11] cortical neuron models [11] – [13] and various models of heart cells [2], [5] – [9] are included in this software package:

Nerve fibre membrane models:

Hodgkin-Huxley model,
Frankenhaeuser-Huxley model,
Fitzhugh-Nagumo model,
Chiu-Ritchie-Rogart-Stagg-Sweeney model,
Schwarz-Eikhof model, and more;

Cortical neuron models:

Wilson regular spiking model,
Wilson fast spiking model,
Wilson bursting model, and more;

Heart ventricular cell models:

Luo-Rudy model,
Hund-Rudy dynamic model,
O'Hara-Rudy model, and more;

Other heart cell models include:

Michaels model of the sinoatrial (SA) node,
Nygren model of the atrial cell.

The cell type branch and consequently the cell model type is selected in the main window of the designed program (Fig. 2, Fig. 4). The following two main parameters can then be set: (1) the number of periods (period is denoting the cycle length) and (2) the duration of one period. A stimulation current of prescribed amplitude and duration is applied to the membrane during each period.

Parameters related to stimulation current, as well as many other cell model parameters, such as intracellular and extracellular ion concentrations, ion channel characteristics and dimensional attributes can be changed in the "Model parameters" window. In the "Initial conditions" window, the user can view and change the values for the initial conditions of model state variables.

After pressing the "Compute" button, new computation is achieved with actual parameter settings. Results are graphically visualized on three panels: the upper panel shows the time course of the membrane potential, the middle one ("Subplot2") shows the time course of the selected state variable, such as intracellular calcium concentration (Fig. 4) and the bottom one ("Subplot3") shows the time course of selected membrane current or a different selected derived variable, as exemplified in the evaluated APD also in Figure 4. After pressing the "More info" button, a new window with a description of the particular cell model is opened.

Nerve fibre membrane models

The Hodgkin-Huxley model of an unmyelinated nerve fibre is one of the most often used models [4]. This model consists of only two types of voltage-sensitive ion channels: the sodium channel and the potassium channel; which are represented by non-linear conductances G_{Na} and G_K (in mS) in Figure 1.

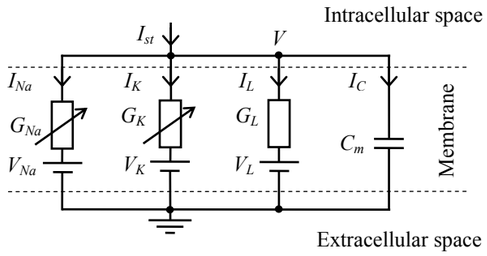

Fig. 1: Circuit scheme of the Hodgkin-Huxley model.

The stimulation current I_{st} (in μA) across the membrane is divided into the ionic current I_{ionic} and capacitive current through the membrane capacity C_m (in μF):

$$I_{st} = I_{ionic} + I_C \quad (1)$$

The time change of the membrane potential (in mV) is then:

$$\frac{dV}{dt} = \left[-i_{ionic} + i_{st}\right] / c_m \quad (2)$$

where i_{ionic} and i_{st} are the current densities (in μA/cm^2), c_{m} is the membrane capacity per 1 cm^2 (in μF/cm^2) and t is time (in ms). For the Hodgkin-Huxley model, the ionic current density is determined only by the sodium, potassium and leakage ion flows:

$$i_{ionic} = i_{Na} + i_K + i_L \quad (3)$$

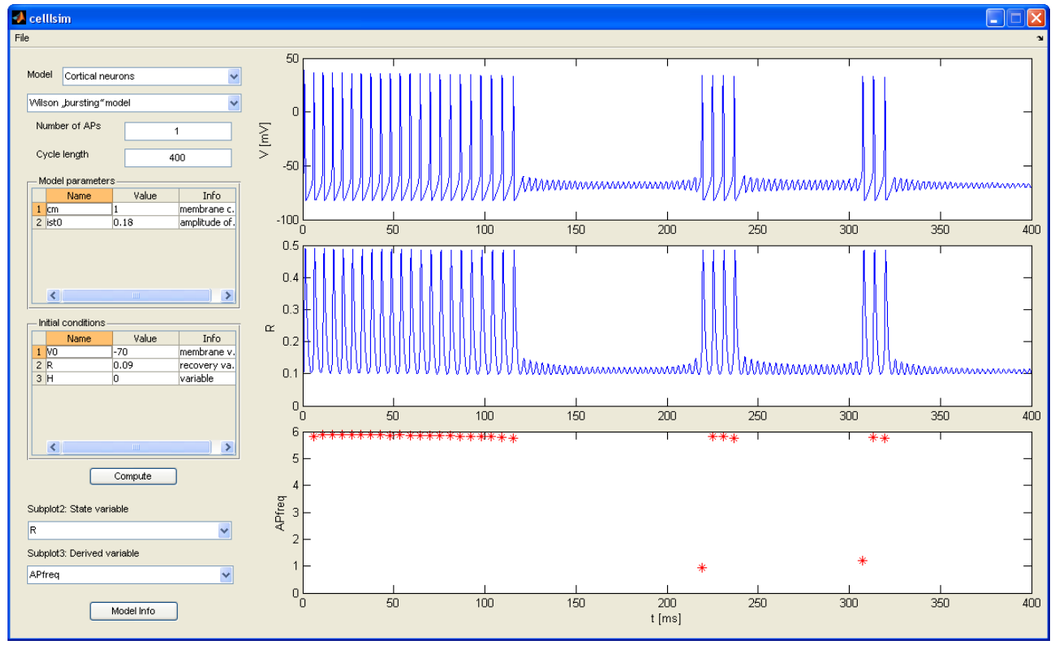

Fig. 2: The main window of the designed software package. Results for the Wilson bursting model of a cortical neuron.

Cortical neurons

The cortical neurons generate a train of nerve impulses with frequency of 1 – 100 Hz or a burst-like activity of nerve impulses (Fig. 2, upper trace: bursts of APs generated by the Wilson bursting model) [12]. The cortical neuron membrane usually contains more types of ion channels than the nerve fibre membrane.

Using the developed software package, the influence of stimulation parameters and model parameters on the AP frequency may be observed (Fig. 2, lower trace).

Heart ventricular cells

The ventricular heart cells (myocytes) comprise many more types of membrane ion channels, ion pumps and exchangers, as depicted in Figure 3. These include channels for the L-type calcium current, the slow and rapid delayed rectifier potassium current, the calcium pump current and the sodium/potassium ATPase current.

Calcium ions play the primary role in the excitation-contraction coupling in myocytes. Advanced models of left ventricular myocytes, such as the Hund-Rudy dynamic model [5], and the O'Hara-Rudy dynamic model [9] contain different calcium buffers, including calmodulin and troponin, and also calcium ion fluxes through the sarcolemmal (cell) membrane and through the membrane of the sarcoplasmic reticulum (SR) which is the main reservoir of calcium ions.

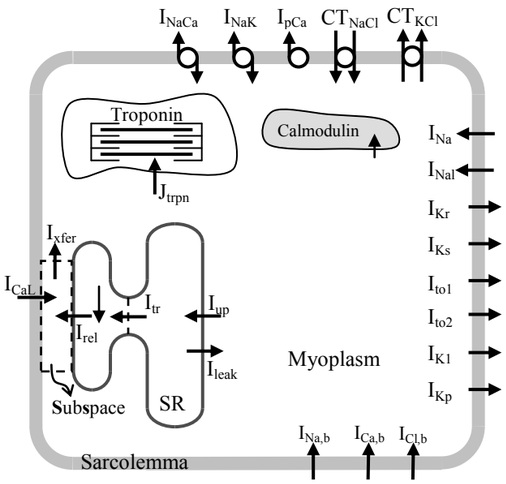

Fig. 3: The scheme of the Hund-Rudy dynamic model.

In the software package, membrane and SR currents, ion concentrations and membrane potential parameters influenced by model parameters and other simulated conditions can be evaluated and observed. These include the AP duration depicted in the lower trace in Figure 4.

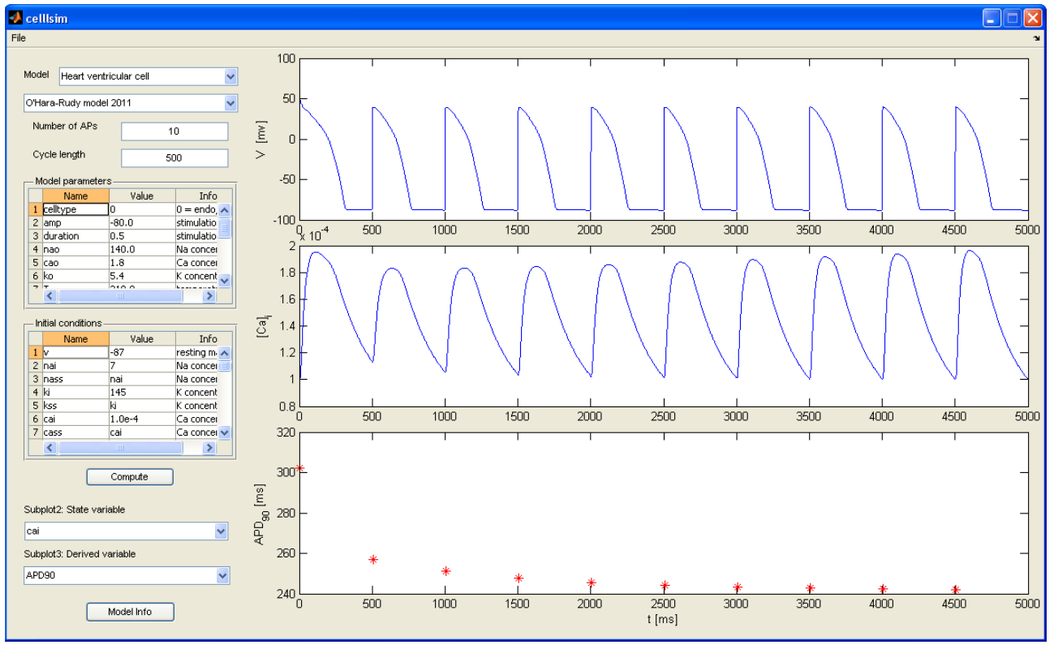

Fig. 4: Main window of the designed software system. Results for the O'Hara-Rudy model of the ventricular heart cell.

Conclusion

The presented software package can help researchers and students to understand the basic and more complex principles related to excitation in neuronal and cardiac cells. This knowledge poses the basis of the electrophysiology of the heart and the nervous system.

The described software package has been developed in the Matlab programming environment and it can be continuously extended by new models of various cell types. This software package can find a great number of applications in different branches of electrophysiological research.

Acknowledgement

The work has been supported by the Slovak Ministry of Education under grants VEGA 1/0987/12, VEGA 2/0210/10 and APVV-0513-10.

References

[1] Cocherová, E. *Refractory period determination in the Hodgkin – Huxley model of the nerve fibre membrane*. In: 4th Electronic Circuits and System Conference, Bratislava, September 11-12 2003, p. 171–174.

[2] Cocherová, E., Zahradníková, A. *Simulation of the effect of changed ionic conductances on the parameters of heart myocyte action potential*. Physiological Research, 2008, vol. 57, no. 2, p. 11P–12P.

[3] Frankenhaeuser, B., Huxley, A. F. *The action potential in the myelinated nerve fibre of Xenopus Laevis as computed on the basis of voltage clamp data*. Journal of Physiology, 1964, vol. 171, p. 302–315.

[4] Hodgkin, A. L., Huxley, A. F. *A quantitative description of membrane current and its application to conduction and excitation in nerve*. Journal of Physiology, 1952, vol. 117, p. 500–544.

[5] Hund, T. J., Rudy, Y. *Rate dependence and regulation of action potential and calcium transient in a canine cardiac ventricular cell model*. Circulation, 2004, vol. 110, p. 3168–3174.

[6] Luo, Ch., Rudy, Y. *A model of the ventricular cardiac action potential. Depolarization, repolarization, and their interaction*. Circulation Research, 1991, vol. 68, p. 1501–1526.

[7] Michaels, D. C., Matyas, E. P., Jalife, J. *A mathematical model of the effects of acetylcholine pulses on sinoatrial pacemaker activity*. Circulation Research, 1984, vol. 55, p. 89–101.

[8] Nygren, A., Fiset, C., Firek, L., Clark, J. W., Lindblad, D. S., Clark, R. B., Giles, W. R. *Mathematical model of an adult human atrial cell: the role of K^+ currents in repolarization*. Circulation Research, 1998, vol. 82, p. 63-81.

[9] O'Hara, T., Virág, L., Varró, A., Rudy, Y. *Simulation of the undiseased human cardiac ventricular action potential: model formulation and experimental validation*. PLoS Computational Biology, 2011, vol. 7, no. 5, e1002061.

[10] Rattay, F. *Electrical nerve stimulation*. Springer-Verlag, Wien, 1990.

[11] Trappenberg, T. P. *Fundamentals of computational neuroscience*. Oxford University Press, Oxford, 2002.

[12] Wilson, H. R. *Simplified dynamics of human and mammalian neocortical neurons*. Journal Theoretical Biology, 1999, vol. 200, p. 375–388.

[13] Wilson, H. R. *Spikes, decisions, and actions. The dynamical foundations of neuroscience*. Oxford University Press, Oxford, 2003.

Elena Cocherová, Ph.D.
Institute of Electronics and Photonics, Faculty of Electrical Engineering and Information Technology
Slovak University of Technology
Ilkovičova 3, 812 19 Bratislava

E-mail: elena.cocherova@stuba.sk
Phone: +421 2 60291174

VENTILATOR CIRCUIT MODEL FOR OPTIMIZATION OF HIGH-FREQUENCY OSCILLATORY VENTILATION

Jan Matějka, Jakub Ráfl, Michal Čech, Martin Rožánek

Czech Technical University in Prague, Faculty of Biomedical Engineering, Kladno, Czech Republic

Abstract
Ventilators for high-frequency oscillatory ventilation (HFOV), Sensormedics 3100, were not designed to tolerate spontaneous breathing of a patient. An experimental Demand Flow System (DFS) is being developed to support spontaneous breathing during HFOV. A control system of the DFS requires a model of the ventilator circuit of Sensormedics 3100. A new model of the circuit was designed, including the oscillating membrane, the inspiratory and expiratory branches of the circuit, the expiratory valve, and a spontaneously breathing patient. The model was implemented in the Multisim software environment. A bench test suggests that the model predicts the basic changes in pressure within the ventilator circuit and that its modified version can be used in the DFS control algorithm.

Keywords
high-frequency oscillatory ventilation (HFOV), ventilator circuit, lumped-parameter model, electro-acoustic analogy

Introduction

High-frequency oscillatory ventilation (HFOV) is an unconventional method of mechanical ventilation. HFOV uses breathing frequencies of 3–15 Hz combined with tidal volumes about four times smaller than in conventional modes of ventilation. Low tidal volumes imply low changes in pressure in the lower airways which reduces mechanical damage to the lungs. That is especially important for patients suffering from Acute Respiratory Distress Syndrome (ARDS) and having reduced lung compliance.

The currently used ventilator for HFOV, Sensormedics 3100 (SensorMedics, USA), has not been designed to support or even tolerate spontaneous breathing of a patient. This is not an issue at severe state of ARDS patients, but it complicates gradual weaning of a patient from mechanical ventilator support: if a patient starts to breathe, his/her work of breathing raises, and high pressure changes in the ventilator circuit caused by spontaneous breathing can even impede the normal functioning of the ventilator.

An experimental device, called the Demand Flow System (DFS), is being developed to facilitate spontaneous breathing during HFOV [1]. The DFS runs concurrently with the Sensormedics 3100, measuring the proximal airway pressure at a patient's airway opening. A control system of the DFS evaluates the proximal airway pressure swings caused by a patient's spontaneous breathing. The spontaneous breathing is compensated by variable gas inflow into the ventilator circuit so that the mean airway pressure (MAP) in the circuit remains unaltered. Therefore, the functioning of the ventilator is not affected. Also, a patient's respiratory effort does not increase.

The control system of the DFS employs the linear quadratic Gaussian (LQG) state feedback controller and requires a model of the ventilator circuit with a connected patient. The model should primarily describe how the proximal airway pressure is affected by a change in the gas inflow into the ventilator circuit. However, the linear model originally employed by the DFS neglects some physical properties of the ventilator circuit. Moreover, approximation of some parameters in the model seems to be oversimplified [1].

The aim of this study is to design a new model of the ventilator circuit of Sensormedics 3100 with revised structure and parameter values. The model should improve the performance of the DFS control algorithm.

Ventilator Circuit

The ventilator circuit of Sensormedics 3100, presented in Fig. 1, connects the ventilator with

a patient, assuring the delivery of fresh gas into a patient airways and removal of the expired gas. The DFS controls the gas inflow into the ventilator circuit. The gas passes through the inspiratory branch and the expiratory branch of the circuit and escapes via an expiratory valve. The expiratory valve flow resistance and gas volume flow rate determine the MAP.

An oscillating membrane is placed at the connection of the circuit and the ventilator. The membrane, similar to a loudspeaker membrane, generates pressure swings that travel through the inspiratory branch to a patient's airway opening (a Y-piece of the circuit) and, while being attenuated, further down to the lungs. Due to the pressure oscillations, a portion of fresh gas flow from the ventilator circuit is diverted into the patient's airways.

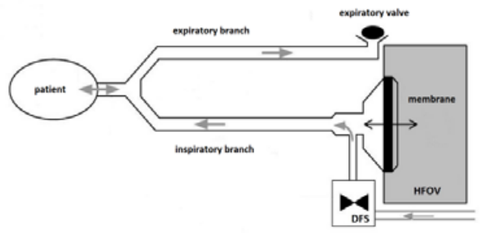

Fig. 1: Ventilator circuit of Sensormedics 3100 with the Demand Flow System. Figure modified from [2].

Model Structure and Parameters

The new model of the ventilator circuit was divided into subsystems according to functional parts of the ventilator circuit with a connected patient: the *membrane*, the *inspiratory branch*, the e*xpiratory branch*, the *expiratory valve*, and the *patient*. The ventilator circuit was disassembled into the functional parts; structure and parameters of each subsystem were identified independently of the rest of the circuit.

Models of the subsystems were based on the electro-acoustic analogy and derived from the combination of theoretical modeling and experimental identification. The theoretical part of the concept was based on similarity of the ventilator circuit components to basic acoustic elements described in [3]. When compared to the circuit dimension, wavelength of oscillations propagating through the circuit was assumed to be long enough to allow construction of a lumped-parameter model.

For the experimental identification, pressure in the subsystems was measured under static conditions at different levels of gas volume flow rate. Alternatively, a step response of the pressure signal was acquired as a reaction to a sudden increase of the gas volume flow rate. Median filters of various window sizes were used to remove the acoustic noise which corrupted the pressure measurements.

The method of least squares was employed to identify a desired parameter from a pressure step response. The method can be described by the equation

$$SSR = \sum_{M=1}^{N} \left(X_M - X_M^p \right)^2 \qquad (1)$$

A measured value of pressure X_M at each of N samples was compared with the value of X_M^p predicted by a model for the same flow input. The parameter of the model was altered by an iterative algorithm so that SSR is minimal [4].

All subsystems and the complete model of the ventilator circuit were implemented and tested in the software Multisim 11.0 (National Instruments, USA).

Membrane

Structure of the subsystem *membrane* is composed of an acoustic elastor ("compliance"), a controlled acoustic resistor and two sources of pressure. The first pressure source represents oscillations of the ventilator membrane. The second pressure source together with a controlled acoustic resistor R_1 (see Fig. 3) represents a proportional valve of the DFS which controls the gas inflow into the circuit.

The membrane structure was identified from pressure step responses measured with and without the membrane oscillations. The step responses corresponded to a response of the first-order RC circuit as illustrated in Fig. 2. The value of the acoustic elastor was calculated using the least squares method as $C_1 = 0.01391 \cdot \mathrm{kPa}^{-1}$.

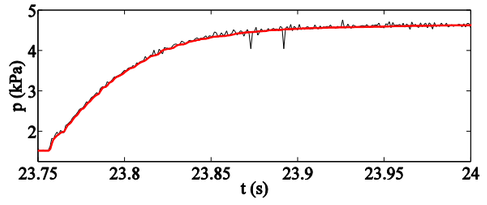

Fig. 2: Pressure recorded in front of the membrane during a step increase of gas inflow from the DFS. The volume flow rate increased from 40 l·min^{-1} to 120 l·min^{-1}. Oscillations were switched off [5].

Inspiratory and expiratory branches

Each of models of the inspiratory and expiratory branches consists of two nonlinear acoustic resistors and two inertors ("inertances") connected in series.

In each branch the nonlinear behavior of the first resistor in described as

$$R_2 = R_5 = 0.0599 q^{0.7161} \qquad (2)$$

and the nonlinear behavior of the second resistor as

$$R_3 = R_6 = 0.0473 q^{0.7557} \qquad (3)$$

where R_2, R_3 are given in $\mathrm{kPa \cdot s \cdot l^{-1}}$ and q is volume flow rate in $\mathrm{l \cdot s^{-1}}$. The equations (2) and (3) were derived from static pressure measurements [6].

A nonlinear resistor was implemented in the software Multisim 11.0 with help of a current source controlled by the current (representing the gas flow) in the model. The current source was connected to a current-controlled voltage source and the voltage source governed the value of the resistor in the model.

The values of inertors L_1, L_2, L_4, and L_5 were calculated from the equation

$$L = \frac{\rho_0 l}{S} \qquad (4)$$

where ρ_0 refers to the gas density, l to the length of a tube, and S to the cross-section area of the tube. In the final model $L_1 = L_4 = 0.0036\ \mathrm{kPa \cdot s^2 \cdot l^{-1}}$ and $L_2 = L_3 = 0.0027\ \mathrm{kPa \cdot s^2 \cdot l^{-1}}$.

Expiratory valve

The expiratory valve exhibits nonlinear resistance which depends on the level of MAP. For MAP of 20 $\mathrm{cmH_2O}$, the relevant resistor is

$$R_7 = 0.0260 q^2 - 0.5612 q + 2.9186 \qquad (5)$$

where R_7 is given in $\mathrm{kPa \cdot s \cdot l^{-1}}$ and q in $\mathrm{l \cdot s^{-1}}$.

Reaction of the valve to a sudden change in flow is modeled by the inertor $L_6 = 0.0046\ \mathrm{kPa \cdot s^2 \cdot l^{-1}}$. The inertance was acquired from a step response measurement.

Model of a patient

The model of a patient was created in two versions. The first one is a patient convalescent from ARDS with spontaneous breathing and the second one is a patient suffering from ARDS without spontaneous breathing. For both the structures a classic single-compartment model was chosen with all elements connected in series.

For the further simulations, the recovering patient version was selected. The subsystem includes the inertance and resistance of an endotracheal tube, the resistance and compliance of a patient's respiratory system, and the work of breathing muscles. Therefore, the model consists of combination of an inertor L_3, a resistor R_4, an elastor C_2, and a pressure source connected in series. The resistor combines both the resistances.

A value of inertance was calculated from (4) as $L_3 = 0.0081\ \mathrm{kPa \cdot s^2 \cdot l^{-1}}$. A value of the resistor was estimated according to [7]–[10] as $R_4 = 3.166\ \mathrm{kPa \cdot s \cdot l^{-1}}$. The elastor was set to $C_2 = 0.501 \cdot \mathrm{kPa^{-1}}$.

Complete model of the ventilator circuit

All subsystems were connected into the complete model of a ventilator circuit and a patient. The final model implemented in Multisim is presented in Fig. 3.

Model Bench Test

The performance of the complete model was compared with the real ventilator circuit. For the purpose of the bench test, the complete ventilator circuit was connected to the ASL 5000 breathing simulator (IngMar Medical, USA). A pressure sensor

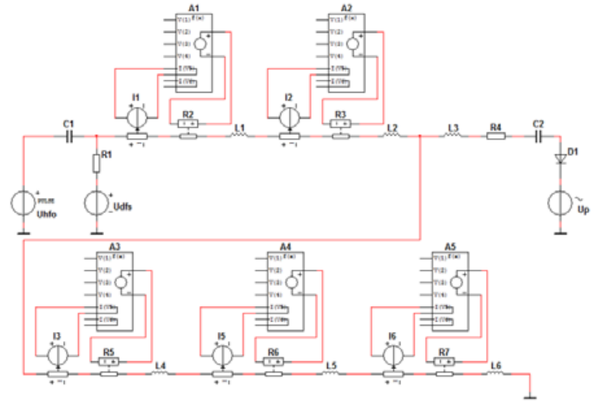

Fig. 3: The final model of the ventilator circuit of Sensormedics 3100 implemented in Multisim [5].

was placed at the Y-piece of ventilator circuit, close to a patient's airway entrance.

A recorded pressure waveform compared to the respective output of the model is in Fig. 4.

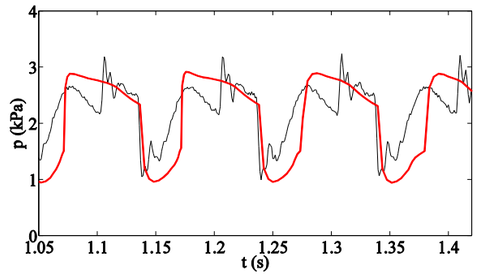

Fig. 4: Pressure waveform recorded at the Y-connection of the ventilator circuit (thin line) compared to the same signal simulated by the final model (bold line) at MAP 20 cmH_2O, frequency of oscillations 10 Hz and amplitude of 15 cmH_2O [5].

Discussion

A mathematical model of the ventilator circuit of Sensormedics 3100 high-frequency oscillatory ventilator was built. The model was implemented in the Multisim software environment, using an electro-acoustic analogy. The model consists of several subsystems that were identified independently of the rest of the circuit. The modular approach enables more detailed identification of the ventilator circuit components, and also allows a gradual improvement of the model in future if more precise measurements are taken or if a part of the circuit is enhanced.

According to the results of the bench test (see Fig. 4), the model correctly predicts the basic pressure changes in the Y-piece of the ventilator circuit caused by the membrane oscillations during a constant gas flow in the circuit. The bench test showed swings in the measured pressure signal that were not observed during the simulation. This could be caused by acoustic compliance of the inspiratory and expiratory branches of the circuit which has been neglected so far.

The pressure signal generated by a model is smoother compared to the measured signal. A model with distributed parameters could achieve a more accurate simulation, involving, for example, reflections of pressure waves.

Finally, one of the problems of the final model is a question how to model the pressure signal generated by the oscillating membrane of the ventilator. In the presented model an ideal source of pressure pulses was used; however, experiments showed that shape and amplitude of the pressure signal is influenced by amount of gas flow from the DFS and by amplitude and frequency of oscillations.

Conclusion

A new model of a ventilator circuit for HFOV ventilation was designed, including a spontaneously breathing patient. Simulations suggest that the model, after some modifications, can be used in a control system supporting spontaneous breathing of a patient on HFOV.

Acknowledgement

The authors thank Ondřej Čadek for construction of a device for accurate real-time pressure measurement.

The work has been supported by grant SGS11/171/OHK4/3T/17 of the Czech Technical University in Prague.

References

[1] Roubík, K., Ráfl, J., van Heerde, M., Markhorst, D. G. *Design and control of a demand flow system assuring spontaneous breathing of a patient connected to an HFO ventilator*. IEEE Trans Biomed Eng, 2011, vol. 58, no. 11, p. 3225–3233.

[2] van Heerde, M., et al. *Unloading work of breathing during high-frequency oscillatory ventilation: A bench study*. Critical Care, 2006, vol. 10, no. 4, p. R103.

[3] Škvor, Z. *Vibrating systems and their equivalent circuits*. 2nd ed. Prague: Academia, 1991.

[4] Bates, J. H. T. *Lung mechanics: An inverse modeling approach*. 1st ed. New York: Cambridge University Press, 2009.

[5] Matějka, J. *Model pacientského okruhu pro optimalizaci vysokofrekvenční oscilační ventilace*. [Bachelor thesis]. Prague: CTU FBMI, 2012.

[6] Čech, M. *Modelování a měření základních komponent v respirační péči*. [Bachelor thesis]. Prague: CTU FBMI, 2012.

[7] van Genderingen, H. R., et al. *Reduction of oscillatory pressure along the endotracheal tube is indicative for maximal respiratory compliance during high-frequency oscillatory ventilation: A mathematical model study*. Pediatric Pulmonology, 2001, vol. 31, no. 6, p. 458–463.

[8] Schranz, C., Moeller, K. *Inverse modeling supports quantification of pressure and time depending effects in ARDS patients*. In: 33rd Annual International Conference of the IEEE EMBS, Boston, Aug 30–Sep 3, 2011, p. 1013–1016.

[9] Schranz, C., Moeller, K. *Model-based quantification of pressure and time depending effects in ARDS patients*. In: 5th International Conference on Bioinformatics and Biomedical Engineering (iCBBE), Wuhan, May 10–12, 2011, p. 1–4.

[10] Pino, A. V., Giannella-Neto, A. *A new method to obtain a positive end-expiratory pressure*. In: Proceedings of the 18th Annual International Conference of the IEEE EMBS, Amsterdam, Oct 31–Nov 3, 1996, p. 1689–1690.

Jakub Ráfl
Department of Biomedical Technology
Faculty of Biomedical Engineering
Czech Technical University in Prague
nám. Sítná 3105, CZ-272 01 Kladno

E-mail: rafl@fbmi.cvut.cz
Phone: +420 728 229 991

REHABILITATION OF PATIENTS USING ACCELEROMETERS: FIRST EXPERIMENTS

Jakub Parak[1], Lucie Talacková[1], Jan Havlik[1], Lenka Lhotska[2]

[1]Deparment of Circuit Theory, Faculty of Electrical Engineering, CTU in Prague

[2]Deparment of Cybernetics, Faculty of Electrical Engineering, CTU in Prague

Abstract

In this article, the use of accelerometers for rehabilitation of patients is described. The appropriate rehabilitation process is a key approach to treat a broad range of different diagnoses. The main problem of rehabilitation processes is a subsequent evaluation of their quality to achieve best results. This initial study describes a possibility of using accelerometers for objective evaluation of quality and monitoring the results. The first measurements with accelerometers were conducted on several exercises which are part of the Tinetti balance assessment tool. For these measurements, the 3D MEMS accelerometer implemented in the STM32-Primer2 development kit was used. After the assessment of results obtained on healthy persons, the clinical tests on senior patients will follow.

Keywords

accelerometer, rehabilitation, Tinetti balance assessment tool, STM32Primer2

Introduction

The rehabilitation of patients is commonly used therapy after traumas or commas. Moreover the rehabilitation is used for the patients who have various problems with a musculoskeletal system.

The main problem of rehabilitations is an objective evaluation of the quality and progress. It means that today the physiotherapist or doctor evaluates the results of rehabilitation only watching the patient. Every physiotherapist or doctor evaluates the progress and results on his way and there is no objective aspect. It means that two conclusions from two doctors can be totally different.

The other problem is that the patients do not have any feedback from therapy process. It means that the patients cannot monitor the progress independently without physiotherapist or doctor.

The use of accelerometers in the rehabilitation process can improve the evaluation of results and make the rehabilitation process more efficient. Based on measured signals, the quality and progress of rehabilitation therapy can be established. A detailed analysis of using the accelerometers in rehabilitation of patients is described in [1].

The diagnostic method which is used mainly in rehabilitation is called the postugraphy. This method is used for used to quantify the postural control in upright stance in either static or dynamic conditions. The objective evaluation of results of postugraphy method is based on accelerometer data during postugraphy tests [2].

The rehabilitation training of a patient with elbow ligament injury was improved by the supplementary monitoring system. This system is based on the wireless accelerometer network and integrates remote monitoring and intelligent crossplatform terminal [3].

The accelerometers are used for monitoring the rehabilitation training of the hemiplegic patients as well [4].

Another usage of the accelerometer is upper extremity rehabilitation of the children with the cerebral palsy. In this rehabilitation is used feedback from trunk wearable accelerometer during playing the game on the multitouch display [5].

In addition the signal from accelerometers is used for physical activity detection. The personal mobility monitoring is very important for patients with physical disabilities or chronic cardiac diseases. This type of monitoring is a part of rehabilitation process for these patients [6, 7].

Several possible solutions and related works which implements accelerometers in rehabilitation process are presented below.

In this article the application of the accelerometers in diagnostic rehabilitation process is described. This initial study is focused on exercises from Tinetti balance assessment tool enhanced with measurements on the accelerometers. The acquired signals show the possibility of using accelerometers for objective quality and results evaluation in this diagnostic method.

Measurement system

The measurement system consists of two main parts: the development kit with integrated accelerometer and the PC application for data acquisition.

Development kit

The development kit STM32-Primer2 was selected for this project. The kit is product of France Company Raisonance. The kit contains 32-bit microprocessor ARM CORTEX STM32F103BVET with maximal clock frequency 72 MHz. The device uses especially these kit components: LCD display, accelerometer, joystick button and external USB connector.

In the development kit there is integrated three-axial MEMS accelerometer LIS3LV02DL. This inertial sensor has a user selectable full scale of ± 2g, ± 6g and it is capable of measuring acceleration over a bandwidth of 640 Hz for all axes. The device bandwidth may be selected accordingly to the application requirements [8].

The precision and accuracy of the accelerometer in the development kit was analyzed on the several measurements with pendulum and gramophone.

In the firmware application for development kit there was implemented USB HID device driver for accelerometer data transmission. An acceleration sampling frequency was set to 50 Hz.

The development kit is shown in the Figure 1.

PC application

The PC application for data acquisition from development kit is based on USB HID Component for C# [10]. The application allows saving raw data from the development kit into a file in real-time. The Realtime Chart and Graph component is integrated in the application for visualization of receiving data [11].

The application screenshot is shown in the Figure 2.

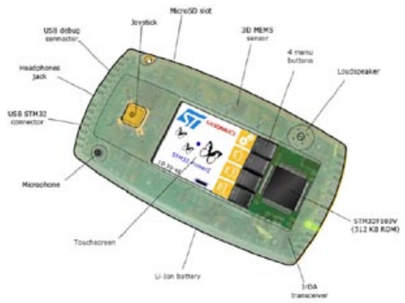

Fig. 1: The STM32-Primer development kit [9].

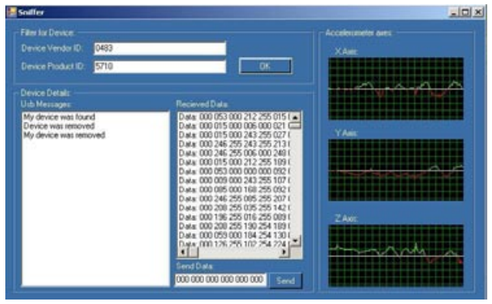

Fig. 2: The screenshot of PC application for data acquisition, logging and visualization.

Signal processing

Signal processing was designed and implemented in Matlab environment.

At the beginning the dynamic acceleration is non linear filtered from raw signal. The signal is decimated to 10 Hz sample frequency firstly. Then the median 10^{th} order filter is applied on the signal. Finally, the signal is interpolated back to 50 Hz sample frequency.

After this filtration the signal contains only the static acceleration. This acceleration is dependent on direction of gravitational acceleration. Further the static acceleration is used for computing tilt of sensor.

The sensor tilt angle in particular axis can be computed by using formula (1). In this formula φ_x is the tilt angle in the axis X, a_x is the actual measured acceleration in X axis depended on tilt angle and g_x is is measured acceleration of gravity in axis X. The analogously same formula can be applied for other two axes. Although the formula is very simple it is not used for determination of the tilt angle.

$$\varphi_x = \arccos\frac{a_x}{g_x} \qquad (1)$$

The other way how to calculate sensor tilt angle is to measure the acceleration of gravity in two specific plane of Cartesian system. This method is explained in the Figure 3. For computing the angle in XY plane was used the formula (2). In this formula α is tilt angle in plane XY, a_x is acceleration in X axis and a_y is acceleration in Y axis.

$$\alpha = \arctan\frac{a_y}{a_x} \qquad (2)$$

The formula (3) was used for computing the angle in XZ plane (1). In this formula β is tilt angle in plane XZ, a_x is acceleration in X axis and a_y is acceleration in Z axis.

$$\beta = \arctan\frac{a_z}{a_x} \qquad (3)$$

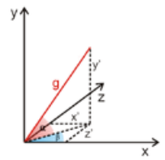

Fig. 3: Representation of x', y' and z' axis after rotation by α and β angles

Experimental measurements

The experimental measurements have been composed of three exercises which are a part of Tinneti balance assessment tool. These exercises are listed in Table 1.

Tab. 1: Selected exercises from Tinneti balance assessment tool [12].

Exercise	Execution of exercise
Rises from chair	Able, uses arms to help Able without use of arms
Standing balance	Unsteady Narrow stance without support
Sitting down	Unsafe (misjudged distance, falls into chair) Uses arms or not a smooth motion

In this first study the exercises are practiced by healthy persons. The measured person tries to simulate health problem during the exercise according to the description in Tinnet's test. The description and the results of the performed measurements are in the next subsections.

Measurement of person who rises from a chair and sits down back

During this experiment the device was set on the side of the tight. The computed tilt angles of the healthy person who rises from a chair and sits down back are displayed in the Figure 4.

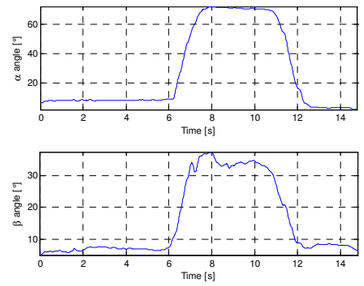

Fig. 4: The computed tilt angles of the healthy person who rises from a chair and sits down.

In the Figure 5 there are displayed the computed tilt angles of measured healthy person who simulates problem with rising from a chair and sitting down. A person stands up with the aid of hands.

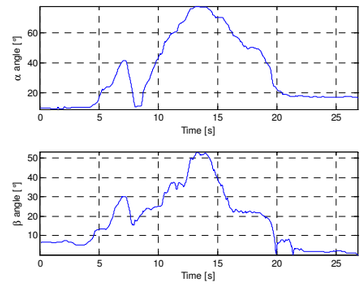

Fig. 5: Tilt angles of simulation problem with rising from chair helping with arms.

The computed tilt angles of the healthy person who simulates trying to stand up without success is shown in the Figure 6.

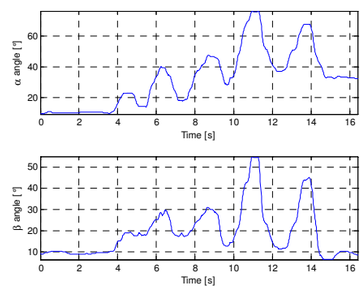

Fig. 6: Tilt angles of simulation problem with rising from chair without final stand up.

Measurement of person balance with opened and closed eyes.

The sensor was attached on the side of the belt during this measurement. In the Figure 7 there are displayed tilt angles computed during simulation of the balance problems with opened eyes. The simulation of the same problem with closed eyes has similar results.

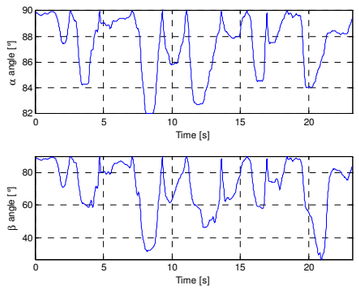

Fig. 7: Tilt angles of simulation balance problems with opened eyes.

Conclusion

The simple measurement system with accelerometer was developed for evaluation of the quality and progress of the rehabilitation. The system can be very easily extended and adapted for other measurements during rehabilitation using the development kit.

Based on experimental measurements applied on exercises from Tinetti balance assessment tool it may be argued that accelerometer can provide suitable information about rehabilitation process.

The proposed method of computing the sensor tilt provides better results than using information only about acceleration in the one specific axis.

The study will be extended with clinical tests on the geriatric department. The exercises from Tinetti assessment tool simulated by healthy people will be measured on real geriatric patients. The data will be acquired periodically during the whole rehabilitation process in order to watch the rehabilitation progress and its quality.

Another parallel research will apply this knowledge in rehabilitation of patients with artificial hip joint

Acknowledgement

This work and the participation in the conference have been supported by the Foundation of Stanislav Hanzl CTU in Prague.

This work has been also supported by the research program No. MSM 6840770012 of the Czech Technical University in Prague (sponsored by the Ministry of Education, Youth and Sports of the Czech Republic).

References

[1] K. M. Culhane, M. O'Connor, D. Lyons, G. M. Lyons, "Accelerometers in rehabilitation medicine for older adults," *Age Ageing*, 2005, vol. 34, no. 6, pp. 556 – 560.

[2] M. Mancini, F. B. Horak, "The relevance of clinical balance assessment tools to differentiate balance deficits," *European Journal of Physical and Rehabilitation Medicine*, 2010, vol. 46, no. 2, pp. 239 – 248.

[3] Ren Wang, Hang Guo, Jiashan Xu, W.H. Ko, "A supplementary system based on wireless accelerometer network for rehabilitation," in *Proc. 5th IEEE International Conference on Nano/Micro Engineered and Molecular Systems (NEMS)*, China 2010, pp. 1124 – 1127.

[4] Y. Higashi, M. Sekimoto, F. Horiuchi, T. Kodama, T. Yuji, T. Fujimoto, M. Sekine, T. Tamura, "Monitoring rehabilitation training for hemiplegic patients by using a tri-axial accelerometer," in Proc. *23rd Annual International Conference of the IEEE Engineering in Medicine and Biology Society*, Turkey 2001, vol. 2, pp. 1472 – 1474.

[5] A. Dunne, Son Do-Lenh, G.O. Laighin, Chia Shen, P. Bonato, "Upper extremity rehabilitation of children with cerebral palsy using accelerometer feedback on a multitouch display," in Proc. *Annual International Conference of the IEEE Engineering in Medicine and Biology Society (EMBC)*, Argentina 2010, pp. 1751 – 1754.

[6] J. Boyle, M. Karunanithi, T. Wark, W. Chan, C. Colavitti, "Quantifying Functional Mobility Progress for Chronic Disease Management," in Proc. 28th *Annual International Conference of the IEEE Engineering in Medicine and Biology Society*, USA 2006, pp. 5916 – 5919.

[7] N. Bidargaddi, A. Sarela, L. Klingbeil, M. Karunanithi, "Detecting walking activity in cardiac rehabilitation by using accelerometer," in Proc. *3rd International Conference on Intelligent Sensors, Sensor Networks and Information*, Australia 2007, pp.555 – 560.

[8] Raisonance. (2010, May). STM32-Primer2 User Manual. [Online]. Available: http://www.stm32circle.com/resources/download.php?STM32-Primer2-Manual.pdf

[9] STMicroelectronis. (2008, January). LIS3LV02DL Datasheet. [Online]. Available: http://www.st.com/internet/com/TECHNICAL_RESOURCES/TECHNICAL_LITERATURE/DATASHEET/CD00091417.pdf

[10] Wimar. (2007, March). A USB HID Component for C#. [Online]. Available: http://www.codeproject.com/Articles/18099/A-USB-HID-Component-for-C

[11] R. Reznik. (2007, May). Realtime Chart and Graph in One. [Online]. Available: http://www.codeproject.com/Articles/15694/Realtime-Chartand-Graph-in-One

[12] M. E. Tinetti, T. F. Williams, R. Mayewski, "Fall Risk Index for elderly patients based on number of chronic disabilities," *American Journal of Medicine,* 1986, vol. 80, pp. 429 – 434.

Ing. Jakub Parak
Department of Circuit Theory
Faculty of Electrical Engineering
Czech Technical University in Prague
Technicka 2, 166 27, Prague, Czech Republic

E-mail: parakjak@fel.cvut.cz
Phone: +420 224 355 86

CHANGES IN BIOIMPEDANCE DEPENDING ON CONDITIONS

J. Hlubik [1], P. Hlubik[2] and L. Lhotska[1]

[1] Gerstner Laboratory, Faculty of Electrical Engineering, Czech Technical University in Prague, Czech Republic

[2] Faculty of Military Health Sciences Hradec Králové, University of Defense, Czech Republic

Souhrn

The aim of the paper is to present results of our ongoing research focused on the influence of measurement condition change on body composition measurements. The performed measurements showed certain influence which must be verified by repeated experiments. These changes can lead to important conclusion and further standardization.

Klíčová slova

Bioimpedance, Body composition, BIA, Body fat

Introduction

Nowadays BMI (body mass index) is a parameter that is often used in studies to indicate degree of obesity (or slimness). BMI is a calculated value that uses patient's height and weight. Thanks to this two persons having the same height and weight can have same BMI but body composition can be diametrically different. Focus only on BMI can lead to biases in classification if no other information is obtained. Hence BMI should be used in big studies as a first approach before further investigation.

It is known that density of bones and quality of muscles influences the weight to a certain degree. That means that two persons having the same height and waist size might have relatively high difference in weight due to the differences in body composition.

Thus, a method allowing measurement of more informative quantities is necessary in order to evaluate the amount of body fat more objectively and precisely. As obesity does not refer to excessive body weight but it refers to the condition in which the individual has an excessive amount of body fat. Many laboratory and field assessment techniques exist for estimating a person's body composition.

The Body Impedance Analysis (BIA) represents one of the methods for classification of body composition.

This method use electrical current that is injected into the body. This current is measured and from these values are calculated parts of body composition such as FFM (fat free mass), TBW (total body water), ICW (intracellular water), ECW (extra cellular water), fat% and so on.

Nowadays devices for impedance measurements are from basic to very complex. Basic machines uses just single frequency measurements and mostly have only one pair of electrodes. Better devices uses for measurements wider range of frequencies and mostly have more electrodes which allow segmental measurements of a body. This feature is important e.g. for measurements of a single body part in case of hydration or other problems.

It is crucial to know which value is needed and due to this choose right device. E.g. for basic examination basic device is enough, but these devices could be often biased. So it is crucial to use proper device.

It is possible to determine patient's obesity in more than one way. One method of the obesity characterization is Body Mass Index (BMI) > 30kg/m² and by body fat increase. But as discussed earlier the question is if BMI alone is sufficient for obesity classification. Another classification of obesity was

determined by WHO as a body fat ranges for standard adults [1].

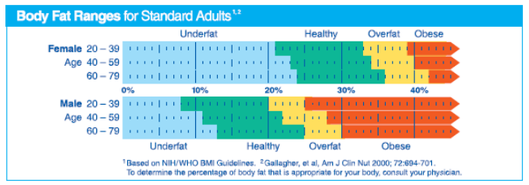

Fig. 1:Ranges of fat mass (FM) from the WHO guidelines.

This obesity classification should be better because it takes into account not just weight and height but also body fat % which is a definition of obesity.
From this perspective method that is able to measure or calculate body fat % should be more precise than just BMI or any other method. For body composition measurement is possible to use several methods and bioimpedance is one of best method.
Many of the studies [2,3,4] performing the BIA for various purposes (e.g. relevance to diagnosing metabolic disorders, cardiovascular risk, assessment of degree of obesity, etc.) usually do not mention patients and electrode status and frequency used during the measurement. Also no information about environmental conditions is given. This led us to formulation of the following two goals of our study.

Goals

The first part of the work deals with a question of measuring human body compositions how and why. The task is to find out what is the role of environmental conditions. The goal is to find out what effects have different hand and feet measuring conditions such as sweat, usage of gels and moistures. It is assumed that changes in measurement conditions may lead to mistakes and biases of values for specific parts of the body.

The second goal is to measure and evaluate body impedance changes and to find out if frequency does have importance on these conditions. And if frequency of 50 kHz is sufficient for measurements of wider range of frequencies should be used.

Methods

Seven subjects of the university in the age group of 25 to 62 years were included in the monitoring in the first task. The height and weight were measured in standard way and the BMI was calculated. BMI mean was 23,05 ± 5,86. All individuals were people having average values of biological parameters. The Tanita MC 180 MA device was used.

Device Tanita MC-180 MA is able to measure on frequencies 5 kHz, 50 kHz, 250 kHz and 500 kHz. It is also possible to do segmental measurements.

All individuals were measured in these conditions: normal conditions, application of water, solution saline, EEG gel, hand cream with oil hand application, oil free hand cream hand application, hand cream with oil hand and foot application, oil free hand cream hand and foot application, oil free hand cream and water based foot cream. For better outcome every measurement was doubled and average values were used.

In the second task, multi-frequency eight-electrode approach of body impedance was considered. BIA was carried out on the following frequencies: 5 kHz, 50 kHz, 250 kHz and 500 kHz.

Results

Results that were measured and observed during changes of conditions are shown in tables one and two. For better understanding also change of body fat % and resistance is shown in Figure 2 and Figure 3.

1) The results of the first set of measurements show that values confirm the hypothesis that the level of body composition can by influenced by measurement conditions. If we consider the first measured values in table 1 is 100% then the values of other measurements vary between 102.49% and 76.42%.

Tab. 1: Changes of body fat % depending on conditions

Body fat %	Patients						
Meas no	1	2	3	4	5	6	7
1	22,05	3	6,15	37,2	24,7	11,3	21,6
2	22,6	3	6,05	37,45	24	11,05	20,9
3	22,15	3	5,8	37,45	23,85	11,1	20,8
4	22,2	3	5,6	36,4	22,95	10,9	20
5	22,1	3	6,05	37,5	24,05	11,25	20,9
6	21,7	3	4,8	37,8	22,9	11,25	20,8
7	22,45	3	4,7	37,55	24,85	11,35	21,6
8	21,9	3	5,15	38,05	24,35	11,15	20,55
9	21,5	3	5,6	37,8	24,3	10,45	19,5

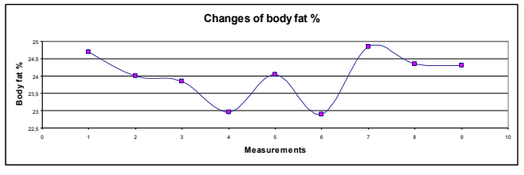

Fig. 2: Changes of body fat % depending on conditions.

Tab. 2: Changes of body fat % depending on conditions

Resistance	Patients						
	1	2	3	4	5	6	7
1	349,4	546	468,9	501,8	594,9	466,6	723
2	355,6	520	468,3	504,3	585,5	463,5	711
3	351,5	533	466,0	504,5	583,9	463,8	710
4	352,2	519	464,6	489,6	572,3	461,6	698
5	350,0	534	469,2	504,9	586,8	466,0	712
6	345,8	534	464,6	508,8	572,6	465,6	710
7	355	534	464	505,7	597,4	467	722
8	349,2	526	469,2	513,8	591,0	465,3	706
9	344,6	525	472,9	509,9	590,3	457,5	697

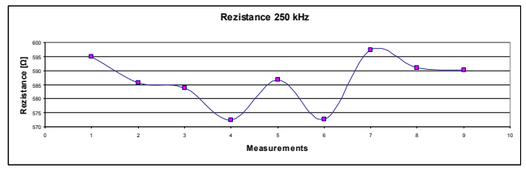

Fig. 3: Changes of resistance depending on conditions.

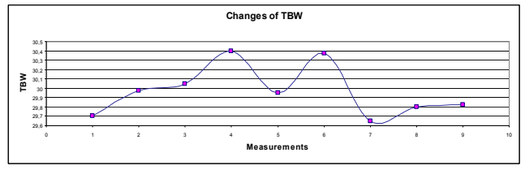

Fig. 4: Changes of TBW depending on conditions.

Tab. 3: Changes of resistance(Ω) depending on conditions

Changes of resistance(Ω) depending on conditions				
Meas no.	R(5kHz)	R(50kHz)	R(250kHz)	R(500kHz)
1	474,65	398,8	349,4	338,45
2	482,8	405,35	355,6	344,15
3	479,9	402,3	351,55	340
4	481,45	402,65	352,2	340,95
5	475,35	399,15	350,05	338,8
6	470,2	394,5	345,8	334,45
7	482,6	405,1	355	344,2
8	476,5	399,45	349,25	337,95
9	470	393,65	344,6	333,25

Although the differences in some cases are not very high it is obvious that conditions can have influence on outcome values. It is also shown that values obtained from persons with low body fat can be biased. Some creams and moistures can dramatically change contact conditions between hand foot and device electrodes.

As shown in Tables 1 and 2 changes in body fat and impedance between measurements differ in range from 4,43% to 21,95% . This shows that knowledge of application of various creams and lotions can be very important.

In Figure 4 changes in total body water (TBW) are shown. These changes correspond to changes of condition as well but in negative correlation.

As show in table 3 changes in resistance differ depending on the conditions from these values from these values correlation have been made and best values for correlation have frequency of 250 kHz.

Conclusion

In this study we have proven that changes in measuring condition can change outcome values of measured subject. Differences between some measurements were significant. Resistance was changed every time those conditions were differed.

This leads to importance of exact specification of measurement conditions. Therefore the importance of patient and device status is necessary to know. In some cases the difference between normal status and status with sweat on hands and feet can play significant role in outcome values. It is necessary to know in which state the measurement is performed. Also the composition of sweat can be very important because sweat differs between patients. This is additional information necessary for correct evaluation. Otherwise the results of such a measurement can be biased.

It is shown that bioimpedance method is suitable for body composition evaluation. Also values of body fat, lean mass, total body water are accessible by this method. This method have better outcome than just BMI and can be easily used in various conditions and patients. This method is fast relatively cheap and has very good outcome values.

In future more measurements should be made to prove importance of measurement conditions in bioimpedance technique. Also further standatization in this field of body composition should be made because no standardization is made nowadays.

Acknowledgement

This research and implementation work has been supported by SGS10/279/OHK3/3T/13 and FRVS 110065.

References

[1] Dympna Gallagher, Steven B Heymsfield, Moonseong Heo, Susan A Jebb, Peter R Murgatroyd, and Yoichi Sakamoto *Healthy percentage body fat ranges: an approach for developing guidelines based on body mass index1* Am J Clin Nutr 2000;72:694–701

[2] Linda Paniagua, Vitool Lohsoonthorna, Somrat Lertmaharit,Wiroj Jiamjarasrangsi, Michelle A. Williams(2008) *Comparison of waist circumference, body mass index, percent body fat and other measure of adiposity in identifying cardiovascular disease risks among Thai adults*. Obesity Research & Clinical Practice (2008) 2, 215—223.

[3] Nayeli Macias, Heliodoro Alemán-Mateo, Julián Esparza-Romero and Mauro E Valencia(2007) *Body fat measurement by bioelectrical impedance and air displacement plethysmography: a cross-validation study to design.* Nutrition Journal 2007, 6:18 doi:10.1186/1475-2891-6-18

[4] Kentaro Shoji, Kazuhisa Maedaa, Tadashi Nakamura, Tohru Funahashi, Yuji Matsuzawa, Iichiro Shimomura(2008) *Measurement of visceral fat by abdominal bioelectrical impedance analysis is beneficial in medical checkup.* Obesity Research & Clinical Practice (2008) 2, 269—275

Jan Hlubik
CTU in Prague department of cybernetics
Faculty of Electrical Engineering
Technicka , Prague
E-mail: hlubikjan@post.cz
tel: +420 22435 5769

THE STRUCTURAL DESIGN AND USE OF HIGHER FORMS OF CONTROL IN REHABILITATION DEVICES

Marián Veseliny[1], Boris Jobbágy[2], Marek Fodor [3], Miloslav Feriančik[4]

[1,2,3,4] Mechanical Engineering Faculty, Technical University of Košice, Slovakia

Abstract

Although the area of artificial intelligence is still progressing, its use in different areas is still insufficient. This article discusses the use of higher forms of control in rehabilitation devices (specifically, the neural networks). Then the article deals with problems of structural design. This proposal is based on the requirements of the rehabilitation process, which must be guaranteed maximum patient safety. This proposed device uses various modern elements. The device will be powered by unconventional actuator, represented by pneumatic artificial muscles.

Keywords

Artificial intelligence, neural networks, JavaNNS, pneumatic artificial muscles, rehabilitation device, construction, exoskeleton

Introduction

The article discusses the use of artificial intelligence in rehabilitation devices. Modern rehabilitation device is designed to replace the work of rehabilitation staff. The process of rehabilitation is increasingly being provided by rehabilitation staff. With the increase in human population is continuously increasing the number of patients. One solution to this situation is a modern rehabilitation device to facilitate the work of rehabilitation staff, or replace them completely. Rehabilitation itself is time-consuming process and personnel. It affects a number of factors such as patient health status, type of damage etc.

This article describes the possibilities of artificial intelligence in modern rehabilitation devices. It is mainly the implementation of neural networks to such device. The role of the neural network is to replace a part the decision in the rehabilitation process. Using a variety of inputs is designed to intelligently load change or rehabilitation program.

Simulations of neural networks were created in JavaNNS. Modern rehabilitation device created by combining a variety of advanced features, such as artificial intelligence and advanced unconventional propulsions. One of these actuators are also pneumatic artificial muscles. Their properties are broadly similar to human muscles. They are therefore suitable for use in the rehabilitation area. Soft and smooth movement needed for the rehabilitation can be done just by pneumatic artificial muscles. This will eliminate the need for constant presence of a rehabilitation staff. Furthermore, the article deals with the design variant design rehabilitation device for the rehabilitation of upper limb. It also deals two proposed design options rehabilitation device.

Rehabilitation devices in present

In spite of major advances in the section of automation is currently in rehabilitation performed principally with the help of rehabilitation operator. This is of time consuming and unrealistic on given capacity. One solution of this situation is research automated rehabilitation devices, which replace work of rehabilitation worker. We know two method of rehabilitation, they are active or passive. With active rehabilitation the patient participate on implementation of exist movement, for example works against movement robot or copying their movement. With passive rehabilitation only robot perform movement, the patient does not perform any movement. Their nervous system "teach in" motion.

Most rehabilitation devices in present focuses on specifically muscle parts and want complex equipment, which could be used to rehabilitate more parts of the body. Essentially we can divide rehabilitation devices onto some groups:

Under rehabilitation body of part, on rehabilitation device practice:

- upper limbs
- lower limbs

- thorax

Under load on rehabilitation device:

- with zero initial load (suitable for patient after operation)
- with nonzero initial load

Rehabilitation device for rehabilitation upper limbs

Robotic device for rehabilitation of upper limb can be divided into:

- JOYSTICK
- EXOSKELETON

In the first case the patient is secured to the arm structure similar to a joystick. Joystick / lever arm to lead positions in accordance with training plan.

In the latter case is a construction attached to the patient. The upper extremity is placed in the exoskeleton. The rehabilitation device may be a stand that serves as a carrier of the structure.

The structural design of rehabilitation device

In order to propose the construction of rehabilitation device, we must first know the requirements of the rehabilitation process. In our case, the rehabilitation of upper limb, which will be powered by artificial muscles. Since we want to rehabilitate the upper limbs, it is appropriate to the patient during rehabilitation was sitting. The draft design options are considered and appropriate design seats. The following steps are described in two variants. Before proposing the first variant, we know design requirements were as follows:

• design must be Easy to install

• for the rehabilitation is necessary to reach 4 degrees of freedom (arm joint 3 ° and 1 ° elbow)

• the possibility of rehabilitation of both upper limbs

•configurability device applicable to different populations.

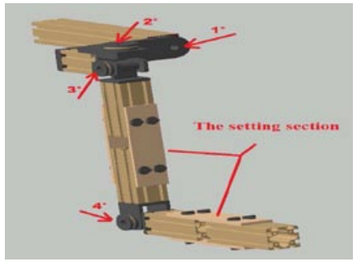

Fig.1: The structural design variants No.1

This structure (shown in Figure No. 1) consists of standard aluminum profiles, which are in terms of low weight and simple application suitable. Aluminium profiles are connected with each part of the adjustment, which allows setting of different sizes of the upper limb. Since this is a rehabilitation device based on artificial muscles, it is necessary to solve the structural design of storage (PAM) muscles. In the design of variant 1 are placed pneumatic artificial muscles at the back of seats and rotation of the joints will be performed by a steel cable attached to the roller. [1]

Variant No. 2 is also designed on the principle of exoskeleton. The device has 4 degrees of freedom of movement. Each joint is powered by a pair of pneumatic muscles that are involved in antagonistic and are connected at joints with cable transfers. Muscles for each joint are placed directly in the design of exoskeleton. Using screws, the exoskeleton can be adapted for different size limbs.

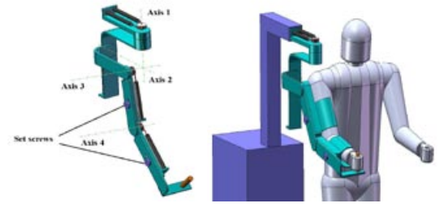

Fig. 2: The structural design variants No.2

Figure No. 2 shows a patient who has a construction rehabilitation devices connected to the right hand. The device is suspended on adjustable stand.

Modern rehabilitation devices

Still missing a device that can respond flexibly to change the various conditions. It therefore seems to be a combination of rehabilitation devices with artificial intelligence, like a good solution. The combination of unconventional actuators and artificial intelligence can build the future of modern rehabilitation device that can respond flexibly to a variety of new situations.

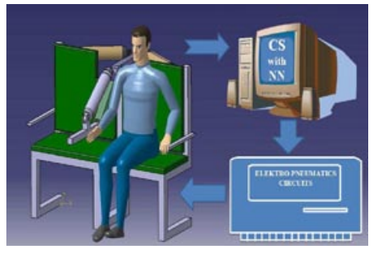

Fig. 3: Modern rehabilitation device, using artificial intelligence and unconventional drives

Figure No. 3 shows a modern rehabilitation device that uses elements of artificial intelligence and unconventional actuators. Description of device:

CS – Control system

NN – Neural network

Electro-pneumatics circuits

The device works as follows: Information is gathered by various sensors. Then they are sent to the control system and neural network. NN gives rise to a control system that sends a control instruction for electro-pneumatic circuits that perform the actual movement of a rehabilitation device. Movement a rehabilitation device is represented by pneumatic artificial muscles. Rehabilitation device must of course have various security features. An example of a security system is described in the publication: "Real-time bezpečnostný systém v automatizovaných rehabilitačných zariadeniach" [2].

Control system

An example of a control system without the neural network is shown in Fig. (Fig. 4)

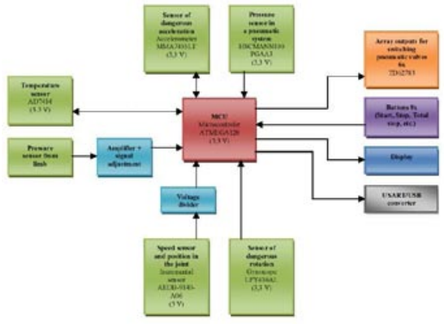

Fig. 4: Blok diagram of control part

The activity of the proposed control system is described by other investigators of the project. Part of the proposed control system is described in: "Design of the control system for rehabilitation device of upper arm" [3].

The most important part of the inputs to the control system mainly consists of inputs from sensors. Sensors placed directly onto the structure, or outside, provide important information needed for control. These sensors include:

- Pressure sensor
- Temperature sensor
- Sensor of dangerous acceleration (Accelerometer)
- Speed sensor (Incremental)
- Sensor of dangerous rotation (Gyroscope)
- and other

Neuron networks in a rehabilitation devices

One possible application of artificial intelligence in a rehabilitation device is the use of neural networks (NN) for the control of a rehabilitation device. It is a part of the control system. NN with input by the sensors provides information control system that performs the actual action and controls rehabilitation device. The NN control system is able to evaluate whether a change is needed load. Modern rehabilitation device is available from the beginning of rehabilitation and is also suitable for patients immediately after surgery. It is used mainly feature NN learn during the process. While rehabilitation is able to detect improvement of physical properties and react by increasing patient load.

Inputs and outputs

When designing a NN learning is the most important definition of inputs and outputs related to them. Neural network decides on the basis of these parameters: speed, load, direction, angle and others. Using these inputs neural network generates outputs.

Tab. 1: Inputs and outputs NN

VSTUPY	VÝSTUPY
SPEED_T	LOAD_1
SPEED_T-1	LOAD_2
LOAD	LOADD_3
PROGRAM	PROGRAM_1
DIRECTION	PROGRAM_2
DIRECTION_T	PROGRAM_3
DIRECTION_T-1	STOP
ANGLE	
PULZ	

Simulation of neural network in JavaNNS

The JavaNNS (JavaNeuralNetwork Simulator) is a program based on its predecessor SNNS (StuttgartNeuralNetwork Simulator). This is the NN simulator. In JavaNNS is improved graphical interface and is much simpler than its predecessor. However, some parts were omitted.

The actual simulation is performed in the following steps:

- Preparation learning and test data
- The design of NN
- NN learning
- Testing the NN

Preparation of learning data is very difficult because it determines the entire functioning of the neural network. Design of the neural network is thanks to graphic interface simpler and more transparent. The proposed NN is shown in (Fig. 5):

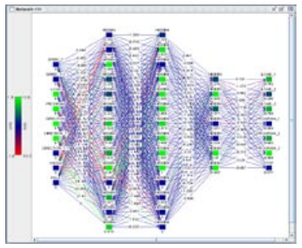

Fig. 5: The proposed NN with three hidden layer

The learning we can use different kinds of learning functions and the process of learning affects many adjustable parameters. Learning is assessed according to NN learning errors, which is shown in Error graph (Fig. 6).

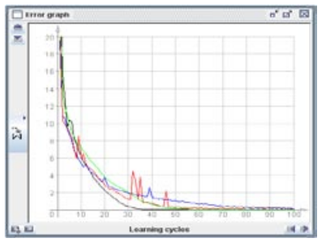

Fig. 6: Error graph with more learning function

The picture (Fig. 10) shows the error graph, which is the result of NN learning using various learning functions. Thus, the proposed NN is able to learn with an acceptable error learning. After learn NN comes the testing process. Evaluation of the NN testing performed on a comparison of actual and expected results. [4]

Conclusion

The combination of artificial muscles and elements of artificial intelligence seems like a promising development in modern rehabilitation device. This proposed rehabilitation device operates largely autonomously. These options meet the design requirements necessary for the rehabilitation process, which was previously entered. Both variants were simulated in the CAD programs, and they allow mobility shoulder and elbow. These devices are suitable for active and passive rehabilitation. Mastering the nonlinearity of pneumatic artificial muscles require advanced management systems. Using artificial intelligence, therefore, appears to be very appropriate. It is not however the only neural networks, but the application can certainly find other elements of artificial intelligence, such as neuro-fuzzy systems, genetic algorithms and fuzzy relational system. Simulation of the proposed neural network has demonstrated the possibility of using artificial intelligence in a rehabilitation device is a realistic perspective.

Acknowledgement

VEGA 1/1162/11 Theoretical principles, methods and instruments of diagnostics a rehabilitation of senior mobility, coordinator: prof. Ing. Dušan Šimšík, PhD.

The research work is supported by the Project of the Structural Funds of the EU, Operational Program Research and Development, Measure 2.2 Transfer of knowledge and technology from research and development into practice: Title of the project: Research and development of the intelligent non-conventional actuators based on artificial muscles ITMS code: 26220220103.

We are support research activities in Slovakia / Project is cofounded from sources of ES.

References

[1] PITEĽ, J., BALARA, M., BORŽÍKOVÁ, J. :Control of the actuator with pneumatic artificial muscles in antagonistic connection. Sborník vědeckých prací Vysoké školy báňské - Technické univerzity Ostrava. Vol. 53, no. 2 (2007), p. 101-106, ISSN 1210-0471

[2] RIGASOVÁ, Eva - ŽIDEK, Kamil, Real-time bezpečnostný systém v automatizovaných rehabilitačných zariadeniach, elektronický optický disk (CD-ROM). In: Automatizácia a riadenie v teórii a praxi 2012 : ARTEP 2012 : workshop odborníkov z univerzít, vysokých škôl a praxe v oblasti automatizácie a riadenia : 22. - 24. február 2012, Stará Lesná, SR. Košice : TU, 2012 S. 54-1-54-7. ISBN 978-80-553-0835-7

[3] ŽUPA, Tomáš - ŽIDEK, Kamil - LÍŠKA, Ondrej, Design of the control system for rehabilitation device of upper arm, Engineering Mechanics 2011 : 17th international conference : May 9-12, 2011, Svratka, Czech Republic. - Žďár nad Sázavou : ŽĎAS, 2011 P. 703-706. - ISBN 978-80-87012-33-8

[4] FISCHER, Igor, HENNECKE, Fabian, BANNES, Christian, ZELL, Andreas: Java Neural Network Simulator - User Manual, Version 1.1, Dostupné na internete: http://www.ra.cs.uni-tuebingen.de/software/JavaNNS/manual/JavaNNS-manual.html

Ing. Marián Veseliny
Department of Automation, Control and Human Machine Interaction
Mechanical Engineering Faculty
Technical University of Košice
Letná 9, 042 00 Košice
E-mail: marian.veseliny@tuke.sk
Phone: +421 55 602

MECHANICAL MODEL OF THE CARDIOVASCULAR SYSTEM: DETERMINATION OF CARDIAC OUTPUT BY DYE DILUTION

Miroslav LOŽEK, Markéta HORÁLKOVÁ, Jan HAVLÍK

Department of Circuit Theory, Czech Technical University in Prague, Czech Republic

Abstract
This paper deals with the experimental implementation of one of the methods for the determination of cardiac output – the dye dilution. Measurement is performed on a mechanical model of the cardiovascular system. It is a specific and experimental measurement intended mainly for educational purposes. It was created a real model of bloodstream at author's workplace. The model enables to set a pulsatile flow of the fluid with defined pressure and flow rate. This experiment is to demonstrate the principle of determination of cardiac output using the dilution methods. This paper is focused only on measuring by dye dilution method. The measurement results are verified by using a Doppler sonography and volumetric containers.

Keywords
cardiovascular system, cardiac output, dye dilution

Introduction

The cardiac output is a very important parameter that helps to diagnose cardiac insufficiency. The determination of cardiac output can be performed using low precision and limited non-invasive methods or high precision but costly and painful invasive methods. [5]

Basic non-invasive methods are Doppler sonography, bio-impedance cardiography and mathematical analysis. Educational demonstration of non-invasive measurement methods is very easy.

Invasive methods of measurement cannot be demonstrated on human being for educational purposes. Based on this fact a mechanical model of the cardiovascular system was developed. The model allows demonstrating the invasive measuring of bloodstream heamodynamic parameters.

This paper focuses primary on the determination of the cardiac output, detailed description of the mechanical model has been published. [1,2]

Principle of dilution methods

The fundament of dilution methods for determination of cardiac output is dilution of the injected substance in the blood. A substance can be special dye or saline with a defined concentration and temperature. There are two types of dilution measurements: the dye dilution method and the thermodilution method. [4,7]

Thermodilution method

This method involves the continuous measurement of the temperature of the pre-cooled blood. The clinical measurement is performed by the Swanz-Ganz catheter. This instrument provides cold saline (4 °C) injected into the blood and then distanced blood temperature measuring.

The result of this process is the thermodilution curve whose mathematic analysis gives value of the Cardiac output. [4,7]

Dye dilution method

The Dye dilution method is based on the measuring of the light absorbance of the dye injected into the blood. The dye (**I**ndo-**C**yanine **G**reen) is injected by special pulmonary catheter. Dyed blood is continuously sucked into the absorption photometer.

$$CO = \frac{Volume_{\,Dye\ Injection}}{Concentration_{\,Relative}} \qquad (1)$$

The result is the dilution curve of the relative concentration of the dye diluted with the blood. Analysis according to equation (1) gives value of the **C**ardiac **O**utput. [4,7]

Mechanical model of the cardiovascular system

The mechanical model of the cardiovascular system was developed for educational purposes at author's workplace. It consists of tubes, valves and a mechanical pump (see Fig. 1). [1,2,5,6]

Various types of the tubes are used for the construction of the arterial, venous and capillary bloodstream. The parameter compliance of the tubes is very important for correct function of the model. Venous vessels are rigid and arterial vessels are elastic. [2]

Hydraulic resistance of the bloodstream is controlled by regulated valve. Aortic valve and minor venous valves are demonstrated by the check valves.

The heart is constructed using a mechanical gear pump. The pump is driven by the pulse mode using special control unit consists of the microprocessor and switching devices. It is possible to choose optional heart rate and heart ratio (power of the pump). [1-3,5]

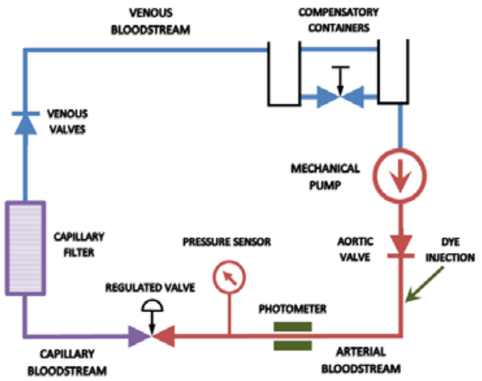

Fig. 1: Overview diagram of the model CVS.

Experimental measurement of the cardiac output

Selection of the type of the dye and its spectral band

First of all, it was necessary to choose the right type of the dye and to tune a suitable spectral wavelength of the photometer. The photometer was constructed of a pair of the IR diode and IR photodiode (λ = 900 nm). It is given by wide availability of these components. Spectral analysis of different types of the dye proved a suitability of the use the Copper sulfate (see Fig. 2).

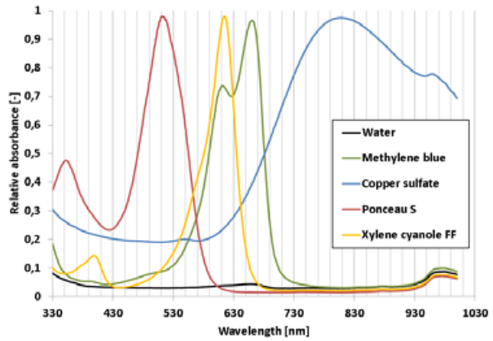

Fig. 2: Spectral analysis of the dyes.

Design of the measuring apparatus

The light source is an infrared light emitting diode with maximum intensity at 900 nm wavelength. For the first experiment it was fully sufficient to supply the light source by constant current. The light passes through arterial vessel and excites the light detector.

The detector is light-sensitive diode with maximum sensitivity at 900 nm wavelength. The photodiode operates at the photovoltaic mode. The output voltage is dependent on light intensity on the detector. The output voltage is amplified by an op-amp and then is sampled into the digital form.

Clean fluid flow does not affect to passage of the infrared beam. The fluid flow with injected dye causes attenuation of the IR beam. It is dependent on concentration of the dye with the fluid.

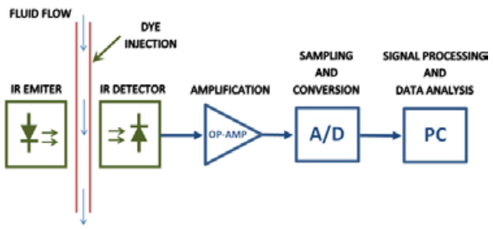

Fig. 3: Measuring diagram

Signal processing and data analysis

The data processing is performed by the Matlab script. Firstly, the data was loaded and the useful components were separated. For very credible demonstration it is measured also blood pressure curve. The data must be converted to the pressure scale.

The calculation of the cardiac output according to the equation (1) is valid only with relative values of the concentration. Reference values are used to relative scale conversion. The reference minimum is the attenuation of the clean fluid flow. The reference maximum is the attenuation of the dye liquid only.

The relative concentration curve is integrated using the cumulative sum. The proportion of the injected dye volume and cumulative sum of the relative concentration values is equal to the cardiac output.

Results of the measuring

Measuring is usually carried out with various settings of the Heart rate and the Heart Ratio parameters. The validation of the results is ensured by the measuring using the Doppler sonography and the volumetric containers. [1,2] The verification is carried out at the same Heart Rate and Heart Ration parameters. Test measurement was performed tree times for each parameter of the model. The results are shown in Tab. 1.

Tab. 1: Result of the measuring with verification.

Model parameters		Cardiac output [ml/min.]		
Heart Rate [bpm]	Heart Ratio [%]	Volumetric containers	Doppler sonography	Dye dilution
55	30	0.450	0.457 (1.6 %)	**0.429 (4.7 %)**
55	70	1.000	1.127 (12.7 %)	**1.171 (17.1 %)**
125	30	0.400	0.462 (15.5 %)	**0.417 (4.3 %)**
125	70	0.950	1.020 (7.4 %)	**1.115 (17.4 %)**

The Matlab script plots dye dilution curve and pulsatile blood pressure curve to the educational compared (see Fig. 4). On the figure is clearly noticeable time point of the dye injection.

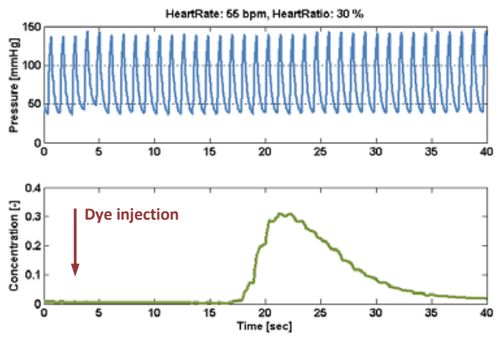

Fig. 4: Dye dilution curve vs. blood pressure curve

Verification methods

This paper is not targeted at the detailed description of the model CVS or Doppler sonography measurement. The next section deals only brief description of the verification methods using Doppler sonography and volumetric containers.

Validation using volumetric containers is very simple and indisputable. It is monitored the quantity of the liquid, which passed through the pump per minute. The accuracy of the validation depends on the correct calibration of the measuring scale of the container.

Validation using Doppler sonography is very similar to clinical determination of the cardiac output. The probe is attached on the tube within fluid flow. This leads to record a velocity profile of the fluid flow (see Fig. 5). The integration of this profile and cross section area multiply give a value of the cardiac output. The data processing performs Doppler sonography device itself.

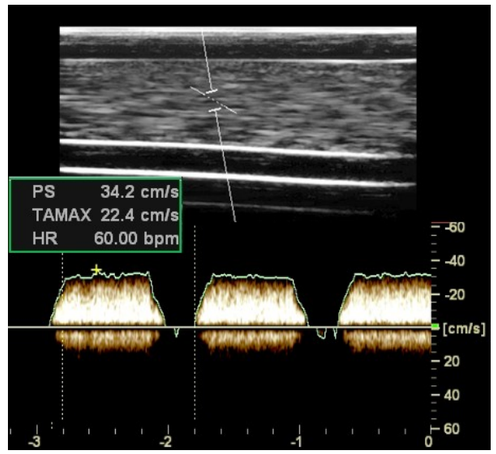

Fig. 5: Example of the measurement of velocity profile on the model CVS by the Doppler sonography device.

Conclusion

The simple model of the cardiovascular system was developed for educational purposes. The model is able to simulate pulsatile fluid flow. Students can measure invasive pulse pressure curve, cardiac output by invasive and non-invasive methods (the doppler sonography and the dye dilution).

The presented method helps the better and the practical understanding of the invasive measurement of the cardiac output, because it is very similar to the clinical determination of the cardiac output. This exercise learns to apply the theoretical equations into the practical measurement.

Relative accuracy of the measurement of the cardiac output is about 15 %. Moreover, it is possible to watch the difference of laminar and turbulent flow by the sonography method on the model.

Acknowledgement

This work has been supported by the grant No. F3a 2177/2012 presented by University Development Foundation and also by the research program No. MSM 6840770012 of the Czech Technical University in Prague (sponsored by the Ministry of Education, Youth and Sports of the Czech Republic).

References

[1] LOŽEK, M.: Model of the Cardiovascular System: Pump Control. *In Proceedings of the 16th International Student Conference on Electrical Engineering Prague*. 2012. ISBN 978-80-01-05043-9.

[2] LOŽEK, M. - HAVLÍK, J. - HORČÍK, Z.: Návrh mechanického modelu kardiovaskulárního systému : *Sborník příspěvků, Letní doktorandské dny*. Praha. 2012. ISBN: 978-80-01-05050-7.

[3] HAVRÁNEK, A.: Klasická mechanika II. *Kontiuum*. Karolinum, 2003. ISBN 80-246-0627-5.

[4] BATZEL, J. J. - KAPPEL, F. - SCHNEDITZ, D. - TRAN, H. T.: Cardiovascular and Respiratory Systems: Modeling, Analysis, and Control. 2006. ISBN 978-0898716177.

[5] WESTERHOF, N. - STERGIOPULOS, N. - NOBLE, M. I. M.: Snapshots of Hemodynamics. *Basic Science for the Cardiologist*, 2005.

[6] COBELLI, C. - CARSIN, E.: Introduction to modeling in physiology and medicine. *Academic Press*.2008. ISBN:978-0-12-160240-6.

[7] LE ROLLE, V. - HERNANDEZ, A. I. - RICHARD, P.Y. - BUISSON, J. - CARRAULT, G.: A Bond Graph Model of the Cardiovascular System. *Acta Biotheorica*, 2005.

Miroslav Ložek
Department of Circuit Theory
Faculty of Electrical Engineering
Czech Technical University in Prague
Technická 2, CZ-166 27 Prague

E-mail: lozekmir@fel.cvut.cz
Phone: +420 224 355 869

AUTOMATIC SEGMENTATION OF PHONEMES DURING THE FAST REPETITION OF (/PA/-/TA/-/KA/) SYLLABLES IN A SPEECH AFFECTED BY HYPOKINETIC DYSARTHRIA

Michal Novotný, Jan Rusz, Roman Čmejla

Czech Technical University, Faculty of Electrical Engineering, Prague, Czech Rep.

Abstract
Hypokinetic dysarthria is a common manifestation of Parkinson's disease (PD). Articulation characteristics can provide useful information to distinguish dysarthric speakers from healthy subjects and monitor the severity of disease and treatment effects. The aim of this study was to design an algorithm for automatic segmentation of consonants and vowels based upon a rapid steady /pa/-/ta/-/ka/ syllable repetition. All syllables were manually labeled at three positions including explosion (E), vowel (V), and occlusion (O). In addition, the representative measurement of voice onset time (VOT) was included as difference between V and E position. When compared to the manual labeled positions, the VOT is detected within the range 5ms to 20ms with a range of a success rate of 68.2 - 90.5%, 44.1 - 75.2%, and 57.2-83.5% for normal, dysarthric, and all speakers. In conclusion, this study shows that algorithm based on the spectral, Bayesian, and polynomial approaches, that can be used to accurately detect the positions of consonant and vowels in normal and dysarthria-related utterances.

Keywords
Parkinson's disease, dysarthria, articulation, diadochokinetic

Introduction

PD affects dopaminergic pathways from substantia nigra to putamen. This causes dopaminergic striatal loss which leads to motoric disorders. Four basic symptoms are tremor, muscular rigidity, akinesis or bradykinesis and stooping unstable posture [1].

According to published study [2], speech pathologies occurred in 70-90% of cases. This speech disorders could be one of the first PD symptoms [2]. Three grades of dysarthria are defined as mild, moderate and severe [3].

This work is aimed to evaluation of mild articulation disorders. For this purpose the diadochokinetic (DDK) task was used. In this exercise are patients asked to repeat the sequence of syllables /pa/-/ta/-/ka/ as fast and as long as possible.

In this paper we are concerned with the segmentation of utterances obtained in DDK task and it's intention is to create an algorithm which will automatically label important positions in the signal. Important positions are beginning of explosives (/p/, /t/, /k/) (E), beginning of the vocal (V) and end of the vocal (O). With known positions of E, V and O can be estimated other characteristics like harmonic to noise ratio, fundamental frequency F0,…

Methodics

Data

Data used for the algorithm design is part of the earlier study [4], within which 46 utterances of native speakers were collected, of which 24 (20 men and 4 women) were diagnosed with early PD stage and their records were created before pharmaceutical treatment. Data of the healthy control group (CG) is acquired from 22 participants (15 men and 7 women) without any neurological disorders.

In terms of the study [4] were recorded DDK task utterances, in which were participants asked to repeat the sequence of syllables /pa/-/ta/-/ka/ as fast and as long as possible [5].

The final training database consists of the 80 records set (1644 syllables /pa/, /ta/ or /ka/), of which 40 (753 syllables) records are PD and 40 records are CG (891 syllables).

Phoneme boundaries

For the purposes of the utterance automatic analysis is necessary to cut the speech record and detect three basic positions. The first position is explosion (E),

beginning of consonants (/p/, /t/, /k/), which is characterized by the release of the oral closure and by the increase of the explosive noise energy.

The second position is beginning of the vowel (V), which represents beginning of the vocal cord vibration. The last one is occlusion (O), which marks voicing end in the signal. One syllable /pa/ with marked positions of E, V, and O is shown on the figure 1.

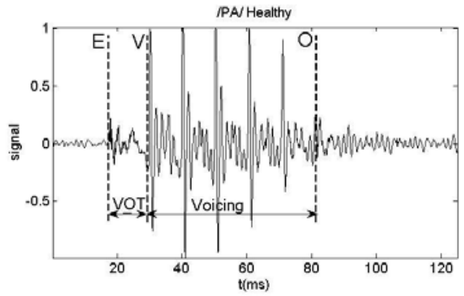

Fig. 1: One labeled syllable recorded from a healthy participant.

Signal segmentation

Due to unknown number of syllables in individual signals is more effective to split the signal into smaller segments containing only one position E, V and O, at first. This results in approximate borders of syllables in the signal.

At the beginning is the signal re-sampled to the sampling frequency fs = 16kHz and filtered by lowpass filter with bandwidth of 300Hz and second one with bandwidth of 1100Hz. This gives two filtered signals on which the peak detector is applied. This peak detector is defined as

$$s(n) = (1 - k(n))|y(n)| + k(n)s(n-1),$$

where the $|y(n)|$ means absolute value of the n-th sample of the signal and the $k(n)$ is defined as

$$k(n) = \begin{cases} 0.9 & |y(n)| < s(n-1) \\ 0.997 & |y(n)| \geq s(n-1) \end{cases}.$$

The peak detector outputs are smoothened by the moving average filter and normalized. Through the smoothened signals are searched local maxima with minimal distance of 800 samples. This procedure helps to prevent false detections.

The vector of found positions in the signal filtered by 1100Hz filter is taken as the initial and is amended by the positions gained from the signal filtered by the 300Hz filter.

The widest range between two locations is computed from this vector. This value is furthermore widened by few samples, which gives the final range of one segment. This range is than divided in the exact ratio which gives approximate borders of syllable shown on the figure 1.

Detection of the explosion

The detection of the E is realized only on the part of the segment, which precedes the position of the local maxima found by the previous segmentation. It is based on the filtration of the spectrogram which is considered to be the matrix **P** with m rows and n columns. For the peak highlight the filtration threshold for each row is computed as weighted average of all values in this row. Every value in the row smaller than this value is set zero and every value higher is kept.

Two energetic envelopes are obtained by the summation of values in each column. The first one is summation of all values and the second one is summation of the values above the 1500Hz. The next step is computation of the centroid for each envelope and elimination of signals with inconvenient position of centroids. In the energetic envelope of the whole filtered spectrogram is then found the approximate position of V and if this position is too underhung the borders of the segment will be moved to avoid missing real position of E behind borders of the segment.

The explosion is than searched in the energetic envelope of frequencies above 1500Hz, because high energy of the vocal on the lower frequencies hides the E peak. This method is illustrated by figure 2.

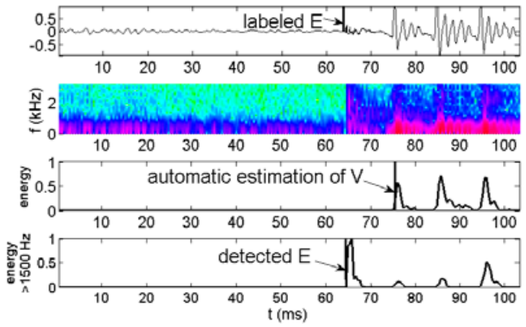

Fig. 2: Principle of the E detection, from the top, labeled part of the signal, spectrogram, energetic envelope for the whole signal and energetic envelope of the signal above 1500Hz.

Detection of the vocal beginning

The V detection counts with rapid growth of the signal energy, which is detected by Bayesian step changepoint detector [6]. Local maxima in the output of BSCD are found and then the one accordant to the position of V is chosen. The selection is based on the shape of the output, because of which we can assume

that peak following the longest gap is the peak matching to the position of V. For the better insight see figure 3.

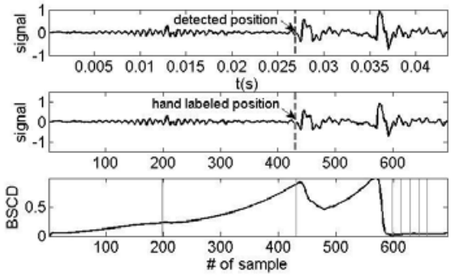

Fig. 3: Methodic of the V detection on the bottom part is shown the BSCD output.

Detection of the vocal ending

The principle of the O detection is to find the flexible threshold, which will optimize itself according to the shape of the signal. Signal is filtered by lowpass with 500Hz bandwidth at first. Next the square of the signal is computed.

The threshold is made by inverted polynomial approximation of the ninth order, which is also moved by the offset computed as two times the average value of the signal energy. This threshold can be written as

$$treshold = \prod_{i=1}^{9}(a_i x + b_i) + 2\bar{x},$$

where the x is a vector of the x axis values with firts value equal to one and with length equal to length of the searched segment. Coefficients a_i and b_i are coefficients of the i-th order of the polynomial and $\bar{x}$ is average value of the signal energy. This threshold is shown on the figure 4.

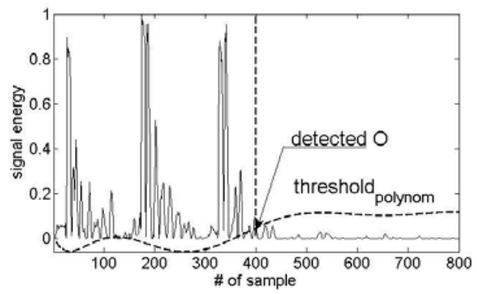

Fig. 4: Detection of the O by the inverted polynomial threshold.

Appraisal of the results

The appraisal of the detection results was made due to the whole count of syllables, not as the appraisal of the single signals. Automatically detected positions were compared to the hand labeled E, V and O positions. The difference between detected and hand labeled positions confronted with three thresholds (5ms, 10ms, and 20ms) and as successful detection was marked value smaller or equal to this threshold. The percentage rating was computed due to the whole number of syllables.

For the VOT evaluation were the differences between detected and hand labeled lengths of VOT compared to the same thresholds as the single E, V and O. For the better view of achieved results the figure 5 is appended.

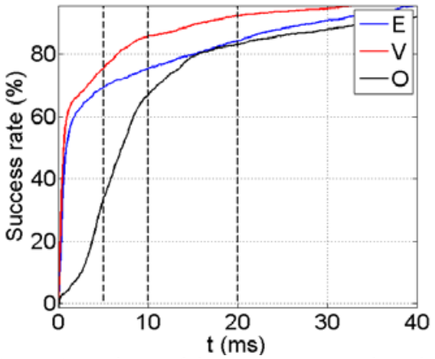

Fig. 5: Dependence of the success rate on the value of the threshold with highlighted 5m, 10ms and 20ms.

Conclusion

It is possible to roughly compare success of the VOT detection with works [7] and [8]. The study [7] is aimed to evaluation of the VOT length for the purpose of the accent distinction. For the comparison were used results of American English native speakers because of their similarity to our data. Correct detections (difference less than 10% of the length) were made in 74.9% of all cases and the average difference of the correct detections is 0.735ms [7]. Our algorithm gives worse score of 57.2% and 1.273ms. Results published in the paper [8], which deals with measurement of the voiced and unvoiced consonants (/b/, /p/, /d/, /t/, /g/ and /k/), are for the 10ms threshold 72.6% and 87.8% for the 20ms threshold. Our results are 68.1% for 10ms and 83.5% for 20ms threshold.

During the comparison is necessary to consider different purposes of each work. For the comparison were used speaker with the most similar accents, however still different. The next limit is presence of PD, which aggravates our results.

The algorithm presented in this paper worked with the strongest 5ms threshold for all participants E, V and VOT at s_E = 64.0%, s_V = 71.2% and s_{VOT}=57.2%. The success rate of the O for all participants for more relevant 10ms threshold is equal to s_O=64.6%. These rates are satisfactory and comparable to other two works, however further improvement is necessary to increase robustness in PD cases.

Currently, all three detections work independently on each other, this gives space for the additional improvement by feedback control. Length of the VOT can be compared to physiological values and in the case that detected VOT is out of bounds positions can be re-estimated. Improvement of the O detection can be achieved through the algorithm for the automatic estimation of the ideal polynomial approximation order. In current time the order is set to fixed empirical value which is not ideal in all cases.

Acknowledgement

The work has been supported by research grants SGS12/185/OHK4/3T/13, GACR 102/12/2230 and NT 12288-5/2011 and by the research program MSM 0021620849 and MSM 6840770012.

References

[1] Rodríguez-Oroz, M., C., Jahanshahi, M., Krack, P., Macias, R., Bezard, E., Obeso, J., A.: *Initial clinical manifestations of Parkinson's disease: features and pathophysical mechanisms*. The Lancest Neurology, 8 (12), 1128 – 1139,2009.

[2] Duffy, J., R.: Motor Speech Disorders: Substrates, Differential Diagnosis and Management. 2nd ed. Mosby, New York, NY, 2005 pp. 1 – 592.

[3] Darley, F., L., Aronson, A., E., Brown, J., R.: *Differential diagnostics patterns of dysarthria.* J. Speech. Hear. Res., 12, 426 – 496,1969.

[4] Rusz, J., Čmejla, R., Růžičková, H., Růžička, E.: *Quantitative acoustic measurements for characterization of speech and voice disorders in early untreated Parkinson's disease.* J. Acoust. Soc. Am., 129 (1), 350 – 367,2011.

[5] Fletcher, S.: *Time – by – count measurement of dyadochokinetic syllable rate.* J.Speech. Hear. Disord., 15, 757 – 762, 1972.

[6] Čmejla, R., Sovka, P.: *Recursive Bayesian Autoregressive Changepoint Detector for Sequential Signal Segmentation.* EUSipco Proceeedings, Wien (2004), 245 – 248.

[7] Hansen, J., H., L., Gray, S., S., Kim, W.: *Automatic voice onset time detection for unvoiced stops (/p/, /t/, /k/) with application to accent classification*. Speech Comunication, 52, 777 – 789, 2010.

[8] Stouten, V., Van Hame, H.: *Automatic voice onset time estimation from reassignment spectra*. Speech Communication, 51, 1194 – 1205, 2009.

Ing. Michal Novotný
Department of Circuit Theory
Faculty of Electrical Engineering
Czech Technical University in Prague
Technická 2, CZ-166 27 Praha 6 – Dejvice

E-mail: novotm26@fel.cvut.cz
Phone: +420 776 643 155

A PHONEME CLASSIFICATION USING PCA AND SSOM METHODS FOR A CHILDREN DISORDER SPEECH ANALYSIS

Josef Vavrina, Pavel Grill, Vaclav Olsansky, Jana Tuckova

Czech Technical University, Prague, Czech Republic

Abstract
Mathematical-engineering methods described in the paper are oriented towards the analysis of disordered children's speech with the diagnosis of Developmental Dysphasia (DD). The paper is divided into three parts. The first one shows briefly our aim to classify consonants using Supervised Self-Organizing Maps (SSOM). The second part is about phoneme parameterization using Mel-Frequency-Cepstral-Coefficients (MFCC), Linear-Predictive-Coding coefficients (LPC) with Principal Component Analysis (PCA). A possibility of clusters visualization is used for a monitoring of disorder proportions and therapy success. The last part describes the importance of vocalic triangle for children with DD and connects the formant frequencies with the second part of the paper.

Keywords
phoneme detection, children speech, PCA, SSOM, vocalic triangle

Introduction

This paper deals with the detection and classification of phonemes (vowels and consonants) extracted from the children's speech. The classification uses two groups – phonemes obtained from utterances of healthy children and utterances of children with developmental dysphasia. The aim of this method is also a graphical representation of phonemes – cluster visualization. Graphic display in 2D or 3D is suitable for diagnose of disease by doctors. Analysis of layout and movement of the features in the SSOM can be one of the symptoms of the neurological disease identification. [1]

The topic is a part of a joint project of the Laboratory of Artificial Neural Network Applications (LANNA) from the Department of Circuit Theory in CTU FEE and the Department of Child Neurology of the Motol University Hospital. Our research in this area is focused on searching for the relation between clinical and electrophysiological symptoms of children with DD. Developmental dysphasia is one of the most frequently occurring neurodevelopment disorders affecting 5% of the paediatric population [2]. The condition is frequently defined as an inability to acquire and learn normal communication skills in proportion to age, even though there is adequate peripheral hearing, intelligence and absence of a broad sensor motor deficit or congenital malformation of the speech or vocal systems.

Utterances were created by clinical psychologist. The aim is the 2D or 3D phoneme representation, so it is necessary to do some dimension reduction of the input speech signal. The proper dimension reduction is parameterization. Parameterized segments of speech signal of particular vowels and consonants became input vectors. Different types of parameterization were used: LPC coefficients, MFCC and formant frequencies [3]. The second dimension reduction used in the paper is PCA [4] and SSOM [6], [7].

Phonemes characterization

It's important for correct classification to focus where consonants are created. They are created by so-called consonant articulation, it means that way for exhaled air is blocked and blowing air around this obstruction is started to ripple. Sound which was created has noisy character. Czech consonants are divided into a few groups according to their origin: explosives (b, d, g, k, t, m, n, p), fricatives (f, h, ch, ř, s, š, v, x, z, ž), sonors (r, l, j) and affricates (c, č). Vowels have a tonal character. They are characterized by the fundamental frequency and vowel formants, which are dependent on the shape of the basic wave tone (the method of vibration of vocal cords). Formants for individual vowels are different and characteristic for them. We distinguish vowels a, e, i, o, u in Czech [7].

Data and Software

Our database contains records of healthy children and children with DD from 8 to 10 years old. We collect data for pilot study from psychologists, speech therapists, neurologists, MRI and EEG records. Our goal is to objectify the degree of DD. There are 12 children with DD in the pilot study. The records contain isolated vowels, several syllabic words and also whole sentences. These records were labelled manually phoneme by phoneme. MFCC were

calculated from the labelled data - 16 MFCC, 20ms long, 50% overlap, Hamming window. 8 LPC were calculated with the same parameters as MFCC. The data of healthy children are used for training and validation, this set contains utterance of more than 60 children. The data of children with DD are used for testing [8].

We use formant analysis for the processing of speech pathology. The existence of formants can be related to the activity of the human brain and movements taking place in a person's articulatory system. FORANA [9] software was developed in the MATLAB. The software was developed to find the formant frequencies correctly. Standardly, the extraction of formant frequencies from speech signals was done by PRAAT [10] - acoustic analysis software. In the classification of formants the results obtained using this approach could not be treated as relevant. A decision was made to develop software, which would be able to classify formants with a minimal error rate. Another factor, which was taken into consideration in designing the FORANA, was the need to automate the process of extracting formants from the recorded speech signals.

The original program SOMLab was used for data processing [11]. Kohonen's SSOM were used for classification of consonants [5].

The original software SpeechLab package [12] in MATLAB was used for speech pre-processing. It is a complex system which was created as a user friendly application of the neural networks in prosody modelling of synthetic speech. The project consists of the tools necessary for utilizing neural networks in prosody modelling. Individual tools can be divided into three categories: pre-processing, processing and post-processing tools. We use pre-processing tool for data preparation, data creation and analysis.

Training ANN for consonants classification

Particular maps were trained separately for words with the same number of syllables and for recordings of children with the same age [1]. Co-articulation had important role at classification of formant frequencies. Explosives were found dominantly in these maps. It shows occurrence formant frequencies, which can be occurring by co-articulation effect of neighbouring vowels. Fig. 1 shows an example of one of the map.

Size of clusters was dependent at occurrence of particular consonant. It turned out during the comparing of maps that polysyllabic words have important role for children with DD.

Method of parameterization and dimension reduction

Principal component analyses which reduce dimensions, is used in method of vowel classification.

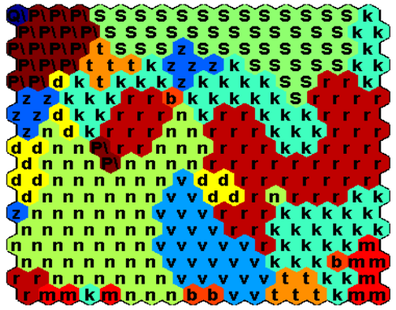

Fig. 1: MFCC, polysyllabic words

It is based on preserving first dimensions (PC – principal component), which contain a maximum information (the largest variance), and inhibiting higher PCs with less valuable information. It is not known in advance, if the MFCC and LPC contain the most information for vowel detection in their first PCs or whether the MFCC or LPC contain different information, which has high variance among speakers, which is not useful for vowel detection. The part of the paper is about finding the best PCs for vowel detection using MFCC and LPC.

Function of classifier

The method for finding the best PCs, is based on correct vowel clustering. The model for vowel classification divides the space into 5 sub-spaces according to 5 vowels in Czech. The space is divided by finding centroid for each vowel – mean of all segments of each vowel. Each new segment is classified to one vowel by finding nearest centroid. The method classifies whole vowel and not only segments. The final classified vowel is the one to which was assigned to most segments.

Finding PCs for parameterization MFCC and LPC

Training data set contains segments with 16 MFCC. If this space is transformed into new dimensions, which PCA produces, the new dimensions (PCs) variance is expressed in Tab. 1, which shows the information value of each dimension. For example, the first three dimensions preserve about 80 % of the original data.

Tab. 1: Amount of information in PCs using MFCC

PC	1	2	3	4	5	6	7	8	9	10	11	12	13	14	15	16
%	47	21	11	5	4	3	2	1	1	1	1	1	1	0	0	0

Individual dimensions may not properly classify vowels. The Tab. 2 summarizes the detection rate of correct classification of vowels for each dimension.

Tab. 2: Correct vowel detection for different PC selection using MFCC

PC	1	2	3	4	5	6	7
1	0,56	0,91	0,69	0,77	0,79	0,62	0,79
2	0,91	0,64	0,85	0,83	0,69	0,68	0,81
3	0,69	0,85	0,5	0,63	0,77	0,54	0,66
4	0,77	0,83	0,63	0,49	0,68	0,57	0,59
5	0,79	0,69	0,77	0,68	0,49	0,58	0,66
6	0,62	0,68	0,54	0,57	0,58	0,35	0,5
7	0,79	0,81	0,66	0,59	0,66	0,5	0,41

Columns and rows in Tab. 2 represent each dimension (PC). The diagonal is the value of correct classification of vowels (for just one dimension). Green cells show the largest values of the correct classification.

Tab. 2 shows that the best results are obtained with PC1 and PC2, respectively. The final model is shown in Fig. 2.

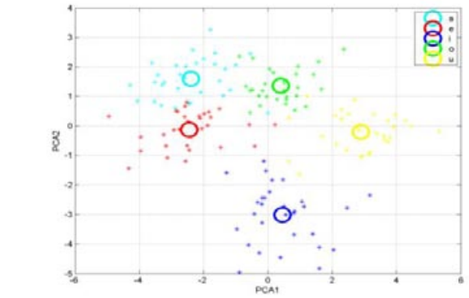

Fig. 2: Final model using MFCC

Circles represent the centroids and stars around them are the vowel of each child. The Fig. 2 shows that the clusters are separable. It corresponds to the large success of correct classification of vowels in Tab. 2. It is also important to note that vowel positions are similar to vocalic triangle.

The same method (the previous paragraphs) was used also for LPC. Similar graphs and tables show very different results for LPC. PC1 does not contain proper information for vowel classification, but also other PCs do not contain enough information for a high degree of correct classification (Tab. 4).

Tab. 3: Amount of information in PCs using LPC

PC	1	2	3	4	5	6	7	8
%	54	18	10	9	4	3	2	1

Tab. 4 does not contain high values of correct vowel detection and the best dimension is PC4. Combination of PC4 and PC5 reaches about 66 % of correct vowel detection. These two dimensions in Fig. 3 do not show good clustering and vocalic triangle is not preserved.

A comparison of the two parameterization shows that MFCC is preferable for the vowel detection by PCA. Without any modifications it achieved more than 90% successful vowel classification and the final model fits vocalic triangle, which is important for diagnostics.

Tab. 4: Correct vowel detection for different PC selection using LPC

	1	2	3	4	5	6	7
1	0,33	0,49	0,48	0,50	0,40	0,35	0,37
2	0,49	0,35	0,45	0,60	0,39	0,39	0,37
3	0,48	0,45	0,31	0,56	0,54	0,43	0,35
4	0,50	0,60	0,56	0,51	0,66	0,60	0,52
5	0,40	0,39	0,54	0,66	0,39	0,48	0,47
6	0,35	0,39	0,43	0,60	0,48	0,36	0,36
7	0,37	0,37	0,35	0,52	0,47	0,36	0,28

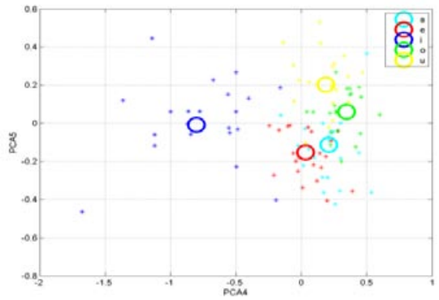

Fig. 3: Final model using LPC

A misclassification between phoneme "a" and "e" is not a serious mistake of classifier, it occurs also in healthy children speech, otherwise a misclassification between "e" and "o" or "i" and "u" is really serious mistake. The results of our previous work shows that these phonemes misclassification are one of the symptoms for DD. Vowel detection method using reduced MFCC proves to be a good method for determining the degree of DD.

Formants

Formants are defined as the spectral peaks of the sound spectrum of the voice. Variations in the basic tone of a person's voice and in the formants of the voice affect prosodic features. Changes to the speaker's basic tone of voice are interpreted as a change in speech melody. Changes to the first formant (F1) correspond to changes in the vertical movement of the speaker's tongue; changes to the second formant (F2) correspond to changes in the horizontal movement of the tongue; while the third formant (F3) changes with actions taking place in the nasal cavity. This means that the first three formants are most important when it comes to vowels (in the order of importance F2, F1 and

F3). Higher formants are identical for all vowels and they contain a significant portion of the information about the intonation of the speaker's voice. We get vocalic triangle as the correlation between F1 and F2 all of vowels (Tab. 5).

Tab. 5: Vocalic triangle [3]

Vertical position of palate	Horizontal position of palate					
		front		central	back	
	high	i,í				u,ú
	mid		e,é		o,ó	
	low			a,á		

Vowels detection and control of the accuracy

Sometimes during labelling children's speech signals that a specific vowel is detecting after listening to an entire word. After the calculation of formants and after the subsequent evaluation of this analysis is it often detected by other vowel. Correction and repair of detection the vowel is done by listening. On the tested sample of speech recordings obtained from healthy children, all of the vowels that were isolated in these recordings were analyzed and subsequently theirs classification by formant analysis. The Tab. 6 shows the parameters for each individual vowel, which were used to classify the vowel.

Tab. 6: Parameters for detection of vowels.

Parameters for detection of vowels	
vowel	formant's parameter
a	"F2-F1" and "F1-F0"
e	"F2-F1" and "F1-F0"
i	"F2/F1" and "F1-F0"
o	"F5/F1"
u	"F2/F1"

Vocalic triangle can be used to check the accuracy of calculation and classification of formant frequencies. Fig. 4 shows the wrong frequency range.

Conclusion

Our research involves an original method for the intensity of speech defect monitoring in child patients with DD. Phoneme classification is part of them. We were drawing upon a body of knowledge consisting of phonetics, acoustics and ANN applications. The PCA and SSOM were chosen for solving part of the project. The LPC reduced by PCA are not good parameterization for solving our problem with determining the degree of DD. The MFCC present much better results. It was shown, that the main

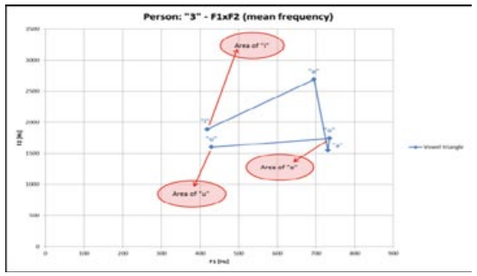

Fig. 4: Vocalic triangle with the wrong range.

information in MFCC contains useful data for vowel classification and it also corresponds with vocalic triangle. It will be probably less complicated to use directly vowel formants for vowel detection.

The consonants detection using SSOM for children with DD are in the beginning of our studies. The SSOM uncovered many results for vowel detection of children with DD, so we expect that the method will be useful also for consonant detection.

Acknowledgement

The work has been supported by research grant No. SGS SGS12/143/OHK3/2T/13 and by IGA MH CR agency, grant No. NT11443-5/2010.

References

[1] Tuckova, J., Komarek, V. Effectiveness of speech analysis by self-organizing maps in children with developmental language disorders. *Neuroendocrinology Letters*, 2009, **29 (**6), 939–948
[2] Dlouha, O., Novak, A., Vokral, J. Central Auditory Processing Disorder (CAPD) in Children with Specific Language Impairment (SLI). In *Int. Journal of Pediatric Otorhinolaryngology,2007,* **71** (6), 903-907.
[3] Psutka, J., Muller, L., Matousek, J., Radová, V.: *Mluvíme s počítačem česky,* Academia Praha, 2006, ISBN 80-200-0203-0.
[4] *Introduction to Machine Learning*, Ethem ALPAYDIN, The MIT Press, October 2004, ISBN 0-262-01211-1.
[5] Kohonen, T. *Self-Organizing Maps,* Springer–Verlag, 3rd edition, 2001.
[6**]** Vesanto, J., Himberg,J., Alhoniemi, E., Parhankangas J., 2000. *SOM Toolbox for Matlab 5,* Helsinki University of Technology, ISBN 951-22-4951-0. www.cis.hut.fi/projects/somtoolbox
[7] Palkova, Z. *Fonetika a fonologie češtiny*. Univerzita Karlova, Praha 1994, ISBN 80-7066-843-1.
[8] Zetocha, P. Design and realization of children speech database. *Ministry of Education grant FRVS, No.2453/2008*.
[9] Grill, P., Tuckova,J., FORANA. In: *Proc. of the Int. Conf. on Technical Computing Prague 2009*. Humusoft, Praha, 2009, pp. 32-39. ISBN 978-80-7080-733-0.
[10] PRAAT: doing phonetics by computer http://www.fon.hum.uva.nl/praat/.
[11] Tuckova, J., Bártů, M., Zetocha, P. *Aplikace umělých neuronových sítí při zpracování signal.* Česká technika, 2009, Praha. ISBN 978-80-01-04400-1.
[12] Tuckova, J., Santarius, J. Neural Network Program Package for Prosody Modelling. *In: Radioengineering,* April 2004, **13 (**1),17-21, ISSN: 1210-2512.

THE REAL-TIME VIZUALIZATION OF PNEUMOGRAM SIGNALS

Jan Sedlák[1], Roman Čmejla[1]

[1]Department of Circuit Theory, Faculty of Electrical Engineering, CTU in Prague

Abstract
The real-time visualization of pneumogram signals is described in this contribution. The device created provides simultaneous measurement of pneumogram and voice. The sampled signals are transmitted to PC software in real time via USB bus, which makes it possible to show the curves from the sampled signals in real-time. In addition, data archiving and printing functions are integrated into the software. Since pneumography is one of the oldest methods to provide information about the technique of respiration, it will be possible for doctors in phoniatric practice to use the created device and programmed application for patient diagnosis. Listed in the results is an example of the recordings acquired from the designed device.

Keywords
pneumography, pneumogram, phoniatry, diagnostics, real-time signal processing, visualization

Introduction

The central focus of this article is the pneumogram acquisition method. Pneumography is one of the oldest methods to provide information about respiration during speaking and singing. A pneumogram consists of the person's voice, the movements of the chest and the movements of the abdominal wall. Pneumography curves are used to measure the respiratory rate, to detect pathological phenomena and to calculate the ratio between the time of inspiration and expiration. Further, the asymmetry and relationship between the curves of the chest movements and abdominal wall are evaluated with this method.

Currently, the pneumography method is not very widespread and is not used in medical practice, having been replaced by pneumotachography (there is no equipment manufacturer in the present market). However, the pneumography method is more suitable for diagnostic purposes, because it provides direct information about the muscle movements participating in the respiration process. Pneumography is also used in cases when a voice teacher needs to gain information about the pupil's breathing technique.

In this article, we have presented a design for a device that is used to capture the pneumography signals. This paper also focuses on description of a PC application that visualizes and records signals in real time. Real-time visualization is necessary, because the measuring sensors have to be correctly set up before the measuring process. Visualization allows for control of the correctness of the record. Listed in the results are the recordings acquired via the designed solution. The design of the device construction is based on descriptions which are specified in references [1].

The hardware description of the designed device

The block diagram in Fig. 1 provides an outline of the hardware solution. A 32-bit microprocessor from ATMEL AT91SAM7S64 [7], which has a maximum clock frequency of 55 MHz, was used for the implementation. The selected type of microprocessor contains all the required peripherals and is easily accessible on the market. The inputs of the device are connected to a pair of strain gauges and a microphone. The signals from the strain gauges are amplified by instrumentation amplifiers [3]. All signals are adjusted to the desired voltage range of the input A/D converter. An electrets microphone, which is commonly used in computer technology, is used to record the voice.

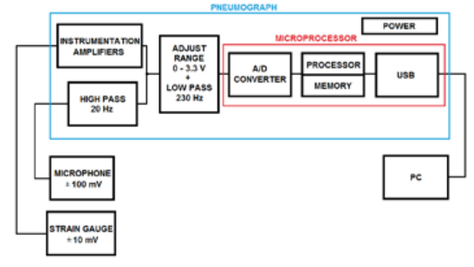

Fig. 2: The block diagram of the hardware solution.

The sampling frequency is set at 500 Hz and the A/D converter has 10-bit resolution; since the voice recording is used only to detect the voice's presence, this sampling frequency is therefore sufficient. Connection to a PC interface is provided by USB. As this device operates in the USB HID class, such as a

keyboard or mouse, no installation of additional drivers is required. The firmware of the microprocessor was created in the programming language C.

The construction of the sensor used for measuring is presented in Fig. 2. The SS5LB BIOPAC [5] sensors used to measure the tension of the strap, inside of which are piezoresistive strain gauges. Similar types of measurement sensors are used, for example, in polysomnography. In an appropriate construction, the sensor should not restrict the test subject, because doing so would affect the measured signal. The sensor sensitivity must be sufficient to register observed pathological phenomena such as hard voice beginnings.

Fig. 2: The sensor for measurement of the tension of the strap.

The final device design is shown in Fig. 3. The device has two inputs for the tension sensors connection and one input for the microphone connection. Potentiometers are used to set the signal offset of the strain gauges. The control LEDs are used for signaling 'power on' and 'recording '.

Fig. 3: The final device design.

The PC application for signal visualization

The block diagram in Fig. 4 provides a description of the functionally designed PC application used for visualization, archiving and further processing of acquired data. First, the data received via USB are converted back from the data transmission format. Nonlinearity was found by measuring the transfer characteristics of the sensor, and the correction table which was calculated from the measured transfer characteristics, was implemented to compensate for nonlinearity. The next block in the diagram serves to compensate the speed streams of the measured and visualized data by selecting and storing data from the queue (FIFO). Implemented in the application is a digital filtering real-time algorithm. The IIR high-pass filter is implemented to remove base line wander, and the FIR low-pass 200th order moving average filter is implemented to eliminate the interference. The following block in the diagram is used to set the display scale. The change of the scale in the time axis is provided by signal decimation. Visualization is performed by rendering each pixel in the graphic user-interface component PictureBox [6], a simple solution that is nonetheless suitable for this application. The application is programmed in the programming language CSharp and is inspired by the design described in reference [4].

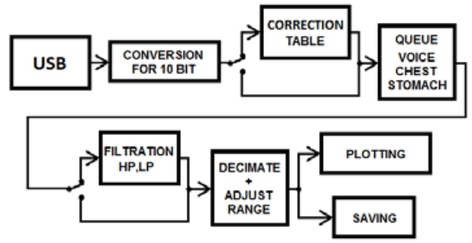

Fig. 4: The block diagram of the application in PC.

The flowchart displayed in Fig. 5 describes the section of the algorithm which ensures the visualization and archiving of data. The greatest problem is to display visualization of the continuous signal curves without

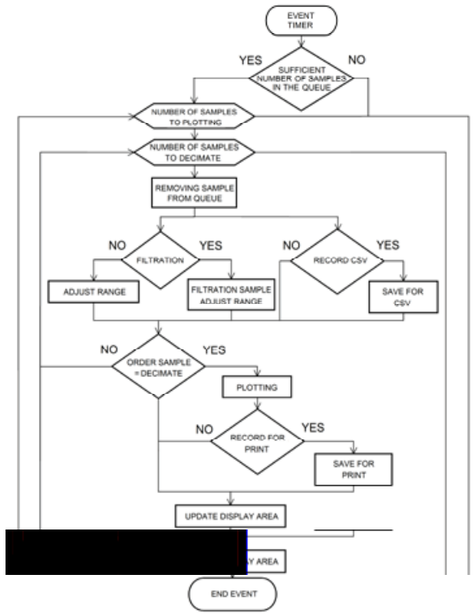

Fig. 5: Flowchart of the algorithm for signal drawing.

having to depend on the performance of the PC. The signal drawing is performed by invoking the timer events. After invoking the event, the conditions of a sufficient number of samples in the queue are evaluated. If the condition is true, the visualization continues. The rendering of more samples at the same time is used to ensure sufficient dynamism of the process. The number of samples plotted in the same time depends on the decimation factor, which can set how the decimated data should be handled when the decimation is applied. It is possible to select only one sample and discard the other or select a sample with maximum value or calculate the average of all decimated samples. Also described in the diagram is the method of storage for archiving and printing.

Shown in Fig. 6 is the design of the graphic user interface. The application includes buttons which provide controlling the recording and inserting information tags on activity during the measurement. The application also allows the user to set options of archiving, printing, using the correction tables, filtration and background color.

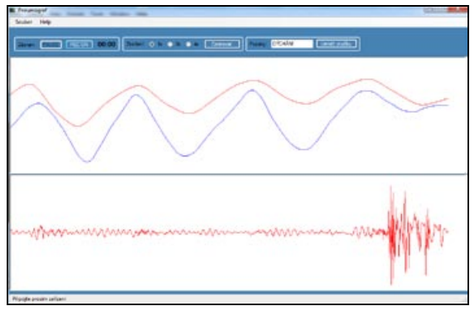

Fig. 6: The graphic user interface designed for pneumograph application in the PC.

Results of the measurements

Fig. 7 shows the results of the measurement acquired by means of the designed and realized solutions.

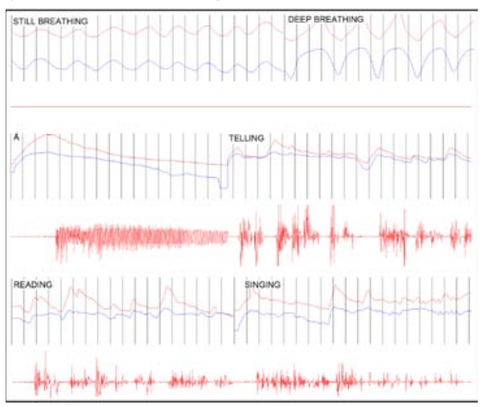

Fig. 7: Record signal optimized for print.

The recordings contains the signal of the voice, chest and abdominal activity, along with the tags providing information on activity during the measurement and tags in time interval 1s. During the recording, it is important to record the correct location of the sensor and the setting of the strap tension.

Conclusion

This article provides a basic description and guide to the use of pneumography. In addition, the article provides a description of a hardware and software solution designed to measure the pneumogram. The created device will be used for diagnosing voice disorders in phoniatrics clinics. Though the device has been tested in cooperation with phoniatric specialists, it has yet to be used in clinical practice.

Suggestions on how to improve the device will be known after more experiences with its use will be attempted, along with implementation of the device in actual clinical practice. Other improvements will include the creation of a database of patient records for better handling of the acquired data.

References

[1] NOVÁK, A. *Foniatrie a pedaudologie II. Poruchy hlasu u dětí a dospělých - základy anatomie a fyziologie hlasu, diagnostika, léčba, reedukace a rehabilitace poruch hlasu.* Praha: UNITISK, 2000.

[2] JANÍKOVÁ, D. *Fyzioterapia funkčná diagnostika lokomočného systému.* Martin: Osvěta, 1998, s. 238. ISBN 80-8063-015-1.

[3] HAASZ, V. - SEDLÁČEK, M.: *Elektrická měření. Přístroje a metody* (2. vydání). Monografie ČVUT, Praha 2003

[4] *The cheapest dual trace scope in the galaxy* [online]. 2012 [cit. 2012-04-25]. Dostupné z WWW: <http://yveslebrac.blogspot.com/2008/10/cheapest-dual-trace-scope-in-galaxy.html>.

[5] Biopac *Respiratory-effort-transducer SS5LB* [online]. 2012 [cit. 2012-04-25]. Dostupné z WWW: <http://www.biopac.com/respiratory-effort-transducer-bsl>.

[6] Microsoft *PictureBox class* [online]. 2012 [cit. 2012-04-25]. Dostupné z WWW: <http://msdn.microsoft.com/en-us/library/system.windows.forms.picturebox.aspx>.

[7] Atmel Inc. *AT91SAM7S64 datasheet* [online]. 2012 [cit. 2012-04-25]. Dostupné z WWW: <http://www.alldatasheet.com/datasheet-pdf/pdf/255484/ATMEL/AT91SAM7S64.html>.

Ing. Jan Sedlák
Department of Circuit Theory
Faculty of Electrical Engineering
Czech Technical University in Prague
Technicka 2, 166 27, Prague, Czech Republic

E-mail: sedlaj15@fel.cvut.cz
Phone: +420 728 760 701

USE OF CORRELATION ANALYSIS FOR ONSET EPILEPTIC SEIZURE DETECTION

Tomáš Havel, Jiří Balach

Faculty of Electrical Engineering, CTU in Prague, Czech Republic

Abstract

In this paper we present our implementation of correlation analysis method used for detecting epileptic seizures during their onset zone. We used matrices of correlation coefficients and their time course to classify seizure. We also developed effective method to reduce number of features. Implemented algorithms were tested on our own dataset acquired in cooperation with the neurological department of FN Motol. The results show this approach as reasonable but the accuracy must be significantly improved before use in practice.

Keywords

scalp EEG, onset seizure detection, epilepsy, correlation analysis, ictal SPECT

Introduction

Surgical treatment is mostly indicated in patients with pharmacoresistant epilepsy. In this case, additional examinations are indicated especially various tomographic scans. One of them is also subtraction of SPECT. This exam displays differences in cerebral perfusion during epileptic seizure. Subtraction image is obtained from ictal and interictal SPECT. These scans use a contrast agent (the radiopharmaceutical, the RP) which are totally recaptured in brain tissue in approximately 30 seconds [1].

When an epileptic patient needs an ictal SPECT scan examination the medical nurse or doctor has to be with the patient all the time, mostly for hours and focus on his behavior for early recognition of the seizure. When the staff realizes the seizure the RP has to be injected. The seizure has to be detected early because if the RP is delivered late, the scan will be less accurate or it can even image a false location instead of a prime epileptic focus.

Our interest is to develop a robust system which will help to the medical personnel to decide whether the patient has the seizure. This system should recognize the seizure from changes in scalp EEG signal and warn the doctor [7].

If the system works robustly enough, the doctor would not have to continuously monitor the EEG and come only when it is necessary. The most advanced idea is to design automatic system which integrates EEG monitor, analyzer machine and linear infusion pump capable to work autonomously or just with doctor confirmation of the RP injection.

Possibilities of seizure detection

Detection of epileptic seizures from EEG is the determination of time zone in which occurs instead interictal physiological EEG course signal, which can be described as ictal pathophysiological course.

There are many different approaches how to determine the seizure from EEG signal. Today's popular methods of seizure detection usually use some type of signal transformation like Fourier, Wavelet etc. These methods are called time-frequency methods after frequency images calculated for time segments [8].

Good results were also achieved by time feature extraction and amplitude-frequency approaches oriented to single or multichannel [2] signal processing [3, 9]. Correlation method can be classify as multichannel time feature extraction technique and were already more-less successfully used for the EEG signal processing. Their usage is mostly oriented for epileptogenic source localization [4] in intracranial EEG inspection.

Another big class of seizure detection methods is pattern recognition. These methods use various analysis and react when some pattern typical for seizure occurs [6].

Description of correlation method

When we use correlation analysis for seizure onset time localization at first we have to segment signals to separate parts and assign timestamps to these parts. We use a windowing method similar to sliding window. It is important to choose right length of segments, because too short segment contains poor information and long segment does not allow good time resolution. To improve time precision we can use overlap of windows but even this method does not solve all problems. When the overlap is too large, computational requirements are unreasonably high and furthermore results are blurred. Segments of multichannel EEG are sets of n short-time signals and one technique to get their mutual information is to calculate cross correlation.

The cross correlation of n EEG channels is calculated in each time window. It gives n-by-n matrix of correlation coefficients (Fig. 1). These coefficients should describe dependence (similarity) and in this application especially synchronicity of signals with zero lag. The final product is map of channel similarities in discrete time steps. Those characteristics change in time. Assuming the neural activity of the brain cells is during seizure abnormally synchronized, this pattern should appear in the correlation maps. The matrix of correlation coefficients is diagonally symmetrical and coefficients on diagonal correspond to autocorrelation which are equal to one. It follows $n(n-1)/2$ coefficients useful for further processing. It is still huge amount of information from which we are trying to extract some results.

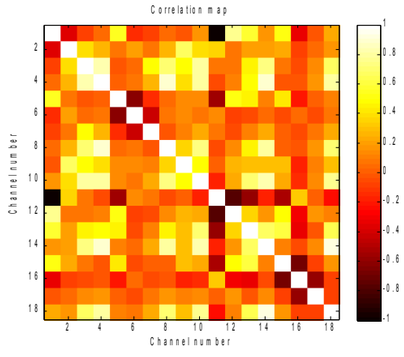

Fig. 1: Correlation map (matrix of correlation coefficients) from ictal zone.

We are using further algorithmic processing to evaluate the time course of correlation maps. For reduction of multivariate data we can calculate eigenvalues of each correlation matrix [5]. The advantage is that the distribution of the eigenvalues λ and their corresponding eigenvectors v of correlation matrix C is directly related to the correlation structure of the multichannel EEG. The eigenvalues are computed by solving the equation (1).

$$C\lambda = \lambda v\,. \tag{1}$$

The eigenvectors form a new orthogonal basis of the n-dimensional vector space spanned by the n EEG channels. Orthogonality ensures uncorrelated state. In the n-dimensional vector space spanned by the original EEG channels, the eigenvector v_{max} is associated with the largest eigenvalue λ_{max}. Due n orthogonal eigenvectors, C may be diagonalized (linearly transformed into a matrix that contains elements only on its main diagonal). The diagonal elements become the eigenvalues λ and their amplitude is proportional to the amount of correlation in the direction of their associated eigenvectors. Under linear transformations the sum of the diagonal elements of a matrix remains unchanged. The sum of the eigenvalues λ then must be equal to the sum of the diagonal elements of the original correlation matrix C and it is equal to number of EEG channels n.

$$\sum_{i=1}^{n} \lambda_i = n\,. \tag{2}$$

The equation (2) must always be respected and consequently, if some eigenvalues increase another one has to decrease to keep the sum constant. Ascending order of eigenvalues called spectrum of the correlation matrix. It can be visualized for each time window in one map (Fig. 2). Illustration of more and less correlated segments are shown on artificialy modified EEG signal in figure (Fig. 3).

Evaluation method uses eigenvalues (spectrum of the correlation matrix) is very useful but each time moment is still described by n features vector. We wanted to found some feature which can represent this vector and approximately specify the situation in time with just one parameter. We tried few possibilities and found one as usable and effective. This method count parameter called s:

$$s = \sqrt{\sum_{i=1}^{n} \lambda_i^2}\,. \tag{3}$$

This parameter s represents distance of the state from the coordinate origin and can reach values between $\sqrt{n}$ and n. Static value of this parameter doesn't bring a lot of information but dynamic changes can demonstrate evolution of correlation between channels in time. When the value is equal to $\sqrt{n}$, the channels are absolutely orthogonal and when is equal to n, they are absolutely correlated. With this knowledge we can use this waveform from interictal segment of signal to set a base line of parameter s of EEG signal. Then we can also set some threshold value for seizure detection based on statistical distribution of interictal signal (Fig. 5).

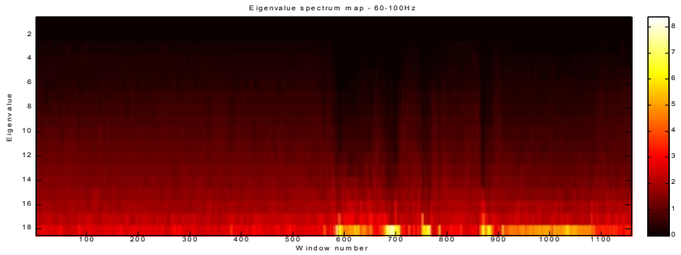

Fig. 2: Spectrum map of the correlation matrix. Seizure detected in onset zone .

Implementation

We implemented algorithms described in previous chapter with the following parameters. Segmentation of signal was realized by windowing technique to segments length 3 s with 3/4 overlap. This setting provides time resolution 0.75 s which we consider as sufficient. We filtered the signals to few frequency bands and calculate cross correlation for each band separately. We used following bands 0-2 Hz, 2-10Hz, 10-20Hz, 20-60Hz and 60-100Hz. Advantege of this technique is higher sensitivity of some frequency band because every patient has different symptoms in ictal EEG. This method proved as good approach because without filtration in most cases correlation maps doesn't show big changes. Correlation maps were evaluated by method uses calculation of eigenvalues followed by calculation of parameter *s* (3). We experimentally discovered that better results are achieved by additional filtration of this waveform with moving average filter with length 3 (Fig. 4). This course is classified by dynamical threshold.

Experimental verification and results

For experimental verification of implemented algorithm were used scalp EEG records with 18 bipolar channels in bipolar longitudinal montage (“Double banana”). All records have sample frequency 200 Hz.

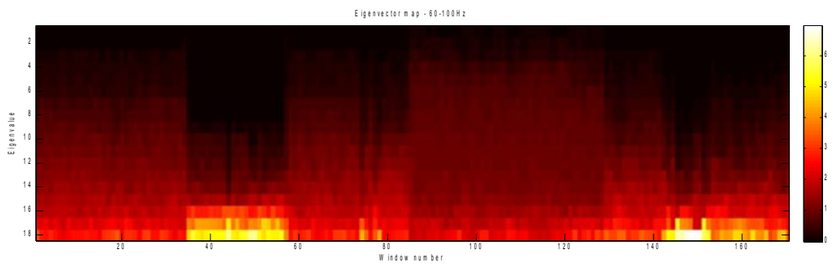

Fig. 3: Spectrum map of the correlation matrix. This map demonstrate effect of more correlated segment from window 37 to 48 and less correlated segment from window 85 to 126. Signals were artificially modified.

We early determine the short records as useless for this technique. It is needed at least 5 minutes prior to seizure onset. That unfortunately limits our resources. We had 11 records complying with these requirements obtained from 6 different patients. Patients were in age from childhood to adult and suffered with various epileptic disease. During implementation we found the time course of correlation maps of unfiltered signals does not correspond to the seizure zones annotated by doctors. When we use signals filtered to bands described above we found the results from some bands as useful for seizure onset detection. Positive results were achieved especially with filtered signals in band 60-100Hz. The interictal zone used for estimation of base line and it's threshold were 30 – 130 s of EEG record. Onset zone was chosen as 20 second after doctor annotation.

The obtained results are as follows: 6 seizures were detected in onset zone, 2 seizures were detected during seizure after onset zone, in 1 record was false detection before seizure starts and in 2 records were seizures not detected. These results show the algorithm was successful in more than half the cases.

The dataset is not big enough for statistically significant conclusions. Further tests with larger dataset should be carried. Currently, we can recommend use of this type of analysis for developing systems for onset seizure detection in combination with another analysis method.

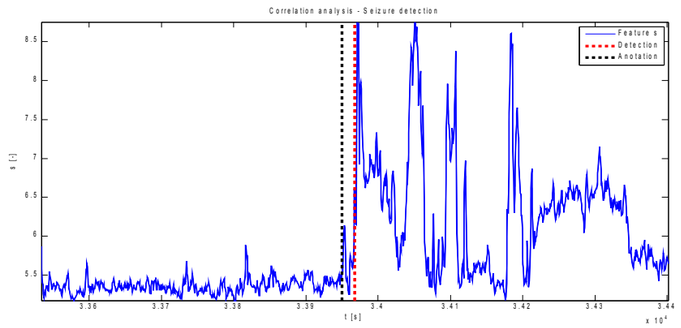

Fig. 4: Waveform of filtered parameter s. Seizure detected in onset zone

Discussion

From the beginning was the method conceived for detection onset zone of epileptic seizure from scalp multichannel EEG record although based on the methods more often used in the analysis of intracranial EEG. Our motivation was make own implementation of this method and experimentally verify it's function on available dateset of EEG records from patients of different ages and epileptic disease. The results show this implementation of correlation analysis successful in 6 of 11 cases as onset seizure detector. Failures were caused by lack of change of synchronicity in EEG records or in case of false detection by spontaneous synchronization in interictal zone. We assume better results would achieve on a more limited group of patients and/or epileptic disease.

We verified our implementation of correlation analysis on our test dataset. Although the results are not very convincing, this method is applicable to the construction of onset seizure detection system.

Acknowledgement

This work has been supported by the grants IGA NT11460-4/2010 Intracranial EEG signal processing; epileptogenic zone identification in non-lesional refractory epilepsy patients, IGA NT13357-4/2012, SGS 10/272/OHK4/3T/13 Analysis of intracranial EEG recording, and resesearch program MSM6840770012 Transdisciplinary Research in Biomedical Engineering.

References

[1] Funkčně zobrazovací vyšetření. Brázdil, M. a Marusič, P. *Epilepsie temporálního laloku*. Vyd. 1. Praha: Triton, 2006, s. 172-187. ISBN 80-7254-836-0.

[2] Duun-Henriksen, J., Kjaer, T. W., Madsen, R. E., Remvig, L. S., Thomsen, C. E., Sorensen, H. B. D. *Channel selection for automatic seizure detection*, Clinical Neurophysiology, Volume 123, Issue 1, January 2012, Pages 84-92, ISSN 1388-2457

[3] Janča, R., Čmejla, R., Jahodová, A. *Rules for Spike Detection in Multichanel Intracranial Electroencephalography* 19th Annual Conference Proceedings Technical Computing Prague 2011 Vydavatelství VŠCHT Praha, 2011, pp. -

[4] Schindler, K., Leung, H., Elger, C. E., & Lehnertz, K. (2007). Assessing seizure dynamics by analysing the correlation structure of multichannel intracranial EEG. *Brain: A journal of neurology, 130*(Pt 1), 65-77. Oxford Univ Press. Retrieved from http://www.ncbi.nlm.nih.gov/pubmed/17082199

[5] Müller, M.; Baier, G.; Galka, A.; Stephani, U. & Muhle, H. Detection and characterization of changes of the correlation structure in multivariate time series Phys. Rev. E, American Physical Society, 2005, 71, 046116, DOI: 10.1103/PhysRevE.71.046116.

[6] Gotman, J. Automatic recognition of epileptic seizures in the EEG. *Electroencephalography and Clinical Neurophysiology*. 1982, roč. 54, č. 5, s. 530-540. ISSN 00134694. DOI: 10.1016/0013-4694(82)90038-4.

[7] Hao Qu, Gotman, J. A patient-specific algorithm for the detection of seizure onset in long-term EEG monitoring: possible use as a warning device. IEEE Transactions on Biomedical Engineering. 1997, roč. 44, č. 2, s. 115-122. ISSN 00189294. DOI: 10.1109/10.552241. Retrieved from http://ieeexplore.ieee.org/lpdocs/epic03/wrapper.htm?Arnumber=552241

[8] Iscan, Z., Dokur, Z., Demiralp, T. Classification of electroencephalogram signals with combined time and frequency features. Expert Systems with Applications. 2011, roč. 38, č. 8, s. 10499-10505. ISSN 09574174. DOI: 10.1016/j.eswa.2011.02.110. Retrieved from http://linkinghub.elsevier.com/retrieve/pii/S0957417411003162

[9] Mcsharry, P. E., He, T., Smith, L. A., Tarassenko, L. Linear and non-linear methods for automatic seizure detection in scalp electro-encephalogram recordings. Medical. 2002, roč. 40, č. 4, s. 447-461. ISSN 0140-0118. DOI: 10.1007/BF02345078. Retrieved from http://www.springerlink.com/index/10.1007/BF02345078

Ing. Tomáš Havel
Department of Circuit Theory
Faculty of Electrical Engineering
Czech Technical University in Prague
Technická 2, 166 27 Praha 6, Czech Republic

E-mail: havelto3@fel.cvut.cz
Phone: +420 604 277 615

FEEDBACK VISUALIZATION INFLUENCE ON A BRAIN-COMPUTER INTERFACE PERFORMANCE

Vladimír Černý[1], Jakub Šťastný[1]

[1]Biological Signal Lab., Faculty of Electrical Engineering

Czech Technical University in Prague, Prague, Czech Republic

Abstract

This paper presents our progress in development of a brain computer interface. We used existing system which was extended to support synchronous experiments with feedback. We use the simplest possible methods as we focus on feedback influence. We examined influence of the way how the feedback is visualized. The abstract feedback, the feedback based on computer game, and the feedback showing real photographs were tested. The classification score 88.5% was achieved with one subject even with simple classification method.

Keywords

BCI, Real-time processing, feedback

Introduction

Our group has been dealing with a research in the field of movement-related EEG recognition towards developing a Brain-Computer Interface (BCI). We have shown that off-line single trial classification of extension and flexion movements of right index finger is possible; classification score of up to 95 % was achieved [1]. The logical next step was to move towards a real-time processing; therefore we have been designing a modular real time processing system [2], [3] and [4].

In the paper [4] we examined how a BCI system is influenced by the presence of feedback. We decided to advance to the online classification of left and right hand movement imagery with visual feedback. This contribution examines the influence of the way how the feedback is presented to the user.

First movement related BCIs

We started with a research on methods used in the oldest movement related BCIs. The first movement related BCIs used synchronous experimental protocol and movements on the opposite side of the body. Synchronous setup means that the user is provided with instruction when and which mental activity he has to perform, in opposite to asynchronous when user performs activities in his own pace.

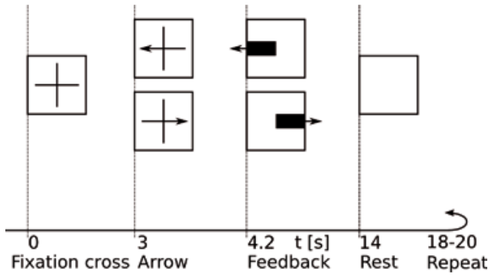

Fig. 1: The synchronous experiments protocol

Works [5],[6],[7], and [8] use the following experimental protocol: at first, the fixation cross is presented to let the subject concentrate, then there is an acoustic beep prior to the instruction of movement to imagine (arrow). Then, the feedback in a form of extending bar is presented, and finally a randomized resting interval is used to avoid adaptation of the subject. Based on these findings we decided to adopt experimental protocol as shown in Figure 1.

Electrode placement was adopted from work [7]. We recorded 3 differential channels connected to the following electrodes (positive - negative): FC3 - CP3, FCZ - CPZ and FC4 - CP4. These channels are simply called C3, C4, and CZ in further text. Linked ears were used as reference.

EPP Architecture

Basic design of our distributed modular EEG Processing Pipeline (EPP) was presented in works [2] and [4]. The system is composed of independent standalone modules connected by a network interface, see Figure 2.

The modules are independent on used operation system and hardware as implemented in the Java language.

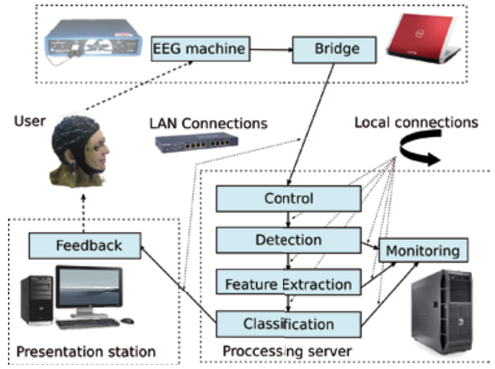

Fig. 2: The system architecture

The communication protocol is based on Real-time Transport Protocol (RTP) to achieve real-time data transfer over the network. Intended purposes of RTP are real-time audio and video streaming. These have very similar requirements as EEG data transfer. And RTP packets are usually prioritized in network devices such as routers.

The latency is most critical parameter for real-time applications. The latency of the pipeline was tested in [2] and was found sufficient for the applications with feedback.

The communication protocol enables to transfer optional parameters defined by the common configuration system. Logging system can store all the communication including all states, messages and commands.

Following modules were implemented:

- BIOPAC Bridge module provides support for a EEG device manufactured by the BIOPAC Company which is available in our department. All the experiments presented in this paper were conducted using this device with a sampling rate of 200 Hz.
- Control module serves for real-time control of the running system, including switching states of the system and sending command to other modules.
- Visualization module serves for visual representation of classification to the experimental subject.
- Perceptron module implements a real-time classification algorithm – a simple one layer Perceptron.
- Feature Extraction module implements a general FIR filtration and a short time power estimation by a leaking integrator filter.
- Detection module computes the power in the same way as the Feature Extraction module and compares the value with a threshold.
- The Data Flow Monitoring module was extended to be capable of showing given experiment setting and all the inter-module communication.

Following modules were implemented in order to support synchronous experiments:

- The Trigger module serves for time synchronization. The module generates sequence of states from the predefined experimental protocol, see Figure 1.
- Feedback module provides instructions and feedback for the experimental subject. Current state of the feedback is picked up from the data flow. The feedback can be displayed as extending horizontal bar, moving image or animation.
- Arkanoid present feedback in the style based on the popular computer game Arkanoid.
- General purpose Generator module, which loads data from log file of any other module and simulates its behavior.
- Threshold module was implemented for the purposes of online classification experiments with asymmetric ratio [9]. The ratio A is defined as

$$A = \frac{R - L}{R + L} \tag{1}$$

where R is the feature extracted from a channel recorder over right hemisphere and L over left hemisphere.

We found out the ratio is usually biased. The bias is subject dependent and differs with each experiment even with same subject. It is caused by electrode placement, contact quality or by asymmetry of brain signal itself. We decided to make normalization of features before computing the ratio. We use balance constant b and we multiply one feature with 1 + b and the other with 1 − b

$$A_{balanc} = \frac{R(1+b) - L(1-b)}{R(1+b) + L(1-b)} \tag{2}$$

The constant can be set by the configuration file or it can be automatically computed. For

automatic balancing we presume long term averages of the normalized features should be equal.

We found out that the modular architecture concept of the system as published in [2] was the right choice because we could easily extend it for new types of experiments.

Synchronous experiments

Synchronous experiments followed the experimental protocol as shown in Figure 1. Modules were connected as shown in Figure 3. The first synchronous experiments were with simulated feedback and the classification was performed offline. The purpose of these experiments was to find simple classification algorithm. Movement imagery of only right hand was used at first as we want to investigate the movement related activity. Stronger movement related activity compared to asynchronous experiment was detected which is in compliance with work [10]. Then two classification algorithms which used signal filtered by an 8-40 Hz band pass filter were tested.

The first algorithm used the Trigger module to compare power from left and right hemisphere. The second algorithm used Support Vector Machine (SVM) and Hjorth features (Activity, Mobility and Complexity). The achieved scores (ratio of correctly classified trials and all trials) were 73 % for power comparison and 75 % for SVM. As the achieved score for SVM was not significantly better we decided to use the Trigger module for feedback comparison experiments [4].

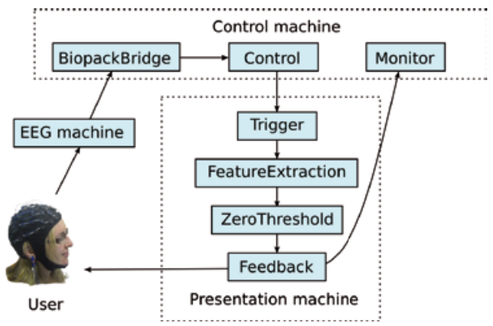

Fig. 3: The synchronous experiments setup

The results with simulated feedback were promising therefore we have attempted to use real feedback based on an online classification. Threshold classification module was activated during the movement period thus the classification results were presented directly to the subject. Subjects reported that it was hard to concentrate on the movement imagery while watching the feedback as the classification results were quite frequently changing during the single movement imagery. The subjects felt more like they are responding to the presented feedback rather than that the system is responding to their imagery. This degraded the signal as offline classification scores have fallen to around 64 %.

We examined the influence of the feedback behavior [11]. The same setting as in previous experiments was used. The Threshold module was used for classification. The feedback was operating in two modes. One was realistic when the feedback bar was extending according to the classification result. The second one was so called optimistic it was expanding when the result of classification was the same as the command and it was still when the result was different. The optimistic feedback was found easier to control and achieved score was better [11].

Fig. 4: Feedback visualization types. From the left: Arkanoid, Realistic, and Bar

The next experiment examined the feedback visualization itself. We were using three different feedback types (Fig. 4).

We were using optimistic feedback as it achieved best results in previous experiment. The experiment was performed with three subjects. These subjects were healthy and had no previous experience with the BCI. Each subject was measured in three sessions in different days. Session consists of 4 to 5 minutes long measurements with short breaks between them. One feedback type was tested in one measurement. There were nine measurements in each session (three of each feedback type). The videos from experiments can be found on research group website [12].

Tab. 1: Average score for individual feedback visualizations

Feedback	Arkanoid	Realistic	Bar
Score [%]	71.7	69.3	64.1

Tab. 2: Average score for individual subjects

Subject	1	2	3
Score [%]	62.8	88.5	56.3

Each cycle command-feedback was considered right or wrong. Right cycle had more samples classified according to the command. The score was computed as ratio of right cycles and all cycles. The score for each feedback type can be found in Table 1.

The best results were with feedback based on Arkanoid probably because it is much more motivating than the others. The Arkanoid feedback shows whatever the user was successful and it even displays score. The subjective opinion about the feedback visualizations differs among subjects. The subject one claimed there is not big difference between feedback visualizations. The subject two founds the Bar feedback most easy to control but he has better results for the Arkanoid. He seemed very motivated when controlling the Arkanoid. The subject three claimed she does not like the Arkanoid feedback because it is much more stressful than the others. But the results for Arkanoid was also better than for other feedback types.

We found out the score is very subject dependent. Our second subject have significantly better results than other two subjects (Table 2).

Conclusion and next steps

We found out that even the simple methods can be used for left and right hand imagined movement classification of EEG. We proven the BCI can be operated even with relatively simple equipment (only two channels EEG) and without need of very special environment such as shielded room. The novel method of asymmetric ratio automatic balancing was achieving high successful rates. This method was used to compare different feedback visualization types. The best results were with feedback which was based on computer game. The second was feedback based on real photographs and last was abstract visualization. The large differences between individual subjects was found. The average score of the best subject was 88.5% but the worst average score was only 56.3% (50% is a baseline).

The significant influence of momental psychical state of subject was also observed. For example stress or insufficient sleep can lower classification score. Subjects also easily lose focus or motivation. This can be partially avoided by right experiment setup and communication with subject.

The subjects were able to use the system almost without training. The results close to average were achieved after less than ten minutes from start of their first experience with BCI.

Because the system is relatively simple it provides large space for future improvements. More advanced classification methods can be used. The modular processing system enables easy adaptation of the new classification methods. The data from realized experiments can be used for design and testing of these methods. The first step in future improvements will probably be adding new class to classification. Thus the classification classes will be left, right, and neutral. This can be done with existing classification with asymmetric ratio even without changes in the source code.

Acknowledgement

Jakub Šťastný is supported by the Grant Agency of the Czech Republic through project P-102/11/1795: Novel selective transforms for non-stationary signal processing and along with the rest of the team by Grant Agency of the Czech Technical University in Prague, grant No. SGS12/143/OHK3/2T/13.

References

[1] J. Doležal, J. Šťastný, P. Sovka. *Recognition of Direction of Finger Movement From EEG Signal Using Markov Models*. In 3rd European Medical and Biological Conference on Biomedical Engineering EMBEC 2005, Prague, pp. 336-341, 2005.

[2] J. Šťastný, J. Doležal, V. Černý, J. Kubový. *Design of a modular brain-computer interface*. In Applied Electronics, pp. 319-322, 2010.

[3] J. Doležal, J. Šťastný, V. Černý, J. Kubák. *Real Time EEG processing*. 57. společný sjezd české a slovenské společnosti pro klinickou neurofyziologii, proceedings, pp. 49, 2010.

[4] J. Doležal, V. Černý, J. Šťastný. *Constructing a Brain-Computer Interface*. In Applied Electronics,. 99-102, 2011.

[5] B. Obermaier, C. Guger, C. Neuper, G. Pfurtscheller. *Hidden Markov models for online classification of single trial EEG data*. In Pattern Recognition Letters, vol 22, pp 1299-1309, 2001.

[6] B. Obermaier, C. Munteanu, A. Rosa, G. Pfurtscheller. *Asymmetric Hemisphere Modeling in an Offline Brain–Computer Interface*. In IEEE Trans. On Systems, Man and Cyber. Part C, vol. 32, pp. 536-540, 2001.

[7] G. Pfurtscheller and C. Neuper. *Motor Imagery and Direct Brain–Computer Communication*. Proceedings of the IEEE, vol. 89, no. 7, pp. 1123-1134, 2001

[8] A. Schloegl, C. Neuper and G. Pfurtscheller. *Subject specific EEG patterns during motor imagery*. In procceding of 19th International conference IEEG/EMGS, pp. 1530-1532, 1997.

[9] H. Ehrlichman, M. S. Wiener, *EEG asymmetry during covert mental activity*. In Psychophysiol, vol. 17, pp. 228-235, 1980.

[10] C. Neuper. *Feedback-Regulated Mental Imagery in BCI Applications: Using Non-Invasive EEG and NIRS Signals*. In BBCI Workshop 2009 – Advances in Neurotechnologies, Berlin, 2009.

[11] J. Doležal, V. Černý, J. Šťastný. *Online motor-imagery based BCI Study on feedback traning.* submitted for publication In Applied Electronics. 2012

[12] J. Šťastný. *Brain-Computer Interface Research Group website*, online: http://amber.feld.cvut.cz/fpga/studenti_kolegove.html

Vladimír Černý
Biological Signal Lab., Faculty of Electrical Engineering, Czech Technical University in Prague, Technická 2, Prague 6, 166 27 Czech Republic

E-mail: cernyvl3@fel.cvut.cz
Phone: +420 603 512 421

EYE TRACKING PRINCIPLES AND I4TRACKING® DEVICE

Marek Polčák, Martin Dobiáš, Vratislav Fabián

Czech Technical University in Prague, Faculty of Electrical Engineering, Prague, CZ

Abstract

The eye tracking principles are well known for more over 50 years, but their commercial usage is still waiting for renaissance. Thanks to fast development of computer performance and imaging chips resolution, video-oculography method became accessible. I4Tracking® device is combination of high resolution, high speed camera, and pupils center detection software.

Keywords

Eye tracking, eye movement detection, image recognition, human interface device

Introduction

Eye tracking principle follows up the idea of pupil as a direct actuator [1]. System of eye nerves is one of the closest to the brain, therefore its reaction time should be one of the shortest. Six different eye muscles are continuously changing its tense, controlling vertical position (superior and inferior recti), horizontal position (lateral and medial recti) and diagonal movement with rotation (superior and inferior oblique). Tense is changing accordingly to internal and external subjects. Feelings, lighting, heard beat even ordinary thoughts have impact on pupil size and focusing.

Different methods are being used to measure eye movement, such as infrared-oculography (IROG).

IROG uses infra light intensity differences. Every eye position has specific reflection factor.

Another method is magneto-oculography (MOG). Contact lens with integrated coils creates induction any time eye moves.

Electro-oculography (EOG) mostly uses 2-4 surface electrodes. Electrodes are attached around the eye to form a cross, and measures electro potential changes on muscles.

VOG method uses a camera device to capture images of eye movement. These images are analyzed afterwards, to determine trajectory of eye ball.

Our research team has developed VOG device called I4Tracking®. This device contains high definition high speed digital camera with analyzing and visualizing software.

Software allows experiments to be recorded and post processed in order to find pupils trajectory and size.
In addition to improve data interpretation, variety of special visualizations has been developed and tested.

Calibration

Calibration process starts before every measurement and controls if enough pictures was captured with open eye. It does not compute center of pupil, only tests if data needed for processing are valid. Images from calibration are saved providing post process recalibration option. Different calibration method can reach better outputs in different environment. I4Tracking® has actually implemented two different methods based on 9 or 5 calibration points.

9 points method works as linearization process. All points from calibration are used to divide space into subsectors with its own calibration formula. This approach is simple to understand, fast to process and used as simple etalon for the other approaches.

New five point calibration is now being tested. It is based on mathematical model derived from 3D model of human head, eyeball and camera positions.

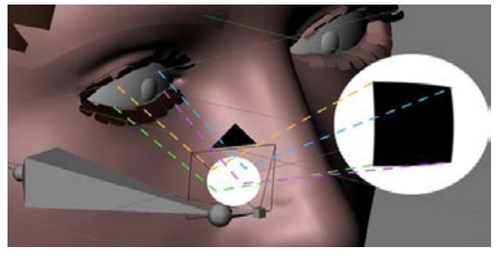

Fig. 1: 3D simulation of camera, head and eye.

Every possible simulation is being tested data are recounted using Matlab application into one correction matrix. This specific method was developed to minimize errors between reality and linearization method.

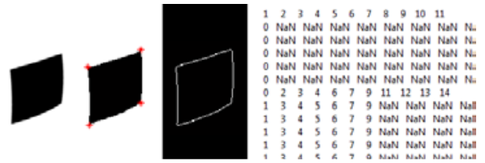

Fig. 2: 3D simulation of camera, head and eye.

Its theoretical preciseness is nearly 100%, but depends on sufficient number of prepared 3D simulations.

At first point, black filled object is created from eye movement trajectory simulation. This picture is imported into Matlab to define x,y positions of each point. All coordinates are mapped to rectangle matrix afterwards.

Detection algorithm finds only nearest neighbor by splitting space into two cells and coparing.

Recording and analyses

Recording

I4Tracking® system can currently record between 1 and 87 frames per second using 720x482 pixels resolution. Size of captured picture is about 400 kB each. Because of high demands, SSD disks are recommended.

Tab. 1: Hard disc needs for continues writing with different camera frame rate setting.

Frames per second	25	40	87
Writing speed MB/s	9,15	14,64	31,842

As transfer protocol is used USB 2.0 standard which allows transfer up to 480Mbit per second.

I4Tracking® software can communicate with Camera API Control Commands allowing pixel clock and timing set. There is also possibility of hardware gamma and brightness auto-gain corrections.

Hardware gamma correction automatically linearise pictures intensity, causing maximization for human recognition.

Auto-gain simply changes intensity of all points to keep stable summation.

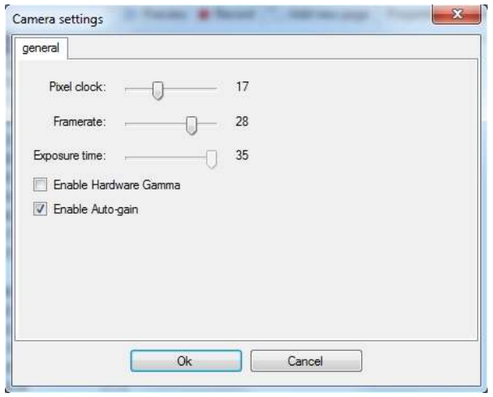

Fig. 3: Digital camera setting possibilities.

Analyses

Current version of I4Tracking® supports a few different recording modes directly connected with analyses. Data Save Mode saves all images to hard drive for post processing. After whole experiment finishes, data can be exported, transferred or processed. Experiment can also be replayed showing detected pupils center. Detection algorithm is based on learning with teacher approach and has been developed by Eyedea Recognition Ltd.

In Real Time Mode all data are directly processed. Here is a problem with CPU performance. All I4Tracking® algorithms are optimized to run on 1, 2, 3 or 4 standalone cores. Even so special algorithm had to be developed for this exact situation, because standard approach was insufficiently slow.

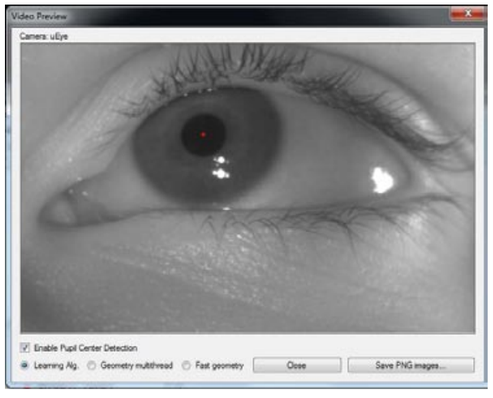

Fig. 4: Real time pupils center detection.

Real time algorithm uses one way principle based on predicted geometry of captured image. I4Tracking® is

now able to work without storage requirements to control computer mouse.

Software application

Graphical user interface

I4Tracking® application is split into two main working areas. In the left column is projects overview. This view allows showing and hiding measurements of any experiment. At the top of projects column is positioned standard set of function icons for creating new project, saving, deleting etc. On the right side is working area. This space is changing accordingly to selection. There is project or measurement overview and additional functions. User can replay experiment, analyze, visualize or export data.

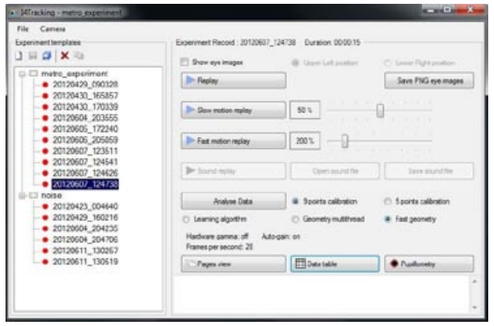

Fig. 5: I4Tracking® graphical user interface.

Data export

Data export is realized by "Copy all" button in "Data table dialog". I4Tracking® application saves exact time in milliseconds for every captured image. Each line is connected with one of these images and adds information of detected center, recounted coordinates on computer display, size of pupil and name of currently focused image.

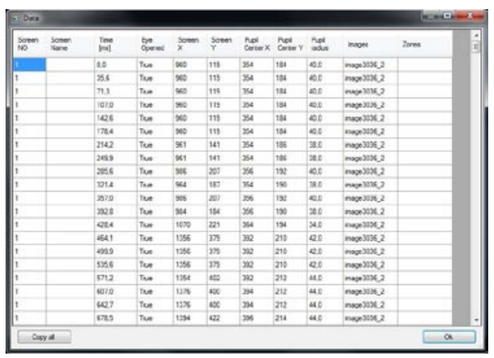

Fig. 6: Data overview table with export button.

Data visualization and usage

Data visualization makes an important part of application. It helps interpreting measurement results more objectively. I4Tracking® program offers variety of different visualizations.

Visualization

The most illustrative visualization is a Simple view. It contains detected points, with time intensity value. User, in this case publisher, can see places of interest for measured subject. This method is used to change positions of important messages in magazines and newspapers.

Fig. 7: Simple view visualization.

Usage

Pupil size detection gives I4Tracking® new possibilities in disease detection. One of many applications is measurement of light wave length reaction.

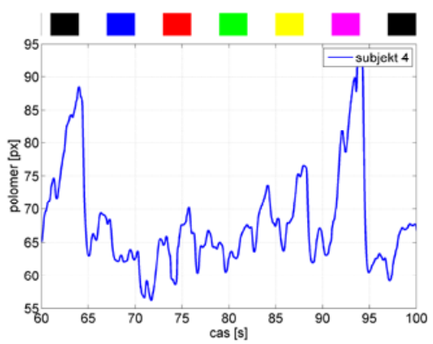

Fig. 8: Pupils reaction to different wave length.

Application usability

I4tracking® core function is providing information about measured subject focus. However this problem is composed from partial problems [2]. We are trying to develop and implement different support functions to help with all of these partial problems.

Calibration setting

Calibration setting allows switching between 5 and 9 points calibration mode. Define random position of trigger points to prevent trigger sequence influence. Background color can be set from prepared palette of colors. And also timing and calibration icons are variable.

Calibration setting

Calibration setting allows switching between 5 and 9 points calibration mode. Define random position of trigger points to prevent trigger sequence influence. Background color can be set from prepared palette of colors. And also timing and calibration icons are variable.

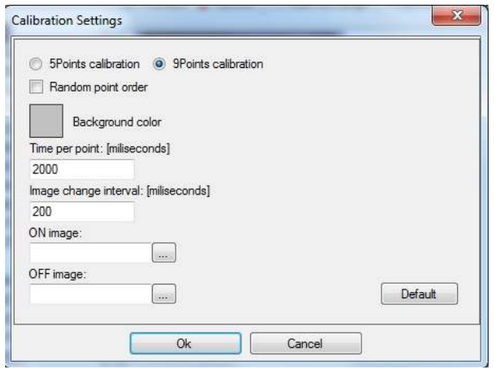

Fig. 9: Calibration setting options.

Experiment setting

Experiment setting provides a lot of different functions. The most important is optional usage of integrated audio player. Each Measurement can have attached audio file which can be looped. Default experiment time can be set and background color changed same as in calibration. Direct processing or saving measurement data can be turned on.

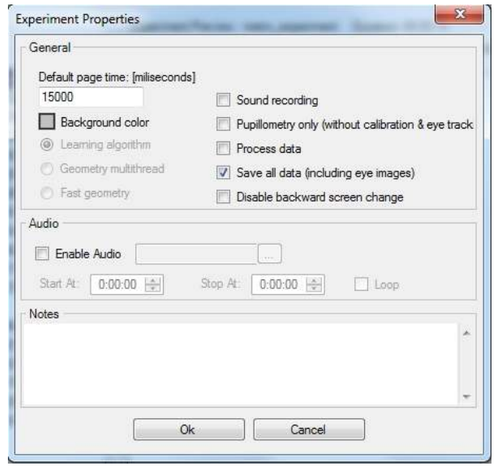

Fig. 10: Experiment setting options.

References

[1] Duchowski a.T.: *Eye Tracking Methodology - Theory and Practice.* Springer-Verlag, 2007.
[2] Wedel M., Pieters R.: *Eye Tracking for Visual Marketing, Foundation and Trends.* Now Publishers, 2008.

Acknowledgement

The work has been supported by research grant No.: SGS10/270/OHK5/3T/13 of The New Technology in Marketing Studies.

Ing. Marek Polčák
Department of Physics
Faculty of Electrical Engineering
Czech Technical University in Prague
E-mail: polcamar@fel.cvut.cz

MODELING OF CIRCULATION DYNAMICS WITH ACAUSAL MODELING TOOLS

Tomáš Kroček[1]

[1]First Faculty of Medicine, Charles University, Czech Republic

Abstract

This paper presents an innovative approach to modeling and simulation using acausal modeling tools, which is representative of the modeling language Modelica. This language allows the description of the modeled relationships directly with the equations. Advantages of this approach are demonstrated on the model circulation dynamics by Guyton, Coleman and Grange of the 1972, which is one of the first models of integrated physiological systems of the organism and opened the domain, which is now engaged in the integrative physiology. The introduction of acausal approach and its comparison to previous methods is the scientific contribution of this paper.

Keywords

Modelica, Guyton, modeling, biomedicine, Dymola

Introduction

This paper aims to introduce an innovative approach to modeling and simulations using the so called acausal modeling tools. These tools, which is representative of the modeling language Modelica, allow to describe the relationships of model directly in tool using equations (we describe the equation and not the solution). Modelica language is now increasingly used in industry. Use in biological applications is still infrequent. Advantages of this approach are demonstrated by the model of circulation dynamics from Guyton, Coleman and Granger of the 1972 [1]. The original article contained as attachment accompanying diagram (see Figure 1), which graphically represents the model equation.

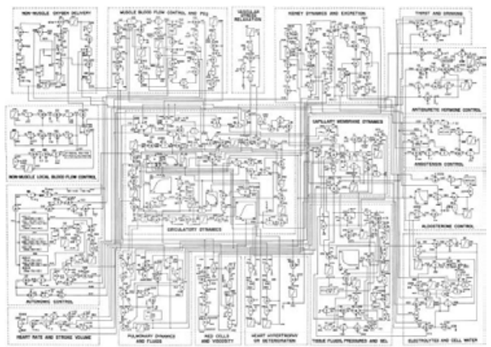

Fig. 1: Guyton's original diagram of the 1972 (in high resolution available from http://patf-biokyb.lf1.cuni.cz/wiki/_media/workshopy/guyton_circulation_an_overall_regulation.pdf).

The model describes the regulation of the circulatory system, including all its connection to other physiological systems of the organism, such as oxygen transport, the volume dynamics, body fluids osmolarity, lymph flow, plasma protein circulation, potassium and sodium homeostasis, kidney model, etc. The model considers the autonomic nervous regulation including the regulation of thirst and drinking, hormonal regulation of angiotensin, aldosterone and ADH. Model represents the broader context of the circulatory system and allows the body to simulate the behavior of normal, during physical activity and in a number of pathological conditions. He was one of the first models of integrated physiological systems of the organism and opened the domain, which is now engaged in the integrative physiology.

Methods

Guyton's chart that was part of the publication is a complex network of interconnected computing elements. The authors originally implemented the model in Fortran. Five years ago in our laboratory was the model implemented in block-oriented tool Simulink. Interconnection in this implementation accurately corresponds to the graphical diagram of the original publication (after correction of some errors in the original graphic diagram) [2]. An implementation where outputs of one block are connected to inputs of other blocks is called causal.

In Simulink, was published, another, more advanced version of Guyton's model (originally implemented in Fortran or C++) - Guyton's model of the 1986, including extensive descriptions can be found at http://physiome.cz/Guyton and Simulink version of Guyton's model 1992 published in 2011 Mangourova et al. [3]. The same model in causal language cellML [4] is not yet fully functional.

New language Modelica [5] allows the implementation of a causal model, where individual elements are connected and visually the same form as the original Guyton's model [6], and also such an implementation, where the behavior of the model expressed by equations. Approach where we focus exclusively on the model equations, are called acausal [7]. Comparison of causal and acausal approach is scientific contribution of this paper.

Let's bring these approaches to calculating the total lung resistance. Yellow highlighted in Figure 2 shows the sequence of individual computing blocks. This sequence graphically expresses the procedure to calculate of total lung resistance (RPT). It was therefore a causal approach. Now let us show an acausal approach. Figure 3 is an icon that represents the total lung resistance. Against the background of this image (Figure 4) are equations whose solution is left on your computer. Acausal modeling leaves the attention of equations and not the solution algorithm, as in causal modeling.

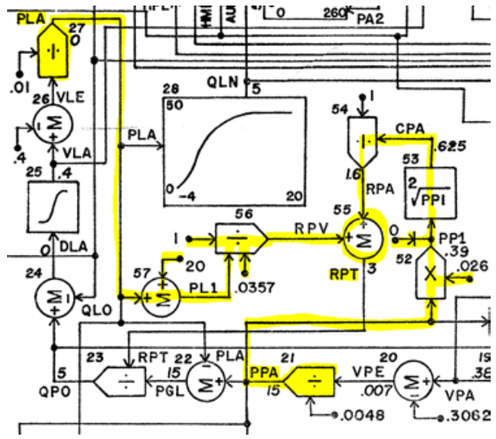

Fig. 2: Causal calculation of the total lungs resistance, where a sequence of computational block implements equation

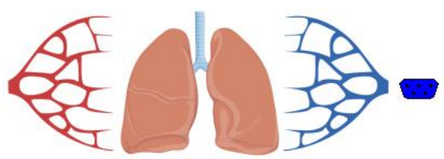

Fig. 3: Acausal block that contains the formula for the calculation of total lungs resistance

```
model PulmonaryBloodFlowControl_
  extends Modelica.Blocks.Interfaces.BlockIcon;

equation
  RPT = 1/(0.0357*(20+PLA)) + 1/(sqrt(if PPA < 0 then 0 else 0.026*PPA));
  a;
end PulmonaryBloodFlowControl_;
```

Fig. 4: Equation in acausal block to calculate the total lungs resistance

Results

According to Guyton's original diagram created three implementations - two causal (in the languages Simulink and Modelica) and an acausal (in the language Modelica - Figure 5). Causal implementation in Modelica was using our labs technology translated into code that is executable in the web browser. The model, which captures the Figure 6 is through a web browser freely available to all Internet users (http://patf-biokyb.lf1.cuni.cz/~tomkro/GuytonModel1972/) without the need to own development environment (Dymola). Causal and acausal model implementation show the same behavior and results.

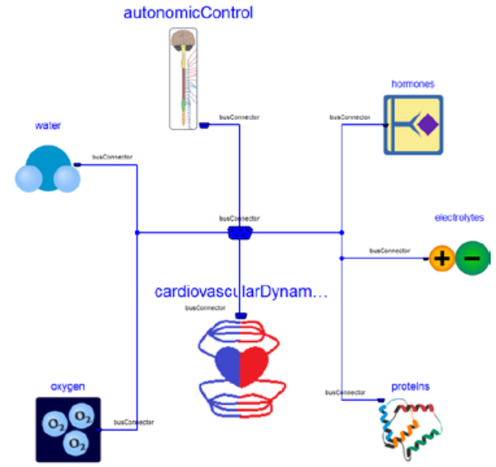

Fig. 5: Acausal implementation of the original Guyton diagram.

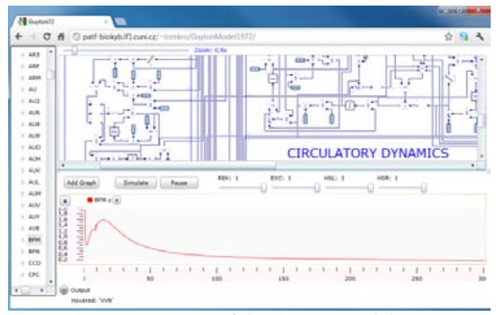

Fig. 6: Internet version of the Guyton model

Discussion

Modelica is a particularly useful tool for creating complex models [8, 9], where the clarity and readability of the most apparent. The current version of the model from Guyton's colleagues and students, under the name HumMod (http://hummod.org) is probably the largest comprehensive model of integrated physiological system of the body. Modelica version of HumMod, which in collaboration with American colleagues engaged in our laboratory (http://physiome.cz/hummod) allows a clear and understandable formalized the expression of complex relationships between the subsystems of the organism. Models of physiological systems, among other things, can serve as a basis for the production of teaching medical simulator. The aim of our work is just making these simulators and their use in teaching physicians [10, 11].

Conclusion

A causal approach focuses on the algorithm calculation and modeling of reality beneath it very often lost. An acausal approach is focused on the model equations and their solution (algorithm) leaves your computer. Figures 7 and 8 demonstrate that the causal structure of the model describes the implementation of the method of calculation rather than the structure of the modeled reality, while acausal approach represented better the modeled reality. Acausal modeling is a way to create understandable physiological models, where it is very important interdisciplinary cooperation of physiologists, technicians and in case of educational applications as well as artists. Acausal modeling using object-oriented and component-based approach, and significantly shortens the development cycle of the model.

Acausal implementations of Guyton model of the 1972 (Figure 5) represents an innovative approach to creating of complex models. Individual components of this model include equations and are represented by icons on the outside. This property is one of the benefits acausal modeling - to express the semantic meaning of each component.

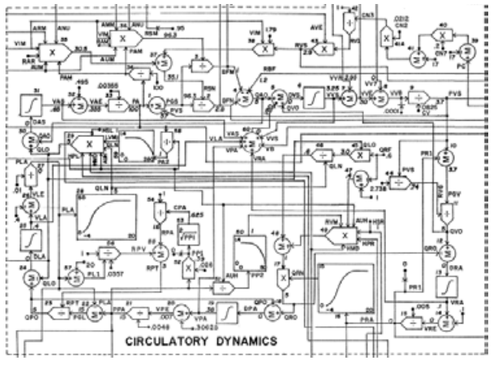

Fig. 7: Causal calculation of circulatory dynamics

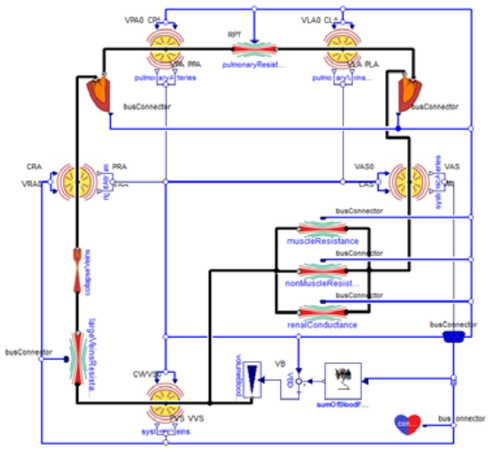

Fig. 8: Acausal calculation of circulatory dynamics

Acknowledgement

This paper describes the outcome of research that has been accomplished as part of research program funded by the grant PRVOUK-P24/LF1/3 and by the grant FR—TI3/869.

References

[1] Guyton, A. C., Coleman, T. G., & Grander, H. J. (1972). Circulation: Overall Regulation. Ann. Rev. Physiol. , 41, stránky 13-41.

[2] Jiří Kofránek, Jan Rusz, Marek Mateják: From Guyton's graphic diagram to multimedia simulators for teaching physiology. (Resurection of Guyton's Chart for educational purpose) Proceedings of the Jackson Cardiovascular-Renal Meeting 2008. (Stephanie Lucas Ed,), CD ROM, 11. pp.

[3] Mangourova, V., Ringwood, J., & Van Vliet, B. (2011). Graphical simulation on environments for modelling and simulation on of integrative physiology. Computer Methods and Programs in Biomedicine, volume 102 (3), pp. 295–304

[4] cellML. (2010). Description of Guyton 1992 Full cardiovascular circulation model. [Online] http://models.cellml.org/exposure/cd10322c000e-6ff64441464f8773ed83/Guyton_Model_1-0.cellml/view

[5] Fritzon, P. (2003). Principles of object-oriented modeling and simulation with Modelica 2.1. Wiley-IEE Press.

[6] Kroček, Tomáš. Implementation of large-scale model of physiological functions in the environment of the language Modelica (in czech). Prague, 2011. Available from: https://cyber.felk.cvut.cz/research/theses/papers/181.pdf. Master thesis. CTU FEE. Supervisor: Doc. MUDr. Jiří Kofránek, CSc.

[7] Jiří Kofránek, Marek Mateják, Pavol Privitzer: Causal or acausal modeling: labour for humans or labour for machines. In Technical Conmputing Prague 2008, 16th Annual Conference Proceedings. (Cleve Moler, Aleš Procházka, Robert bartko, Martin Folin, Jan Houška, Petr Byron Eds). Humusoft s.r.o., Prague, 2008, ISBN 978-80-7080-692-0. CD ROM, str. 1-16, [Online] http://www2.humusoft.cz/kofranek/058_Kofranek.pdf

[8] Jiří Kofránek, Marek Mateják, Pavol Privitzer: HumMod - large scale physiological model in Modelica. Proceedings of 8th. International Modelica conference 2011, Dresden*, internetový sborník (12 stran): https://www.modelica.org/events/modelica2011/Proceedings/pages/papers/23_poster_ID_175_a_fv.pdf

[9] Hester R, Brown A, Husband L, Iliescu R, Pruett WA, Summers RL and Coleman T (2011). HumMod: A modeling environment for the simulation of integrative human physiology. Front. Physio. 2:12. doi: 10.3389/fphys.2011.00012

[10] Kofránek, Jiří Privitzer, Pavol, Mateják, Marek, Matoušek, Stanislav: Use of web multimedia simulation in biomedical teaching. In Proceedings of the 2011 International Conference on Frontiers in Education: Computer Science & Computer Engineering, Las Vegas, July 18-21, 2011, (H. R. Arabia, V. A. Cincy, L. Deligianidis, Eds.), ISBN 1-60132-180-5, CSREA Press, Las Vegas, Nevada, 2011, 282-288.

[11] Kofránek, Jiří, Matoušek, Stanislav, Rusz, Jan, Stodulka, Petr, Privitzer, Pavol, Mateják, Marek, Tribula Martin: The Atlas of physiology and pathophysiology: web-based multimedia enabled interactive simulations. Computer Methods and Programs in Biomedicine, 104(2), 143-153, 2011 IF 1.44

Ing. Tomáš Kroček
Department of Pathological Physiology
First Faculty of Medicine
Charles University in Prague
U nemocnice 5, CZ-120 00 Praha

E-mail: tomas.krocek@lf1.cuni.cz
tel: +420 224 965 912

METHODOLOGY OF THERMOGRAPHIC ATLAS OF THE HUMAN BODY

Viktoria Rajtukova, Monika Michalikova, Teodor Toth, Jozef Zivcak[1]

[1] Technical University of Kosice, Faculty of Mechanical Engineering, Department of Biomedical Engineering and Measurement, Kosice, Slovakia

Abstract

Thermography allows contactless measurement of surface temperature of objects; it displays temperature digitally and enables to record graduate fields. Nowadays, this field of biomedical engineering has received an increased attention due to potential of medical thermography applied in the daily normal clinical practice. It is a noninvasive diagnostic method that enables an early diagnostics of several diseases, e.g. vascular system disorders, skin diseases, cancer, etc. The core of research was to establish a reference sample of thermograms using thermovision devices that convert emitted thermal energy into thermographs. These reference samples are to be used to determine the potential pathology in the obtained thermograms using mutual comparisons. To create thermography atlas there were 30 volunteers (15 male, 15 female, with physiological BMI index and the age ranging between 16 and 28 years) participating the study. All subjects were instructed about the measurement principle, process of measurement and requirements for precise measurement before the experiments. Each volunteer was measured in 18 different positions in the constant laboratory conditions. All the obtained thermograms were used for the creation of thermal atlas of the human body that was a result of the research.

Keywords

methodic, infrared thermograph, reference sample, atlas

INTRODUCTION

The main advantages of infrared thermograph are a contactless, noninvasive, painless and no-radiation character of this image technique [1].

In order to clearly state that the image describes the pathological changes, it is important to be able to compare the thermograms of the same healthy individual.

The study is devoted to the research of the temperature distribution of healthy human bodies that was measured by infrared thermograph. We have used Infrared Imager with detector type 320x240 Focal Plane Array, Vanadium Oxide. A database of 540 thermograms of various positions and/or localities of human body was created. The following 18 various positions of human body were captured: ***TBA*** (total body anterior), ***TBD*** (total body dorsal), ***TBAA*** (total body anterior abduction), ***TBDA*** (total body dorsal abduction), ***TBR*** (total body lateral view right), ***TBL*** (total body lateral view left), ***CA*** (chest - anterior view), ***UB*** (upper back), ***RAA*** (right arm anterior), ***RAD*** (right arm dorsal), ***LAA*** (left arm anterior), ***LAD*** (left arm dorsal), ***RHA*** (right hand dorsal), ***RHP*** (right hand plantar), ***LHD*** (left hand dorsal), ***LHP*** (left hand plantar), ***FA*** (face), ***FP*** (foot plantar).

BASIC CONCEPTS

Physiological temperature distribution is defined as temperature distribution measured from certain position and locality of healthy human individual [2],[3].

Atlas of normal thermograms can be describes as a database that consists of physiological healthy human volunteers data measured by infrared thermovision camera [3],[4].

Medical thermography is a technique that uses infrared imaging and measurements recorded by thermocamera to “see“ and “measure” invisible infrared energy emitted from an object. It is a tool for the study of surface temperature distribution of living organisms [5].

METHODICS OF MEASUREMENT

Skin temperature of the human body (number of database samples, n=540) was measured with an infrared camera (Infrared Thermal Imaging Camera Imager, Fluke Ti55/20, Fluke, USA). This thermovision camera generates a matrix (representing image points) of temperature values. They feature 320 x 240 (76 800 pixels) detectors with industry leading thermal sensitivity (≤0.05 °C; 50 mK NETD) for high resolution. The camera works in the spectral range from 8 to 14 μm. Human body infrared radiation is the highest in the spectral range around 9.66 μm. The calibrated temperature ranges from -20 °C to 100 °C. Data were obtained through high-speed (60 Hz) analysis [1].

Emissivity of the skin was set up 0.98 in the camera. The ambient temperature was measured with an infrared (laser) thermometer (Pyrometer Testo 810) [6].

The camera was calibrated using the system's internal calibration process before each recording.

Conditions of Measurement

The room, where the thermographic measurements are done has to meet certain conditions including constant room temperature, certain humidity, lightness, and room equipment. In this case examining room had air conditioning by which we could reach needed temperature of 22.5 degrees of Celsius (±1.7 °C). If we had higher or lower room temperature, examined person could end up sweating or having shivers; this would discard the measurements. Room temperature was controlled by TESTO 810. Having window blinds is an advantage. If we perform these kinds of measurements in daylight, we will get a classical photography (except of a thermogram). There cannot be a heater in or close to the room. Metal objects and reflective surfaces have to be removed as well. The thermovision camera has to be at a sufficient distance from measured person (app. 2 m), that means the bigger room is necessary to perform the measurements (optimal room dimensions 3x4 m) [7]

Methodology of the sensing system preparation

Fluke IR-Fusion technology captures a visible light image in addition to the infrared image. It joins two images and makes one image or it makes a combination of picture in picture. IR-Fusion technology helps us to identify and record suspicious components and helps us to repair them right at the first time. The head of camera with lens is rotating within 180 degrees and allows us to show and record images in areas that are hard to reach. Software Smart View provides us with tools that analyze infrared images, add explanations and prepare reports. It allows us to edit those reports in a way that will satisfy specific workflows and its requirements.

Before measuring, room temperature and emissivity have to be adjusted on Fluke Ti 55-20 and the right kind of lenses has to be chosen. The emissivity value for a human body is 0.98 [6], [8].

Methodology of the thermovision somathometry

With a modern thermovision camera one should count with a fact that it takes a few seconds to start it working. First of all, camera has to be set properly away from the scanned subject. To have a thermogram on the entire screen of thermovision camera, it is necessary to decide on an appropriate distance, height and angle of measuring. It should be ensured that while measuring a subject, the image should not show heaters, reflective components or any other subjects. We have to be able to see visible end points on the screen of a thermovision camera.

Software packages distributed with the camera are used for processing the obtained thermograms. Software allows us to archive images made with thermovision camera.

Methodology of the subject preparation

A measured subject has to be instructed a day before about following:

- The body should be dressed in loose clothing. Tight clothing on the skin leaving body prints and causes a reduction in blood flow to the body,
- subject should not eat food, drink hot drinks, alcoholic beverages, use drugs or smoke 4-6 hours before the measurement,
- subject should not take part in any physiotherapy treatment, exercise or increase physical activity 6 hours before measurements are conducted,
- subject should not wear make – up and use body lotion,
- subjects need to be in good physical and mental condition (sample of healthy subjects for this study),
- subjects is informed to be aware of the thermovision method as painless, noninvasive and safety measurement method.

At the beginning of the experimental part of the study it is important to complete the "Questionnaire". Based on the information included in it we find out important information for the statistical analysis of thermovisual measuring. Thermal stabilization of the subject consists of acclimatization which takes 15 - 20 minutes. Before the measuring, subject is informed about the positions that he/she will be captured in.

Reports

Each report includes date and time of thermal image, information about the subject, technical parameters of

the camera. The color scale can be set before the measuring. In this case we have set grey scale because we wanted to focus on the details of human body.

By processing the range of temperatures we will find regions which help us to identify temperatures for the selected polygon. Using the software Smart View we can detect changes of temperature on the surface of human body. We can detect changes in symmetries on different parts of the body and deviations from the standards. Based on the measurements and other personal information about the subject, we can provide a general description of thermogram and make an evaluation of it together with histogram. The evaluated thermogram enables us to see signs determining the center position, see center frame, pointer of the warmest and the coldest point on the body. Those signs can be turned over - that means we can set the sign which we want to have or do not want to have shown on the thermogram.

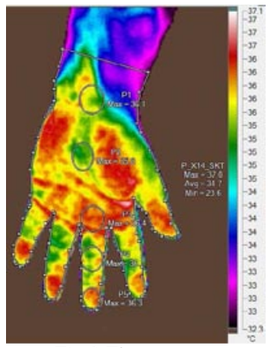

Fig.1 Thermogram

Results and Conclusion

Thermography enables us to measure the temperature of objects on the surface without any contact, to display it on the computer and to differentiate the captured temperature fields.

Nowadays, the attention is paid to thermography worldwide because we want to start using thermography in everyday clinical practice. This project is following-up a worldwide research. Its aim is to create a database of "physiological thermograms" made with healthy people living in Slovakia (mild temperature zone), with "physiological anthropological parameters".

Our database consists of 30 physiological healthy volunteers (n1=30; 15 male, Mn1=15; 15 female, Fn1=15) aged from 16 to 28 to create „Thermographic atlas of the human body". These subjects were captured by infrared camera in 18 different positions. We had 540 thermograms (nTG=540) as a result of the study.

The study results in a database of physiological thermograms and reviews physiological temperature distributions. Obtained temperature values can be used as a reference for medical thermography, where positive/negative findings of the disease or injury can be quantitatively assessed in the future.

The Fig. 2 shows the thermograph of the subject standing on a pad, arms and legs slightly abducted, palms (TBA) or dorsum (TBD) of the hands point forwards, head is a vertical position, neither rotated nor tilted to the side. The most cranial point of the head is in the upper edge of the image) and soles of the feet are lower edge of the image.

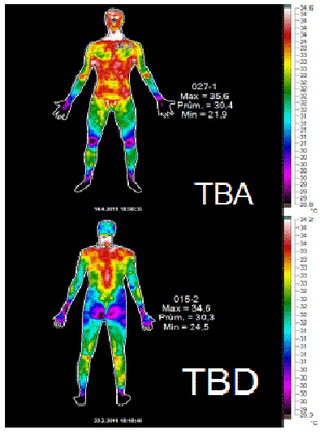

Fig.2. Example, characterizing the first position in "Thermographic Atlas of the Human Body".

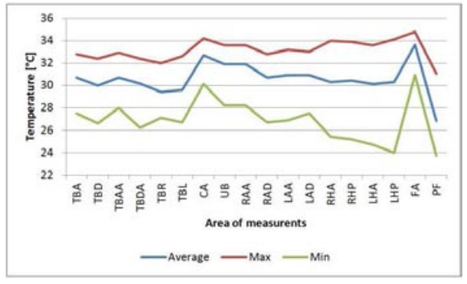

Fig.3. Comparison of the temperatures.

In Fig. 3 there is a comparison of average, maximum and minimum temperatures for each view displayed. The temperatures are calculated (arithmetic mean of all measured subjects in the selected projection) from marked body region, for example see Fig. 2.

From the Fig. 4 one can see that the range for the first step (Rv=5.3°C) is the simplest measure of variation to find. It is simply the highest value (32.8°C) minus the lowest value (27.5°C). Male (Mn1=15) and female (Mn2=15) databases were divided into class of intervals (k, Mk=Fk=6). Temperature distribution in male database was in interval from 29°C to 31.7°C and the highest multiplicity (Mk4=47%) in class interval

<30; 30.9>. Temperature distribution in female database was in interval from 27°C to 32.8°C and the highest multiplicity (Fk4=33%) in class interval <31; 31.9>. Accuracy of the used thermal imager (Fluke Ti55/20) is ±2°C.

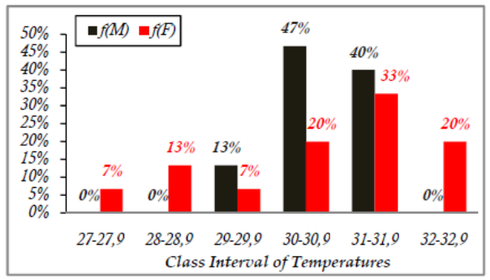

Fig.4. Temperature comparison between male and female volunteers, view in frontal plane ventral side in determined classes

Acknowledgement

This contribution is the result of the project implementation: Center for research of control of technical, environmental and human risks for permanent development of production and products in mechanical engineering (ITMS:26220120060) supported by the Research & Development Operational Programme founded by the ERDF.

References

[1] http://www.fluketi55.com/assets/images/pdfs/ti55/2674273_0000_ENG_C_Wti55datasheet.pdf.
[2] Ring, E. F., The historical development of thermometry and thermal imaging in medicine, Journal of Medical Engineering & Technology, 2006 Jul-Aug;30(4):192-8Please, use Times New Roman, 8 points and this format for writing the list of references.
[3] http://www.comp.glam.ac.uk/pages/staff/pplassma/MedImaging/Projects/IR/Atlas/index.html.
[4] Ring, E. F. J.: The historical development of temperature measurement in medicine, Infrared Physics & Technology, Volume 49, Issue 3, 2007, Pages 297-301
[5] Ring, E. F. J.: The historical development of temperature measurement in medicine, Infrared Physics & Technology, Volume 49, Issue 3, 2007, Pages 297-301
[6] https://www.comp.glam.ac.uk/pages/staff/pplassma/MedImaging/Projects/IR/Atlas/index.html
[7] Hudák, R.: Termografická diagnostika v procese rehabilitácie paraplegických a tetraplegických pacientov. Doktorandská práca. Košice: Technická univerzita v Košiciach, Strojnícka fakulta, 2007. 144s.
[8] http://iopscience.iop.org/0031-9155/18/5/307
[9] Tkáčová, M., Hudák, R., Živčák, J. and Sidun. J.: Thermographic Atlas of the Human Body, INES 2011, Pages 417-420, ISBN 978-4244-8955-8
[10] Awerbuch, M.S.: Thermogrraphy – its current diagnostic status in musculoskeletal medicine, Pain Management Unit, Memorial Medical Centre, North Adelaide, SA., Med J AUST. 1991 Apr 1; 154 (7): 441.
[11] Ammer, K.: Thermology 2009- a computer- assisted literature survey; In: Thermology International; Published by the Austrian Society of Thermology and European Association of Thermology; Vol.20, No.1;2012; p.5-10;ISSN 1560-604X.
[12] Gold, J.E. – Cherniack, M. – Buchnolz, B.: Infrared thermography for examination of skin temperature in the dorsal hand of office workers, European Journal of Applied Physiology, Publisher: Springer Berlin/ Heidelberg, ISSN 1439-6319, Issue: volume 93, Numbers 1-2 / October, 2004
[13] Takashino, S.- Nakata, R. – Kohashi, R. – Nozaki, S. – Mizuma, H. – Inada, I. – Harashima, K. – Iizuka, H. – Nishimura, N.: A Thermmographic Study on the Alteration of Facial Skin Temperature in Autistic Patient by Exercise Loading, Journal of the Kyorin Medical Society, ISSN 0368-5829, Vol.31, No.3, pp. 357 – 364 (2000).
[14] Jain, R.K., Gullino, P.M.: Thermal Characteristics of Tumors: Applications in Detection and Treatment, Annals of the New York Academy of Science, Volume 335, ANYAA 9 335 1-542, 1980
[15] Kerr, J.: Review of the effectiveness of infrared thermal imaging (thermography) for population screening and diagnostic testing of breast cancer, NZHTA Tech Brief Series, July 2004 Volume 3 Number 3
[16] Sidun, J., Wejrzanowski, T., Dąbrowski, J.R., Kurzydłowski, K. J.: Quantitative description of cancellous bone by image analysis techniques. Journal of Vibroengineering, Vol.11, nr 3 2009, pp. 547-550.
[17] Živčák, J. – Hudák, R. – Kneppo, P.: Application of Infrared Imaging in Rehabilitation Medicine in Spinal Cord Injured Individuals, INES 2005: Procceding: 9th International Conference on Intelligent Engineering Systems, September 16-19. 2005, ISBN 0-7803-9474-7, pp. 221-224.
[18] Živčák, J. – Kneppo, P – Hudák, R.: Methodics of IR Imaging in SCI Individuals Rehabilitation, Inovation from Biomolecules to Biosystems: 27th Annual International Conference of the IEEE Engineering in Medicine and Biology Society, Shanghai, September 1 -4, 2005, ISBN 0-07803-8741-4.
[19] Hudák, R - Živčák, J – Tóth, T. – Michalíková, M.: Spinal cord injured individual' s diagnostics via thernographic measurements, Thermo – Bridge: 14th International Conference on Thermal Engineering and Thermogrammetry, 22 – 24 June, 2005, Hungary, Budapest, MATE 2005.

Viktória Rajťúková, Ing.
Katedra biomedicínskeho inžinierstva a merania
Strojnícka fakulta
Technická Univerzita v Košiciach
Letná 9, 04200 Košice

E-mail: viktoria.rajtukova@tuke.sk
Phone: +421 55 602 2657